

## Ice-induced vibrations of vertically sided offshore structures

Hendrikse, Hayo

**DOI**

[10.4233/uuid:325ebcfb-f920-400c-8ef6-21b2305b6920](https://doi.org/10.4233/uuid:325ebcfb-f920-400c-8ef6-21b2305b6920)

**Publication date**

2017

**Document Version**

Final published version

**Citation (APA)**

Hendrikse, H. (2017). *Ice-induced vibrations of vertically sided offshore structures*. [Dissertation (TU Delft), Delft University of Technology]. <https://doi.org/10.4233/uuid:325ebcfb-f920-400c-8ef6-21b2305b6920>

**Important note**

To cite this publication, please use the final published version (if applicable).  
Please check the document version above.

**Copyright**

Other than for strictly personal use, it is not permitted to download, forward or distribute the text or part of it, without the consent of the author(s) and/or copyright holder(s), unless the work is under an open content license such as Creative Commons.

**Takedown policy**

Please contact us and provide details if you believe this document breaches copyrights.  
We will remove access to the work immediately and investigate your claim.

**ICE-INDUCED VIBRATIONS**  
OF VERTICALLY SIDED OFFSHORE STRUCTURES



**ICE-INDUCED VIBRATIONS**  
OF VERTICALLY SIDED OFFSHORE STRUCTURES

**Proefschrift**

ter verkrijging van de graad van doctor  
aan de Technische Universiteit Delft,  
op gezag van de Rector Magnificus prof. ir. K. C. A. M. Luyben,  
voorzitter van het College voor Promoties,  
in het openbaar te verdedigen op 20 januari 2017 om 10:00 uur

door

**Hayo HENDRIKSE**

civiel ingenieur  
geboren te Woerden

Dit proefschrift is goedgekeurd door de promotoren:

Prof. dr. A.V. Metrikine  
Prof. dr. S. Løset

Samenstelling promotiecommissie:

Rector Magnificus,	voorzitter
Prof. dr. A.V. Metrikine,	Technische Universiteit Delft
Prof. dr. S. Løset,	Norges Teknisk-Naturvitenskapelige Universitet

*onafhankelijke leden:*

Prof. dr. K.A. Riska,	Norges Teknisk-Naturvitenskapelige Universitet
Prof. dr. P. Sammonds,	University College London
Prof. dr. J. Tuhkuri,	Aalto University
Prof. dr. M.L. Kaminski,	Technische Universiteit Delft
Prof. ir. A.C.W.M. Vrouwenvelder,	Technische Universiteit Delft



This thesis was financed by the Research Council of Norway through NTNU's Research Centre for *Sustainable Arctic Marine and Coastal Technology* (SAMCoT CRI). The work described in this thesis was supported by the European Community's 7<sup>th</sup> Framework Programme through a grant from the budget of the Integrated Infrastructure Initiative HYDRALAB-IV, Contract no. 261520.

Copyright © 2017 by H. Hendrikse

All rights reserved. No part of this publication may be reproduced or distributed in any form or by any means, or stored in a database or retrieval system, without the prior written permission of the publisher.

*Printed by:* Gildeprint

*Cover design:* Tamara Hendrikse



ISBN 978-94-6186-746-9

An electronic version of this dissertation is available at  
<http://repository.tudelft.nl/>.

*Nature is relentless and unchangeable, and it is indifferent as to whether its hidden reasons and actions are understandable to man or not*

Galileo Galilei



# SUMMARY

Offshore developments in ice-covered waters have received increasing attention from the petroleum and wind power industries over the past decade. The petroleum industry seeks to develop the Arctic region which contains a major portion of undiscovered conventional oil and gas in the world. The wind power industry seeks to develop offshore wind farms at locations with more moderate ice conditions such as the Baltic Sea and the Great Lakes of North America. These developments are motivated by the global push for green energy and the greater energy potential of offshore wind compared to onshore wind.

Sustainable developments in icy waters can contribute to a balanced energy future provided that the deployed offshore structures are designed to be safe. Safe design requires understanding of the loads exerted by floating ice on offshore structures and the resulting ice-structure interaction. The possible development of ice-induced vibrations has to be considered in the design of bottom founded offshore structures with a vertically sided waterline cross-section subject to level ice. These vibrations originating from dynamic interaction between the ice and structure can result in high global peak loads and significantly contribute to the fatigue of structures. Ice-induced vibrations is the main topic of this thesis.

Two main theories for explanation of the development of ice-induced vibrations which originated in the late sixties are still the most commonly applied, despite the discrepancies between these theories and experimental observations. None of the models based on the mechanisms which have been proposed in the past capture level ice action on vertically sided structures over a broad range of conditions. A re-evaluation of the existing data with the aim to identify a physical mechanism which can explain all, or at least a majority of the observations, and which allows for the development of a widely applicable model is therefore warranted.

The main objective of this study is to define a physical mechanism which can explain the development of ice-induced vibrations when level ice acts on flexible, vertically sided offshore structures. In order to achieve this objective existing experimental observations of ice action on rigid and flexible structures have been analyzed. This analysis resulted in a definition of key features of the interaction process which a governing theory should encompass. New experimental data have been gathered by performing forced vibration experiments in order to elucidate in more detail the processes in the contact zone between ice and structure.

On the basis of the literature study and performed indentation experiments a new theory has been proposed. The theory is based on the observation that ice action on a vertically sided structure is controlled by the velocity dependent deformation and failure behavior of ice. At low loading rates a large real contact area between ice and structure can



develop as a result of ductile deformations of the ice. This results in high global loads on the structure. At high loading rates the ice behaves more or less elastic before failure and contact is only attained in specific zones of high pressure across the ice-structure interface. When a flexible structure is interacting with the ice the loading rate changes continuously. Once it reaches a sufficiently small value, an increase of the contact area between ice and structure takes place resulting in an increased global load on the structure. Ice-induced vibrations develop when this increase in global load is large enough in magnitude to provide sufficient energy to enable sustained vibration of the structure.

Based on this theory a novel phenomenological model for the prediction of ice-induced vibrations has been developed. Consistency of the model with experimental observations has been demonstrated and it has been shown that the majority of observations are captured within the model. The effect of buckling on ice-induced vibrations has been theoretically studied with the model illustrating that buckling of ice generally limits the development of ice-induced vibrations. However, cases may exist in which the ice-induced vibrations prevent ice buckling. Practical application of the model has been discussed on the basis of simulation examples considering the implementation of multi-degree-of-freedom models and the design of model-scale experiments.

# CONTENTS

<b>Summary</b>	<b>vii</b>
<b>1 Introduction</b>	<b>1</b>
1.1 Icy waters: the next energy frontier . . . . .	1
1.2 The phenomenon of ice-induced vibrations . . . . .	3
1.3 Historical overview of research with respect to ice-induced vibrations . . . . .	5
1.4 Thesis objective and scope . . . . .	7
1.5 Thesis outline . . . . .	8
<b>2 Ice action on a rigid structure</b>	<b>11</b>
2.1 Introduction . . . . .	11
2.2 Failure of ice during indentation . . . . .	12
2.3 Global ice load on a structure . . . . .	14
2.4 Details of the ice crushing process . . . . .	17
2.5 Conclusion . . . . .	18
<b>3 Ice-induced vibrations</b>	<b>21</b>
3.1 Introduction . . . . .	21
3.2 Intermittent crushing . . . . .	23
3.2.1 Local contact during intermittent crushing . . . . .	23
3.3 Frequency lock-in . . . . .	24
3.3.1 The frequency lock-in relation . . . . .	26
3.3.2 Boundaries of the lock-in regime. . . . .	27
3.4 Continuous brittle crushing. . . . .	28
3.5 Conclusion . . . . .	28
<b>4 Forced vibration experiments in ice</b>	<b>31</b>
4.1 Introduction . . . . .	31
4.2 Design of the experiment . . . . .	32
4.2.1 Experimental setup . . . . .	32
4.2.2 Experimental procedure and test matrix . . . . .	34
4.3 Results on global and local ice behavior. . . . .	35
4.3.1 General observations during a cycle of forced vibration . . . . .	36
4.3.2 Increase in global load resulting from an increase in contact area . . . . .	38
4.3.3 Dependence of the increase in global load on the duration of ductile ice behavior . . . . .	40
4.3.4 Application of the results to frequency lock-in . . . . .	40
4.4 Added mass and added damping from ice . . . . .	42
4.4.1 Experimental results . . . . .	43
4.4.2 Comparison with fluid-structure interaction. . . . .	44

4.5	Conclusion . . . . .	46
<b>5</b>	<b>Physical mechanism and developed model for ice-induced vibrations</b>	<b>47</b>
5.1	Introduction . . . . .	47
5.2	Contact area variation as a source of ice-induced vibrations . . . . .	49
5.3	Phenomenological model of ice-structure interaction . . . . .	53
5.3.1	Model description . . . . .	53
5.3.2	Definition of model input parameters . . . . .	55
5.4	Consistency of the model and physical mechanism. . . . .	58
5.4.1	Ice action on a rigid structure . . . . .	59
5.4.2	Ice-induced vibrations. . . . .	61
5.4.3	Forced vibration . . . . .	72
5.5	Validation and further development . . . . .	74
5.6	Conclusion . . . . .	76
<b>6</b>	<b>Ice-induced vibrations and ice buckling</b>	<b>79</b>
6.1	Introduction . . . . .	79
6.2	Model description . . . . .	80
6.3	Model application for ice action on rigid structures. . . . .	82
6.4	Ice-induced vibrations and ice buckling . . . . .	88
6.4.1	A structure with scaled dynamic properties . . . . .	88
6.4.2	Intermittent crushing limiting the development of buckling failure . . . . .	92
6.4.3	A structure in conditions of different ice thickness. . . . .	93
6.5	Discussion . . . . .	95
6.6	Conclusion . . . . .	96
<b>7</b>	<b>Practical application</b>	<b>99</b>
7.1	Introduction . . . . .	99
7.2	Implementation of MDOF structural models . . . . .	100
7.2.1	A simplified 1D beam model of an offshore wind turbine . . . . .	100
7.2.2	Structural shape . . . . .	105
7.2.3	Multi-legged structures . . . . .	107
7.3	Variation in ice properties. . . . .	109
7.4	Design of model-scale experiments. . . . .	112
7.5	Conclusion . . . . .	117
<b>8</b>	<b>Conclusion</b>	<b>121</b>
	<b>References</b>	<b>125</b>
<b>A</b>	<b>Post-processing of tactile sensor measurements</b>	<b>135</b>
<b>B</b>	<b>Determination of added mass and added damping</b>	<b>139</b>
B.1	Theory for determination of added mass and added damping . . . . .	139
B.2	Problems encountered during the forced vibration experiments . . . . .	141
<b>C</b>	<b>Implementation of structural models</b>	<b>143</b>
C.1	Implementation of a simplified offshore wind turbine . . . . .	143
C.2	Implementation of a cylindrical structure. . . . .	146

---

<b>Acknowledgements</b>	<b>149</b>
<b>Publications by the author</b>	<b>151</b>
<b>Samenvatting</b>	<b>153</b>
<b>Curriculum Vitae</b>	<b>155</b>



# 1

## INTRODUCTION

### 1.1. ICY WATERS: THE NEXT ENERGY FRONTIER

Offshore developments in ice-infested waters have received increasing attention from the petroleum and wind power industries over the past decade. The petroleum industry seeks to develop the Arctic region which contains a major portion of undiscovered conventional oil and gas in the world (Gautier et al., 2009). Recently the majority of projects in this region have been put on hold as a consequence of the significant drop in oil price, but future developments in the energy market may result in a revival. The wind power industry seeks to develop offshore wind farms at locations with more moderate ice conditions such as the Baltic Sea and the Great Lakes of North America. These developments are motivated by the global push for green energy and the greater energy potential of offshore wind compared to onshore wind.

Sustainable developments in ice covered waters can contribute to a balanced energy future provided that the deployed offshore structures are designed to be safe. Safe design requires understanding of the loads exerted by floating ice on offshore structures and the resulting ice-structure interaction. Sea ice and lake ice come in various types and may contain features such as icebergs and ice ridges. As a result the actual ice regime varies from location to location, which calls for tailor-made design of structures. As an example one could think of a location where icebergs can be present. For such locations a bottom founded structure able to withstand iceberg impacts can be engineered, as has been done in the past (Sédillot, 1998). However, a more feasible and perhaps safer solution is to design a floating structure which can move out of the path of the iceberg if necessary.

In shallow waters with predominantly sea ice conditions, level ice or floe ice, the most feasible solution is often to deploy a bottom founded structure. The relatively cheap monopile foundation for offshore wind turbines is a preferred solution, as cost reduction is a focal point of the wind power industry. In the petroleum industry experience with



Figure 1.1: Lunskeye-A platform in level ice conditions in the Sea of Okhotsk, Russia (photo courtesy of Sakhalin Energy Investment Company Ltd.).

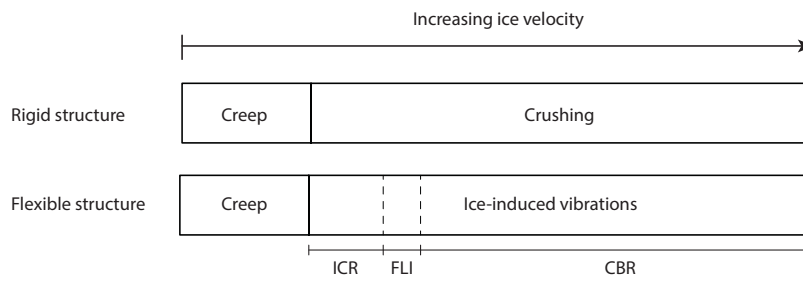


Figure 1.2: Regimes of ice action and ice-structure interaction for level ice acting on a vertically sided offshore structure. Ice-induced vibrations encompass the interaction regimes of intermittent crushing (ICR), frequency lock-in (FLI), and continuous brittle crushing (CBR). Intermittent crushing and frequency lock-in do not always develop and the range of velocities associated with these two regimes as shown in this Figure is only an example.

bottom founded structures in open water is vast and they are currently the most widely employed structures in locations with sea ice presence. An example of a successfully deployed gravity based structure at such location is the Lunskeye-A platform shown in Figure 1.1, which is located in the Sea of Okhotsk, Russia.

Level ice acting on a vertically sided offshore structure may fail and deform in multiple ways depending on ice properties, structural properties, and situation specific parameters. Small ice floes fail by splitting when cracks originating at the ice-structure interface propagate to one of the nearby free edges of the ice floe. For large and thin ice sheets buckling is often observed, resulting in circumferential cracks to be formed in the ice close to the structure. For thicker ice floes acting on relatively stiff structures either creep or crushing is observed depending on the velocity of the ice floe as illustrated in Figure 1.2. Flexible structures can experience three distinct types of structural vibrations as a result of the interaction between ice and structure in the crushing regime. These vibrations are defined as ice-induced vibrations.

The occurrence of ice-induced vibrations has to be considered in the design of bottom founded offshore structures with a vertically sided waterline cross-section subject to level ice. These vibrations, originating from dynamic interaction between the ice and structure, can result in high global peak loads and significantly contribute to the fatigue of structures. The prediction of effects ice-induced vibrations may have on specific structures in terms of fatigue and limit-state performance is outside of the scope of this work. In this thesis the focus is on the mechanism of ice-induced vibrations.

## 1.2. THE PHENOMENON OF ICE-INDUCED VIBRATIONS

Ice-induced vibrations are structural vibrations which can develop as a result of level ice interacting with a vertically sided offshore structure. During interaction the ice fails in compression at the contact zone between ice and structure by crushing into small ice pieces. Larger pieces can sometimes be observed in the hereby generated rubble which originate from cleavage cracks in the ice propagating to the free surface thereby creating spalls or flakes. Flexibility of the structure plays an important role in the process as the interaction is driven by changes in relative velocity between the ice and structure. Ice-induced vibrations are not observed for relatively rigid structures, which displace and deform marginally when subject to ice loading.

Three regimes of ice-induced vibration are commonly defined depending on the velocity of the incoming ice as shown in Figure 1.2. Typical time signatures of the structural response and global ice load in these three regimes are shown in Figure 1.3. At low velocities intermittent crushing may develop which is the regime resulting in the highest global peak loads and which is characterized by saw-tooth patterns in the time dependencies of the global ice load and structural displacement. For intermediate velocities frequency lock-in may develop which is a truly dynamic interaction regime. In this regime the structure oscillates at a frequency close to one of its natural frequencies. The third regime is the continuous brittle crushing regime which occurs at high velocities and results in a small response of the structure.

With respect to the design of structures the regimes of intermittent crushing and frequency lock-in are the most important and can lead to structural failure or adverse working conditions if not taken into consideration properly. Neglecting the ice loads during design in the early stages of the Bohai Sea oil exploitation has led to the push over of two jacket platforms and difficult sleeping and working conditions on board (Yue and Li, 2003). Severe ice-induced vibrations have resulted in damage of lighthouses in the Gulf of Bothnia (Bjork, 1981). An example of one of the pioneering Swedish lighthouses which toppled over as a result of high global ice loads is shown in Figure 1.4. It must be mentioned that this is a structure for which design guidelines had not been developed at the time of construction. Most well-known case of intermittent crushing on a large scale is the Molikpaq May 12<sup>th</sup> 1986 event (Jefferies and Wright, 1988; Jefferies et al., 2011). In this particular case interaction with a thick first-year ice floe with several multi-year ice inclusions resulted in severe intermittent crushing endangering the stability of the platform.

Several solutions have been proposed for mitigation of ice-induced vibrations. The most



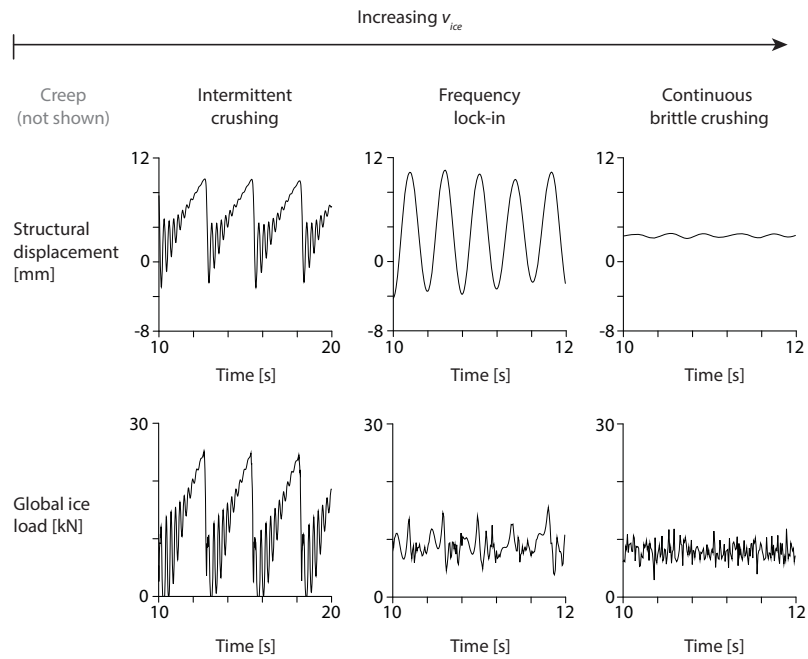


Figure 1.3: Illustration of structural response and global ice load in the three regimes of ice-induced vibrations. Global ice load and structural displacement values have been obtained by numerical simulations and do not reflect real measurements.



Figure 1.4: A Swedish lighthouse toppled by level ice (photo courtesy of Lennart Fransson).

common approach is to apply cones at the ice-structure interface. The sloping cones at the waterline make the ice to move up or down and fail by bending rather than crushing thereby reducing the possibility for ice-induced vibrations to develop (Brown and Määttä, 2009). However, bending failure can still result in a periodic load on the structure leading to structural vibrations and damage (Yue et al., 2007). Furthermore, adding cones to structures comes at an additional cost, can increase the loads resulting from wave action during the time of the year when no ice is present, and introduces additional fatigue-prone zones in the structure. A new approach to mitigation of ice-induced vibrations are the so-called spall initiators proposed by Gagnon (2014). Extruding elements are attached to the structure surface with the aim of initiating cleavage cracks and spalls thereby disturbing the crushing process and preventing ice-induced vibrations to develop. Development and proof of concept studies with respect to this approach are ongoing.

Mitigation measures have either not sufficiently matured to be considered in design or only come at additional cost, which especially for the wind industry reduces the economic feasibility of offshore developments. The capability to predict the frequency of occurrence and severeness of ice-induced vibrations is therefore still of key importance for designing safe and feasible structures. Multiple theories for explaining the physics governing ice-induced vibrations have been proposed in the past. This resulted in a large number of predictive models and approaches which can be used to simulate the interaction. A brief historical overview of significant contributions in the field is presented in the next section.

### 1.3. HISTORICAL OVERVIEW OF RESEARCH WITH RESPECT TO ICE-INDUCED VIBRATIONS

First documented cases and theoretical explanations of ice-induced vibrations date back to the late 1960's from observations on offshore platforms at the Cook Inlet, Alaska (Peyton, 1968; Blenkarn, 1970). Being the first major subarctic region for oil- and gas exploitation in the world, design information applicable to the conditions of Cook Inlet was absent and large measurement campaigns were undertaken. Analysis of the obtained data resulted in the proposal of two different mechanisms for explanation of the development of ice-induced vibrations. Blenkarn (1970) proposed that there exists a source of negative damping in the ice-structure system which provides the energy required for sustained vibration. Peyton (1968) concluded from his analysis that ice possesses a characteristic failure length. He explained the observed periodic structural vibrations during intermittent crushing and frequency lock-in as a resonance condition which can occur when the natural frequency of the structure lies close to the failure frequency of the ice. The latter being defined by the characteristic failure length and indentation velocity. To date these two mechanisms are still the most commonly adopted explanations for the occurrence of ice-induced vibrations.

Neill (1976) presents a summary of the research in the late sixties and seventies with respect to analytical approaches, full-scale data, and small-scale laboratory investigations.

## 1

The main conclusion he draws is that after ten years of research more data were still necessary, full-scale as well as small-scale, in order to obtain a better understanding of the dynamic ice-structure interaction process. During these early years two phenomenological models were introduced which are still used to date in research and design studies. The model by Matlock et al. (1969) is the first model which contains the characteristic failure length of ice. The model by Määttänen (1978) predicts ice-induced vibrations to occur as a result of negative damping. As the source of negative damping a decrease in ice strength with increasing loading rate was proposed based on measurements of the uniaxial compressive strength of ice (Michel and Toussaint, 1977).

In the beginning of the eighties several small-scale experimental campaigns were initiated in order to increase the understanding of the phenomenon of ice-induced vibrations and gather more data for model validation. During these campaigns it was first observed that frequency lock-in occurs over a range of velocities (Määttänen, 1983; Toyama et al., 1983; Tsuchiya et al., 1985). Another key discovery was the linear relation between ice velocity and amplitude of structural vibrations in the frequency lock-in regime found by Toyama et al. (1983). Tsuchiya et al. (1985) developed the first model to incorporate both the characteristic failure length of ice and the dependence of ice strength on loading rate - an approach still used in research and which has been refined in a more recent model by Huang and Liu (2009).

Until the end of the eighties most experimental and modeling work was focused on slender vertical piles. This changed with the observations of ice action on the Molikpaq structure which were presented in 1988 (Jefferies and Wright, 1988). This wide structure experienced significant intermittent crushing while interacting with a first-year ice floe with multi-year inclusions. In one case this induced fatigue of the sand core thereby degrading the platform's ability to withstand ice loading. The first model applicable for simulation of such wide structures in ice conditions has been developed by Kärnä (Kärnä et al., 1999, see also Kärnä, 1992; Eranti, 1992; Kärnä and Turunen, 1989). The 'PSSII' model is the first to apply a zonal approach with specific ice-structure interaction points to model both simultaneous and non-simultaneous crushing during interaction. The model incorporates a dependence of ice strength on indentation velocity as the mechanism governing the development of ice-induced vibrations.

Extensive overviews of the research on ice-induced vibrations until 1988 by Sodhi (1988) and Määttänen (1988) show that still no consensus had been reached on the mechanism causing ice-induced vibrations. Sodhi criticizes the self-excited vibrations models and proposes a model which is based on the concept of a characteristic failure length in ice (Sodhi, 1995). He further draws the attention to the lack of high-speed indentation data and data of indentation with wide structures. Määttänen defends the self-excited vibration concept by stating that self-excited vibration type models are the only models which can represent ice loads on rigid structures. This is still the main argument against models which employ the theory of a characteristic failure length in the ice.

During the nineties significant steps were made to fill the data gap identified by Sodhi in the Japanese JOIA project (Saeki et al., 1996) as well as the full-scale measurement campaigns LOLEIF and STRICE on the Norströmsgrund lighthouse in the Gulf of Bothnia (Schwarz and Jochmann, 2001). Novel approaches employing predefined force functions

were introduced (Shih, 1991; Vershinin and Iliady, 1990), however such approaches are generally limited in terms of applicability as they do not explicitly model the interaction process between ice and structure. Muhonen (1996) gives an evaluation and comparison between ice-structure interaction models concluding that none of the considered models performs well due to oversimplification of ice behavior. He proposed that further development of models should take into account the obtained knowledge about the physics of the interaction process.

In 2000 Dempsey (2000) presented an extensive overview on the research trends in ice mechanics. He concludes that the importance of contact area, ice sheet velocity, and ratio between structure width and ice thickness on the global ice force is not sufficiently well understood. Dempsey states that this knowledge needs to be gained first, before the further development of ice-structure interaction models can effectively continue. The objectives of a more recent Joint Industry Project on ice-induced vibrations (Kärnä et al., 2013) which was completed in 2012, show that there is still a gap in the understanding of the physics of the interaction process which needs to be dealt with in order to develop design tools the industry needs.

Most recent new approaches for dynamic ice-structure interaction include the use of more advanced numerical procedures such as discrete element and lattice modeling techniques (Dorival et al., 2008; Shkhinek et al., 2011), the use of numerical FE techniques with cohesive elements (Gürtner et al., 2010), and a foam analogue for modeling of ice crushing (Gagnon, 2011b). All approaches show to have a potential for use in simulations of the dynamic ice-structure interaction. However, the mechanism governing ice-induced vibrations has not been recovered yet in these models. With the aim of defining a widely applicable model for prediction of ice-induced vibrations further development and evaluation of the two primary theories is still ongoing (Gagnon, 2012; Huang and Liu, 2009; Jeong and Baddour, 2008, 2010; Venturella et al., 2011; Withalm and Hoffmann, 2010; Gagnon, 2012).

#### 1.4. THESIS OBJECTIVE AND SCOPE

The most recent developments described above illustrate that the physical explanation for ice-induced vibrations remains under debate and needs to be defined in order to develop numerical models which can be used for prediction of the behavior of vertically sided structures in level ice conditions. The two main theories which date back to the late sixties are still commonly applied, despite the discrepancies between these theories and experimental observations. None of the models based on the mechanisms which have been proposed in the past capture level ice action on vertically sided structures over a large range of conditions. A good model should, at least, capture ice action on both rigid and flexible structures without the need of changing ice properties or ice behavior in the model when different structural properties are considered. Based on the existing theories such model cannot be developed. A re-evaluation of the existing data with the aim to define a physical mechanism which can explain all, or at least a majority of observations, and which allows for the development of a widely applicable model is therefore warranted.

## 1

The main objective of this study is to define a physical mechanism which can explain the development of ice-induced vibrations when level ice acts on flexible, vertically sided offshore structures. In order to achieve this objective existing experimental observations of ice action on rigid and flexible structures are first analyzed. This analysis results in the definition of key observations which a governing theory should encompass. New experimental data is gathered by execution of forced-vibration experiments in order to elucidate in more detail the processes in the contact zone between ice and structure during a controlled harmonic motion closely resembling frequency lock-in vibration. The result of this literature study and experiment is the formulation of a theory which can explain the phenomenon of ice-induced vibrations.

The second objective of this study is to develop a phenomenological model for the simulation of vertically sided structures in level ice conditions. A simplified analogy is developed based on the defined mechanism. Consistency of the model with experimental observations is demonstrated and application of the model for practical cases is discussed.

The focus in this study is on large level ice floes acting on vertically sided structures. The extent of the ice floes is assumed to be such that their drift velocity is not influenced by the interaction with the structure. Specific ice features which may be included in the ice such as ridges, rafted ice, and icebergs are not taken into consideration. Effects of rubble, or failed ice, present at the ice-structure interface, are not considered as the loads associated with this rubble are generally small compared to the loads resulting from interaction between intact ice and structures. Material science studies with respect to ice have not matured enough to allow for the development of a full physical material model of ice, its deformation behavior, and fracture. In this thesis a phenomenological approach to model the deformation and fracture of ice is therefore chosen.

With respect to the structure, only bottom founded offshore structures are considered in this thesis. The presented results may be extended to scenarios with floating structures as long as the level ice acts on a vertical side of the structure. Throughout the thesis the structure is treated in a simplified manner as being rectangular and its dynamics being described by a single-degree-of-freedom oscillator model. This simplification allows to focus mainly on the ice behavior in the developed model. The implementation of more detailed structural models is discussed with respect to the practical implementation of the developed theory.

## 1.5. THESIS OUTLINE

This thesis consists of three main parts. The first part includes Chapters 2 to 4 and deals with full-scale and experimental observations of ice actions on rigid structures and ice-structure interaction. These observations form the basis for the theory developed in this work. The second part, consisting of Chapters 5 and 6, presents a description of the mechanism that is proposed to explain the development of ice-induced vibrations as well as the developed phenomenological model for ice-structure interaction. The third part, Chapter 7, deals with practical aspects in relation to application of the theory and phenomenological model and defines some possible directions for further research.

Chapter 2 contains a literature review with respect to ice actions on rigid structures. An overview of experimental and full-scale observations is given to illustrate the deformation and failure of level ice during indentation. The ice failure modes of creep, crushing, and buckling are introduced and details of the crushing process are described.

In Chapter 3, experimental and full-scale observations with respect to ice-induced vibrations are summarized and a definition of the regimes of intermittent crushing, frequency lock-in, and continuous brittle crushing is given. The focus in this chapter is on experimental observations which can be used to verify and validate theories and models for simulation of dynamic ice-structure interaction.

Chapter 4 deals with the novel forced vibration experiments in ice carried out as part of this research. The experiments were designed for investigation of controlled cyclic indentation of ice. Results of these experiments show how ice deforms and fails when the rate by which it is loaded varies during indentation. An attempt has been made to identify the added mass and added damping from ice. A comparison with forced vibration experiments for cylinders submerged in fluid is made, the latter being commonly applied for the definition of added mass and added damping in the field of research concerned with vortex induced vibrations. The presented results provide unique data for the validation of theories and models for simulation of the behavior of vertically sided structures in level ice conditions.

In Chapter 5 a theory is introduced which explains how ice-induced vibrations develop and encompasses the experimental observations introduced in Chapters 2 to 4. It is proposed that variations in the contact area between intact ice and structure govern ice-induced vibrations. These variations occur as the loading rate between ice and structure changes during indentation where ductile deformation of ice, at low loading rates plays a major role. A phenomenological model is developed based on the defined mechanism. Consistency of the defined theory and model is verified by comparing model predictions with the key experimental observations and trends identified in Chapters 2 to 4.

In Chapter 6, ice buckling as a limiting mechanism for ice-induced vibrations is investigated. The phenomenological model for ice-structure interaction as introduced in Chapter 5 is expanded to include ice buckling in a simplified manner. In this way a model is obtained which captures creep, crushing, and buckling of ice and the transitions between these failure modes as observed in laboratory conditions. It is shown that ice buckling generally limits the development and duration of ice-induced vibrations, but that for specific conditions the opposite, namely the ice-induced vibrations limiting the development of buckling, can occur.

Chapter 7 deals with the practical aspects in relation to application of the developed numerical model and theory. Conditions for which frequency lock-in can occur at higher structural modes are illustrated by simulation of a simplified offshore wind turbine in level-ice conditions. The incorporation of different structural shapes and multi-legged structures is discussed. Examples are given to illustrate the importance of initial conditions for the development of frequency lock-in. Finally, the design of model-scale tests for ice-induced vibrations is discussed.

In Chapter 8, the main findings of this thesis are summarized.



# 2

## ICE ACTION ON A RIGID STRUCTURE

### 2.1. INTRODUCTION

The study of ice-induced vibrations concerns flexible, vertically sided structures interacting with level ice. The case of a rigid structure, defined here as immovable and undeformable, that indents into the ice might therefore not be the most obvious choice to start our investigation. When considering the response of ice to an indenting load it is important to understand that the ice does not differentiate between different types of structures, but merely responds to the behavior of the object it meets. In this context the rigid structure is a special case of flexible structure, and hence any sound theory or model for ice-induced vibrations should capture ice action on a rigid structure as well. Studying ice action on rigid structures allows to define ice behavior in absence of structural motion based purely on ice properties and the boundary conditions of the indentation problem.

In this Chapter experimental and full-scale observations of ice action on rigid, vertically sided structures from literature are summarized. In Section 2.2 first the different failure modes which can occur and their dependence on indentation velocity and aspect ratio, the ratio between structure width and ice thickness, are introduced. In Section 2.3 characteristics of the time dependencies of the global load for each of the different failure modes are treated. In Section 2.4 details of the crushing process are summarized, crushing being the main failure mode associated with ice-induced vibrations. The chapter ends with summarizing conclusions in Section 2.5.

---

Parts of this chapter have been published in *Cold Regions Science and Technology*, 2016 (Hendrikse and Metrikine, 2016b).



## 2.2. FAILURE OF ICE DURING INDENTATION

Level ice acting on a vertically sided structure may fail in multiple ways depending on indentation velocity, aspect ratio, and ice properties (Blanchet et al., 1988; Timco, 1991). Splitting failure occurs when a crack initiating at the ice-structure interface propagates to a free edge (Lu et al., 2014). Splitting mainly occurs for ice floes limited in size. In this work it is assumed that the extend of the ice floes is sufficient such that splitting does not occur. The terms creep, crushing failure, and buckling failure are used here as generalized terms each of which combines several deformation and crack formation processes in the ice. In Figure 2.1 the different crack formation processes are sketched, indicating which of those are encompassed by creep, crushing failure, and buckling failure. A failure map indicating the dependence of ice failure on indentation velocity and aspect ratio based on model-scale data from Timco (1991) is shown to illustrate the transition between different types of failure. In full-scale the data shows to be more scattered compared to model-scale, and especially the transitions from crushing to buckling failure change (Blanchet et al., 1988; Kärnä and Jochmann, 2003). What follows is a brief description of creep, crushing failure, buckling failure, and the transition between those.

Creep governs the deformation and failure of ice at low indentation velocities and low aspect ratios. This type of failure is sometimes referred to as ductile failure. Creep is characterized by full contact between the ice and structure and a relatively uniform pressure at the ice-structure interface. Large creep deformations can develop over long periods of time. Failure occurs by plane creep in which case the ice deforms in a plastic manner in front of the structure and material flows slowly from the interface to form solidified ice in front of and at the sides of the structure. Creep of ice is treated in detail by Schulson and Duval (2009), and Ponter et al. (1983).

Crushing defines the ice deformation and failure at high indentation velocities and low aspect ratios which is characterized by local contacts and quasi-random ice load signals (Jordaan, 2001; Sodhi, 2001). The term crushing is used to define the combined pulverization of ice, formation of spalls and flakes as a result of cleavage cracks propagating to the free surface, and formation of radial cracks. Spalls and flakes generally occur for aspect ratios above one, the range of interest for ice-induced vibrations, resulting in a wedge shaped front of the ice when looking from the side. Radial crack formation results in a wedge shaped geometry of the ice in front of the structure when looking from above, but does not necessarily have a measurable effect on the load on the structure (Palmer et al., 1983). Deformation of ice during crushing prior to failure is mainly elastic at high indentation velocities. At indentation velocities around the transition from creep to crushing, ductile deformation, i.e. visco-elastic or visco-plastic deformation, forms a more pronounced part of the total deformation, even though the ice still fails locally by fracturing. The difference between ductile and creep deformation is related to the time scales associated with them. Ductile deformation develops at similar time scales as the elastic deformation and creep takes significantly longer to develop.

Buckling failure is defined as the out-of-plane deformation of the ice sheet resulting in failure as soon as the bending stress caused by the buckling exceeds the bending strength of the ice plate. This mechanism leads to the formation of circumferential cracks in the

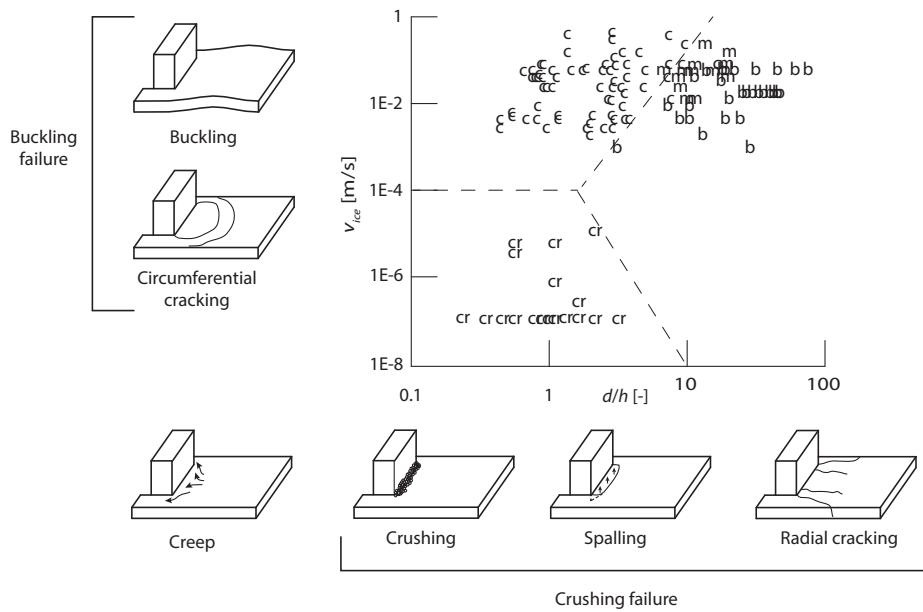


Figure 2.1: Failure mode map for model-scale conditions based on the data reported by Timco (1991). On the vertical axis the ice velocity is plotted. On the horizontal axis the aspect ratio is plotted defined as the ratio of structure width, or diameter,  $d$  to ice thickness  $h$ . Dashed lines are added here to indicate the expected transitions between different failure modes. Sketches of distinct types of failure and fracture are shown. Legend: cr – creep, c – crushing failure (crushing, crushing with spalling, and crushing with radial cracking), b – buckling failure, m – mixed crushing and buckling failure.

ice (Michel and Blanchet, 1983). The buckling failure occurs for high aspect ratios and can develop at both high and low velocities of ice. When buckling failure at high velocities occurs after a period of ice crushing against the structure it is referred to as failure in mixed crushing and buckling. It is noted that in general distinguishing between bending and buckling failure is difficult, as both result in a similar failure pattern. However, the term bending is normally associated with deformations imposed by vertical loads acting on the ice sheet, for example large rubble piles may cause the ice sheet to bend. In laboratory conditions it is expected that the circumferential cracks originate mainly from buckling caused by in-plane loads induced by the structure.

The transitions between different failure modes, as they are expected to occur, are indicated in Figure 2.1 by dashed lines. A transition velocity can be identified, corresponding to the horizontal dashed line in the figure, which marks the change from creep to crushing failure. The transition velocity is expected to depend on ice properties similar to the ductile-to-brittle transition strain rate in compression of small ice-samples (Schulson and Duval, 2009). Transitions from creep to buckling failure and from crushing to buckling failure, indicated by diagonal dashed lines in Figure 2.1, occur for high aspect ratios or thin ice when the critical buckling load of the ice sheet is less than the maximum in-plane load due to crushing or creep.

### 2.3. GLOBAL ICE LOAD ON A STRUCTURE

Each failure mode of ice results in a distinct time dependence of the global load the ice exerts on a structure. Typical time traces of the global load on a structure for the different failure modes are illustrated in Figure 2.2, and can be found in Timco (1987). In creep the global ice load increases gradually over time towards a peak value, after which the load reduces to a steady-state value (Sodhi, 1991). In crushing the time traces are generally quasi-random around a mean value owing to the uncorrelated local failures in the contact zone between ice and structure. In case of buckling the time traces are characterized by periods of load build-up followed by global failure and then intervals of zero or low load from ice rubble when new contact is being established. Mixed crushing and buckling results in short periods of crushing abruptly ending when buckling failure occurs, followed by periods of small or zero loading as new contact between the ice and structure is being established.

Besides the time dependencies the statistical features of the global ice load are of importance for ice-structure interaction. Especially the dependence on indentation velocity of the maximum, mean, and standard deviation of the global ice load. Typical dependencies for low and high aspect ratios are shown in Figure 2.3 based on data from experiments with rigid indenters by Sodhi and Morris (1984).

For low aspect ratios, the left graph in Figure 2.3, the global load on a structure is typically largest at or around the transition velocity which marks the transition from creep to crushing and can be up to four times the maximum load during crushing at high velocities (Singh et al., 1990). In the creep range, not included in Figure 2.3, the maximum ice load increases roughly linearly with indentation velocity (Ponter et al., 1983) as a result of strain-rate hardening. In the crushing range the mean global ice load is highest around

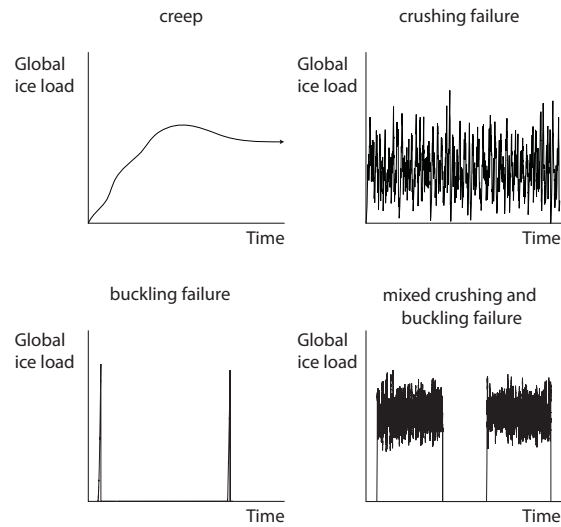


Figure 2.2: Illustration of typical time traces of the global load for different failure modes. Illustrations are not to scale.

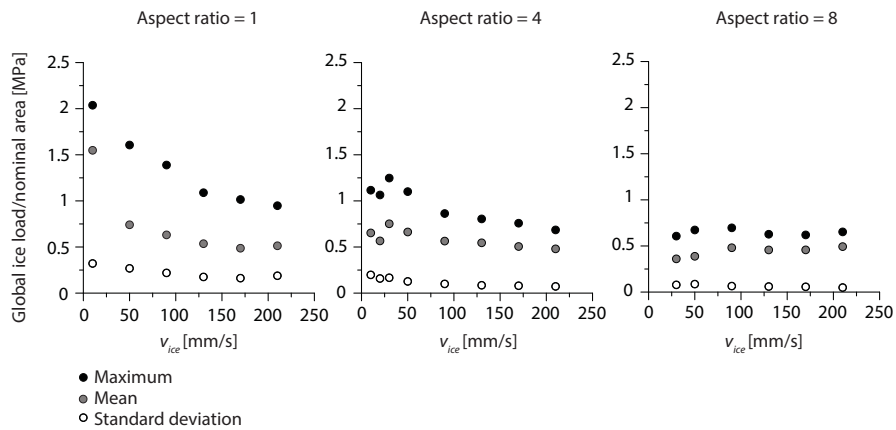


Figure 2.3: Dependence of maximum, mean, and standard deviation of the global ice load on indentation velocity for low and high aspect ratios from experiments with rigid indenters (Sodhi and Morris, 1984). The loads are scaled with the nominal contact area defined by the indenter diameter and ice thickness, the latter being approximately 55 mm for all tests. Results cover only the crushing regime and not the low ice velocity regime in which global creep occurs.

the transition velocity and reduces to a more or less constant value for high indentation velocities. The maximum load shows a similar trend, whereas the standard deviation remains more or less constant irrespective of velocity (Sodhi and Morris, 1984).

**2**

For high aspect ratios, the right graph in Figure 2.3, the maximum global load no longer occurs at the transition velocity but at high velocities where crushing, or mixed crushing and buckling failure is observed (Sodhi and Morris, 1984). This result is obtained in cases for which the critical buckling load is lower than the global load required for crushing or in-plane creep of the ice. Especially around the transition velocity buckling failure may be triggered before the high global loads which occur as a result of creep and crushing have fully developed. It is interesting to note from Figure 2.3 that the scaled mean global ice load at high velocities seems to scale linearly with structure width, while the standard deviation reduces with increasing structure width.

The decrease in mean and maximum global ice load with increasing ice velocity observed for low aspect ratios is of importance with respect to ice-induced vibrations as this dependence facilitates the energy flow from ice to structure. The global load is generally considered as a summation of pressures in local contact areas where a distinction can be made between intact ice, which carries the majority of the load, and broken ice pieces or rubble, which do not generally carry a significant portion of the load. The higher global ice load around the transition from creep to crushing can be a result of a larger contact area, higher pressures in the contact zone, or both.

Observations by Takeuchi et al. (2001) from field tests show that the contact area between ice and structure changes significantly around the transition from creep to crushing. Results in terms of the contact ratio, defined as the area of contact between ice and structure over the total area given by the ice thickness and structure width are replotted in Figure 2.4. In creep almost full contact can be attained indicated by the high values of the contact ratio, while during brittle crushing the mean load is carried by only roughly ten percent of the total area. A decreasing trend is observed starting from the transition between creep and crushing, however the amount of data in this range is limited. Nevertheless, the contact area shows to change around the transition velocity which indicates it might play a role in the high global load level observed at such velocity of indentation. Further illustrations of the difference in contact area in the creep and crushing range can be found in Sodhi et al. (1998).

With respect to pressures in the contact zone different opinions exist. It is commonly stated that the ice strength, and as a result pressure in the contact zone, decreases with increasing velocity of indentation causing the decrease in global load with increasing velocity for low aspect ratios as shown in Figure 2.3. This statement is based on uniaxial compressive strength tests of small ice samples (Michel and Toussaint, 1977). Such dependence of strength is however not always recovered in case of warm ice in field conditions (Schwarz, 1971). When looking at pressure measurements in the creep and crushing regimes even the opposite is observed, local peak pressures show to be generally higher in case of crushing at high indentation velocities (Sodhi et al., 1998). There is no existing compelling evidence which shows that local pressures in the contact zone between ice and structure follow a dependence on indentation velocity similar to that observed for the uniaxial compressive strength of ice in lab conditions.

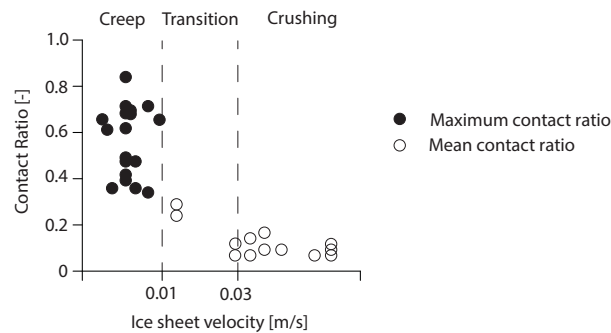


Figure 2.4: Dependence of contact ratio on indentation velocity from experiments by Takeuchi et al. (2001).

## 2.4. DETAILS OF THE ICE CRUSHING PROCESS

Ice-induced vibrations are mostly associated with the failure mode of crushing and it is therefore of interest to describe the details of this process. Descriptions of ice crushing are given by Jordaan (2001) and Sodhi (2001). Crushing is a dynamic process associated with the pulverization of ice into small particles, the occurrence of spalls, and local contact between the ice and structure in zones of high pressure.

The contact between ice and structure during crushing is established in local spots distributed in a line-like zone across the width of the indenter as first described by Joensuu and Riska (1988) and illustrated in Figure 2.5. The wedge shaped front of the ice occurs as a result of horizontal cleavage cracks originating near the ice-structure contact and propagating to the free surface. This process is often referred to as spalling or flaking. Pressures fluctuate considerably both in space and in time, with most of the force concentrated intensely in so-called high-pressure zones (Jordaan, 2001). The position and number of high-pressure zones changes continuously resulting in fluctuations in the global ice load. Regularity of the processes in high-pressure zones is interrupted by the formation of spalls.

Spalling and crushing show to be periodic processes with recurrence periods in the order of 0.02 seconds up to 2 seconds (Blanchet et al., 1988). Especially spalling shows to be highly periodic in controlled small-scale experiments (Gagnon, 1999, 2011a), although these experiments show some interaction between ice and the test apparatus which might affect the observed periodicity. The periodicity of the crushing process is of interest as it can be important in the development of ice-induced vibrations. When looking at the global interaction a more or less linear dependence of the peak frequency in the spectrum of the global ice load on indentation velocity is observed (Sodhi and Morris, 1984), indicating that the process is not random, but on a local scale the crushing and spalling process are perhaps periodic. For indentation against rigid structures global periodic failure is however never observed to occur in the crushing range.

2

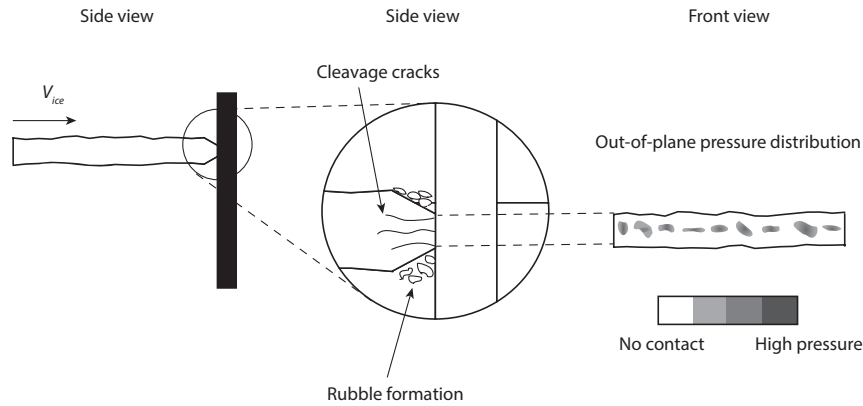


Figure 2.5: Local line-like contact in crushing with high-pressure zones carrying the majority of the global load. The front of the ice is typically wedge shaped as a result of spalling.

## 2.5. CONCLUSION

Large ice floes acting on a rigid vertically sided structure can fail in creep, crushing, buckling, or a combination of those. Creep characterizes the deformation and failure process in ice at low indentation velocities. Crushing failure defines the pulverization of ice, spalling, and formation of radial cracks. The deformation of ice is almost purely elastic at high indentation velocities and ductile, containing larger contributions of visco-elastic or visco-plastic deformation, at low velocities around the transition from creep to crushing. Buckling failure defines the formation of circumferential cracks due to exceedance of the bending strength in the ice as a result of instability of the horizontally flat equilibrium. Transitions between the different failure modes depend on indentation velocity and aspect ratio besides ice properties and boundary conditions.

The global ice load shows typical time dependencies and trends in statistical characteristics for the different failure modes. In creep the global load builds up to a peak value over a significant amount of time after which the load reduces to a steady value. In crushing the load is apparently aperiodic around a mean value. Buckling results in periods of load build-up followed by global failure and times of zero or low loads as new contact is established. For low aspect ratios the maximum global load generally occurs around the transition from creep to crushing. For high aspect ratios this is not recovered as buckling of ice becomes the limiting failure mechanism. The higher global ice load around the transition can be explained to result from an increased contact area between ice and structure, which has been observed to develop around the transition from creep to crushing.

Ice crushing is characterized by discrete failure, local contact, high pressure zones and a wedge shaped front of the ice sheet as a result of spalling. The frequency of failure shows to be rather constant in small-scale experiments with only one or few zones of contact, but to be distributed around a peak value in cases of indentation against larger structures.

When modeling level-ice action on vertically sided structures the ice failure modes and deformation behavior of the ice described in this Chapter need to be considered. The aspects described herein serve as a basis for the development of a theory and phenomenological model for dynamic ice-structure interaction which is presented in Chapter 5. In the next Chapter level ice interacting with flexible structures is treated for which the interaction between ice and moving structure can result in the development of ice-induced vibrations.





# 3

## ICE-INDUCED VIBRATIONS

### 3.1. INTRODUCTION

In the previous chapter it is shown that level ice may fail in different ways when acting against a rigid, vertically sided structure. When a flexible structure is introduced the ice and structure start to interact which can lead to the development of ice-induced vibrations. In this Chapter the different regimes of ice-induced vibrations are introduced. Ice-induced vibrations are mostly associated with the crushing failure mode of ice and therefore seen often in cases where the aspect ratio is low or the ice is relatively thick. Creep and buckling failure which generally result in small amplitude vibrations, or transient vibrations of the structure are not considered here.

Three regimes of ice-induced vibrations can be distinguished for ice sheet velocities exceeding velocities resulting in global creep. These three regimes are defined as intermittent crushing, frequency lock-in, and continuous brittle crushing. An illustration of the time dependence of the global load and structural displacement in each of these regimes is given in Figure 3.1. Not all regimes occur for each type of flexible structure, but typically intermittent crushing is observed for the lowest indentation velocities, followed by frequency lock-in, and ultimately continuous brittle crushing for the highest velocities. The interaction during intermittent crushing and frequency lock-in is of particular interest for design of structures, as these types of interaction result in the largest global loads and largest amplitudes of structural oscillation.

In this Chapter the three regimes of ice-induced vibrations are introduced in more detail based on model-scale and full-scale observations from literature. References to experimental campaigns where ice-induced vibrations have been observed are given, but not all campaigns are discussed in detail. In Section 3.2 intermittent crushing is first introduced, showing typical characteristics of the interaction process and some key observations which can be used for model validation. Frequency lock-in is treated in Section

---

Parts of this Chapter have been published in International Journal of Solids and Structures, 2015 (Hendrikse and Metrikine, 2015).

## 3

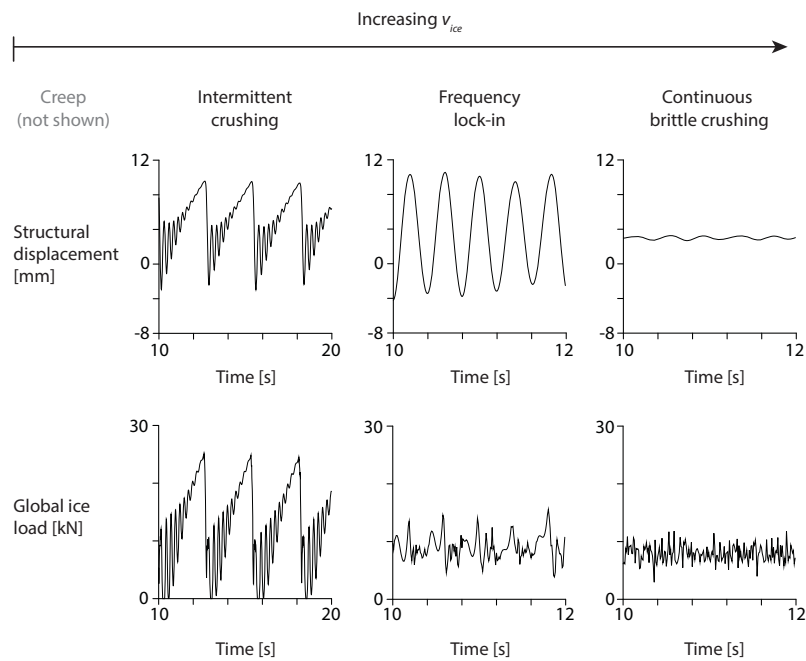


Figure 3.1: Illustration of structural response and global ice load in the three regimes of ice-induced vibrations. Global ice load and structural displacement values have been obtained by numerical simulations and do not reflect real measurements.

3.3 where subsections deal with the relation between structural amplitude and indentation velocity and the dependence of the range of velocities over which frequency lock-in occurs on changes in structural properties. In Section 3.4 continuous brittle crushing is defined and summarizing conclusions are given in Section 3.5.

## 3.2. INTERMITTENT CRUSHING

Intermittent crushing occurs when a relatively flexible structure interacts with a slowly moving ice sheet (Blenkarn, 1970; Finn et al., 1993; Izumiyama and Uto, 1997; Jefferies and Wright, 1988; Kamesaki et al., 1996; Kärnä and Muhonen, 1990; Kärnä et al., 2003; Määttänen, 1983; Muhonen et al., 1992; Nakazawa and Sodhi, 1990; Sodhi, 1991, 2001; Toyama et al., 1983; Tsuchiya et al., 1985; Yue et al., 2002). This regime of ice-induced vibration is characterized by a saw-tooth like pattern in both the time traces of global ice load and structural displacement as illustrated in Figure 3.1. The saw-tooth frequency shows to be approximately constant for a specific structure in non-varying ice conditions and increases with increasing ice sheet velocity until frequency lock-in or continuous brittle crushing becomes the dominant mode of interaction (Sodhi, 2001). The amplitude of structural displacement is mainly determined by the ratio between global ice load and structural stiffness. For this reason the interaction is often referred to as quasi-static interaction. Dynamic properties of the structure do play a role in the observed interaction after a moment of global ice failure and at the start of a saw-tooth interaction cycle.

The observations of intermittent crushing on the Molikpaq structure have been of historical importance with respect to ice-induced vibrations (Jefferies and Wright, 1988). The Molikpaq suffered from severe intermittent crushing on May 12th, 1986, when interaction with a large first-year ice floe with multi-year inclusions resulted in the stability of the platform being endangered. This was the first time ice-induced vibrations on a wide structure had been reported. The observations show that even such stiff and heavy platforms can suffer from ice-induced vibrations, given the right ice conditions.

The maximum global ice load during intermittent crushing is significantly higher than that observed during continuous brittle crushing. Reports from model-scale experiments indicate that the peak loads increase by a factor 1.7 - 2.2 approximately (Finn et al., 1993; Kärnä and Muhonen, 1990). This increase is comparable to the increase in global load that is observed when ice failure against rigid structures changes from crushing to creep as explained in Chapter 2. Detailed processes in the contact area can be studied in order to reveal the cause of these high peak loads during intermittent crushing. This is shown in the next Section.

### 3.2.1. LOCAL CONTACT DURING INTERMITTENT CRUSHING

Intermittent crushing has been observed often in the experiments with a compliant structure executed as part of this thesis in the large ice basin at HSVA, Hamburg (Määttänen et al., 2012). During the experiments a tactile sensor was used to measure the local

pressures and contact at the ice-structure interface. A single case of intermittent crushing is discussed here to illustrate the development of local contact and pressure, but the results are applicable to all cases of intermittent crushing observed in the experiments.

Figure 3.2 shows a typical observation in the case of intermittent crushing for a constant ice sheet velocity of  $40 \text{ mm s}^{-1}$ . A cycle of intermittent crushing starts at the time moment A, preceded by several events of brittle fracture at a high relative velocity. A rough line-like contact between ice and structure is established and the ice starts to load the structure. Due to the structural motion the relative velocity quickly reduces allowing for ductile deformations in the ice to develop. These ductile deformations cause a delay of local brittle fracture and result in a growth of the contact area and increase in mean pressure. The resulting larger load on the structure pushes it further from its equilibrium. At time moment B the maximum deformation in a local high pressure zone is reached and local brittle fracture is initiated. This results in a reduction of the global load and causes the structure to start moving back towards its equilibrium position gradually increasing the relative velocity. The contact area is almost instantaneously reduced as seen from the tactile sensor measurements at time moment C. The large load drop is sometimes referred to as spatially synchronized failure or simultaneous failure. In reality several events of local brittle fracture occur subsequently, even though on the time scale considered the fracture seems to happen more or less simultaneously. As the structure moves towards its equilibrium position it is slowed down by this fracturing process and a new cycle starts.

It is concluded that the relative velocity between ice and structure plays an important role during intermittent crushing. At low relative velocities the contact area shows to expand and local pressures increase more simultaneously allowing for a large global load to develop. At high relative velocities the load is mainly carried by several local zones of high pressure as is typical of the crushing process of ice. Unfortunately, the pressure measurements are not detailed enough to draw quantitative conclusions on the maximum local pressures, size of individual interaction zones, and exact increase in contact area.

### 3.3. FREQUENCY LOCK-IN

Frequency lock-in vibrations typically occur over a range of velocities for structures with low damping and low natural frequencies (Engelbrektson, 1983; Huang et al., 2007; Izumiyama et al., 1994; Izumiyama and Uto, 1997; Kärnä and Muhonen, 1990; Määttänen, 1983; Määttänen and Järvinen, 2003; Nordlund et al., 1988; Singh et al., 1990; Sodhi, 1991; Toyama et al., 1983; Yue et al., 2001; Yue and Li, 2003). The vibrations are characterized by periodic oscillation of the structure at a frequency slightly below one of its natural frequencies. Example time dependencies of the global ice load and structural displacement are shown in Figure 3.3. The motion of the structure is close to harmonic with a small deviation close to the time moment of major ice fracture. At this point the ice temporarily prevents the structure from moving back towards its equilibrium position. The global ice load shows a quasi-random, typical for crushing failure of ice, pattern when the relative velocity between ice and structure is high. Also a fast increase in ice load

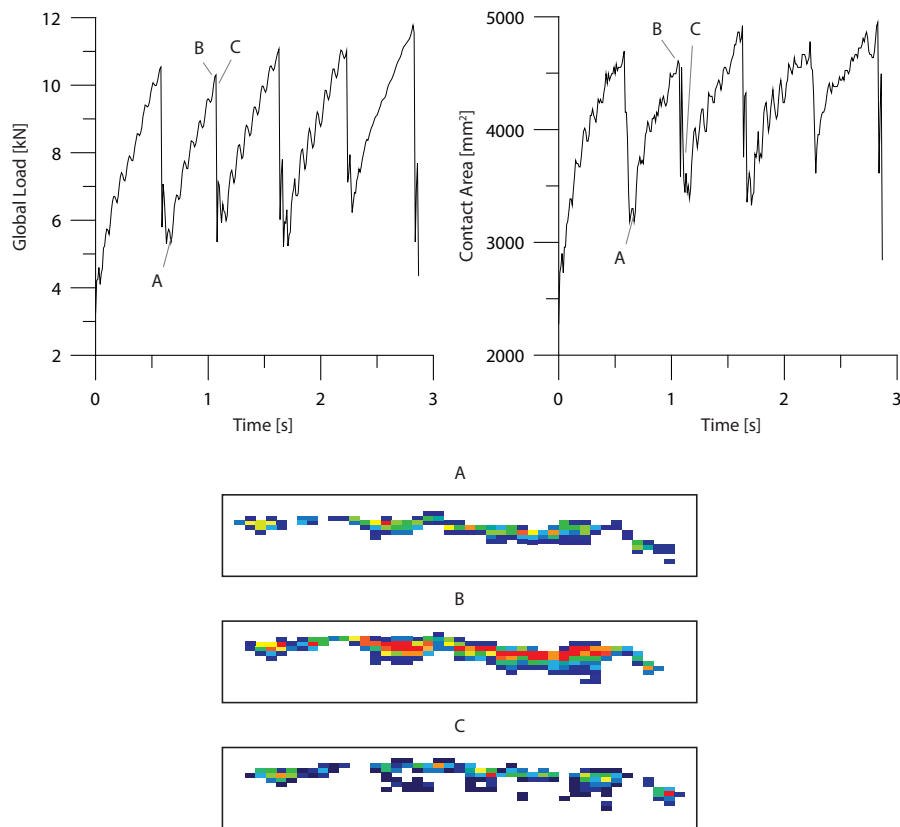


Figure 3.2: Development of the global load and contact area during intermittent crushing in the experiments described in Määttänen et al. (2012). Below the graphs local pressures across the interface at three points during a cycle of intermittent crushing are shown. Blue indicates areas of low pressure and red indicates areas of high pressure.

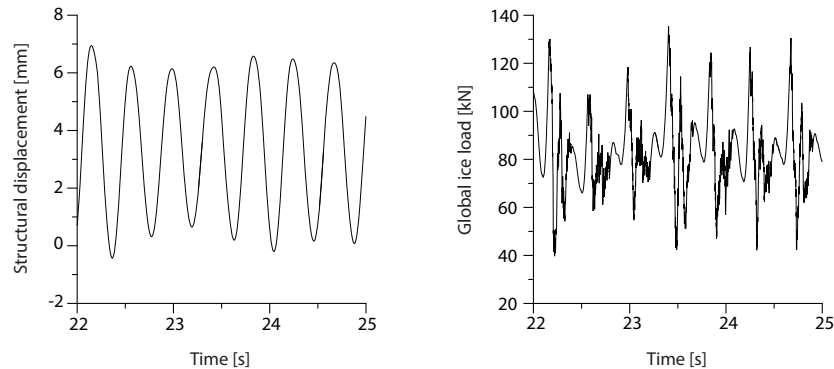


Figure 3.3: Typical (simulated) time traces of structural displacement and global ice load during frequency lock-in.

is observed after a period of time during which the relative velocity is low. Sometimes a brief moment of reduction in ice load is observed to occur when the structure briefly moves faster than the ice causing temporary unloading of the ice edge.

Frequency lock-in has mainly been observed to occur for natural frequencies in the range of 0 to 10 Hz. Some reports exist of frequency lock-in at very high frequencies for structures up to 60 Hz (Määttänen and Järvinen, 2003) and in specific small-scale tests up to 900 Hz (Gagnon, 2011a). The latter report discusses lock-in vibrations which could be explained as synchronization or resonance type vibrations occurring when the frequency of brittle ice fracture comes close to the natural frequency of the structure. Such vibrations are different from frequency lock-in vibrations for which the brittle fracture frequency of ice is significantly higher than the interaction frequency. In order to distinguish frequency lock-in from other types of periodic vibrations the frequency lock-in relation can be used as a guidance. This relation is defined in the next subsection.

### 3.3.1. THE FREQUENCY LOCK-IN RELATION

During frequency lock-in a more or less linear relation exists between the velocity amplitude of the structure and the ice sheet velocity. This relation has first been found by Toyama et al. (1983) during model-scale experiments in the Saroma Lagoon, and has later been confirmed in other experimental campaigns (Huang et al., 2007; Izumiyama et al., 1994; Izumiyama and Uto, 1997; Timco et al., 1992). The experimental results from these campaigns are replotted in Figure 3.4. The relation between the maximum velocity of the structure in the direction of ice drift at the location of ice action to the ice sheet velocity is given by:

$$\dot{u}_{max} = \beta v_{ice} \quad (3.1)$$

The value for  $\beta$  varies between 1.0 and 1.5 for the different experimental campaigns, but is not necessarily limited to that range. The underlying physical mechanism which causes this relation to exist is not clear. The observed trend could indicate an importance

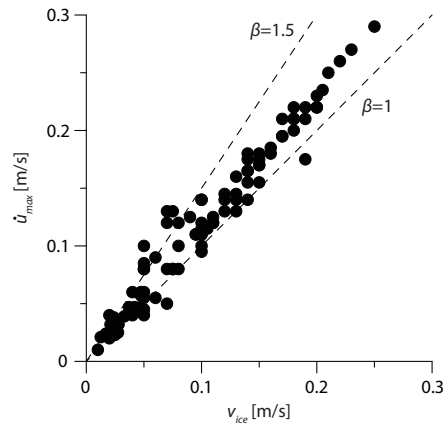


Figure 3.4: Maximum velocity of structural oscillation versus ice sheet velocity during frequency lock-in. Results from several experimental campaigns are plotted (Huang et al., 2007; Izumiyama et al., 1994; Izumiyama and Uto, 1997; Timco et al., 1992; Toyama et al., 1983).

of low relative velocities during interaction. Such low relative velocities occur when the structure moves with the same velocity as the ice. The observed trend can be used to distinguish frequency lock-in measurements from other observations where the oscillations of the structure tend to be close to harmonic, such as vibrations resulting from resonance in the ice-structure system or the response of single-degree-of-freedom structures to an aperiodic excitation.

### 3.3.2. BOUNDARIES OF THE LOCK-IN REGIME

The effects of changes in structural stiffness and mass on the range of velocities over which frequency lock-in occurs have been studied in the experimental campaign by Huang et al. (2007). During this campaign four structures with different properties experienced frequency lock-in vibration in similar ice conditions. The boundaries of the range of velocities where frequency lock-in was observed for each of the structures are shown in Figure 3.5 as well as the structural properties. Damping is not reported upon, but can be assumed to be small as each of the structures experienced frequency lock-in over a large range of velocities.

From Figure 3.5 it can be seen that the boundaries of the frequency lock-in regime shift to lower velocities with increasing stiffness and natural frequency. Furthermore the extend of the range of velocities over which frequency lock-in occurs seems to decrease with increasing stiffness and natural frequency. This conclusion is slightly different from the one made by Huang et al. in their report as they consider the effect to purely result from an increasing stiffness. However, as the mass of the structures was simultaneously varied the observed effect has to be considered in terms of a simultaneous change of two parameters. Unfortunately damping values are not reported upon. It is therefore not possible to draw conclusions on the general applicability of the observed trend.



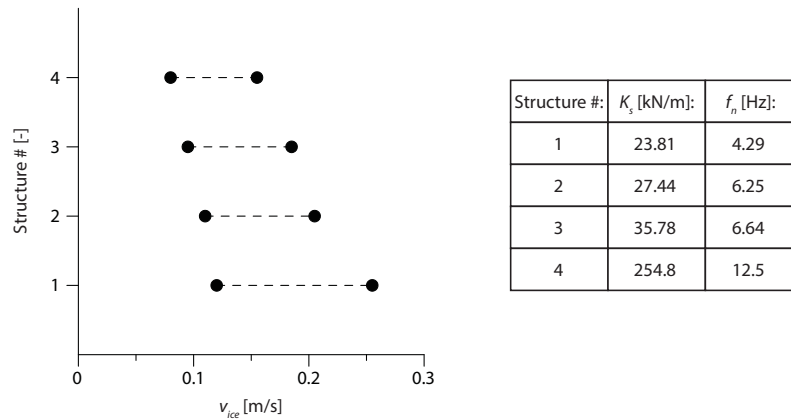


Figure 3.5: Changes in boundaries of the frequency lock-in regime for four different structures in similar ice conditions according to Huang et al. (2007). Structural properties are shown in the table to the right of the graph.

### 3.4. CONTINUOUS BRITTLE CRUSHING

Continuous brittle crushing occurs for all flexible structures at high ice sheet velocities. A typical load and displacement signal are shown in Figure 3.1. The ice load is apparently random and oscillates around a mean value. The mean value is roughly constant in ice conditions which vary little, for example in an ice basin, but does vary with for example varying ice thickness and strength in full-scale. Structural oscillations are typical for a structure excited by an aperiodic load. The amplitude of oscillation of the structure and maximum global ice load are significantly smaller than those observed in the frequency lock-in and intermittent crushing regimes.

The ice deformation and failure during continuous brittle crushing is comparable to the behavior observed on rigid structures at high indentation velocities as treated in Chapter 2. This indicates that during continuous brittle crushing the interaction between ice and structure is insignificant.

### 3.5. CONCLUSION

Three regimes of ice-induced vibrations are distinguished for flexible, vertically sided structures in level ice conditions where the ice fails in crushing. With respect to indentation velocity from low to high values these are intermittent crushing, frequency lock-in, and continuous brittle crushing. Frequency lock-in and intermittent crushing are not always observed depending on the ratio between ice properties and structural properties.

The intermittent crushing regime is defined by saw-tooth structural displacement and global ice load time traces. The frequency of saw-tooth occurrence is dependent on both the structural and ice properties and the structural stiffness is most important in

this regime. During interaction the local contact area and pressure increase as a result of ductile ice behavior when the relative velocity between ice and structure becomes small. This allows for the development of a large global load and large displacement of the structure from its equilibrium. Upon fracture of the ice the structure rebounds resulting in a high relative velocity and lower global load. As soon as the transient oscillations of the structure as a result of the large drop in global load have decayed, the cycle starts over. The ice behavior at different relative velocities during a cycle of interaction is consistent with what is observed during low and high velocity indentation on rigid structures.

Frequency lock-in vibrations can develop for flexible structures with a low natural frequency and low structural damping. The vibrations are characterized by being close to harmonic at a frequency slightly below a natural frequency of the structure. The maximum velocity of the structure in the direction of ice motion has been observed to be between 1.0 and 1.5 times the ice velocity, but is not necessarily limited to this range. For structures with larger stiffness and natural frequency the boundaries of the lock-in regime can shift to lower velocities. During frequency lock-in the ice load is often larger in magnitude during the time the structure and ice move in the same direction as compared to the time during which they move in opposite direction.

Continuous brittle crushing occurs for all flexible structures at high enough ice sheet velocities. The global ice load signal in this regime is aperiodic and ice fractures locally in a brittle manner. The ice behavior is similar to that observed during crushing against rigid structures at high velocities. The structural response is characterized by small-amplitude oscillations around a mean value which is a typical response to an aperiodic excitation.

The regimes of ice-induced vibrations and key characteristics described in this Chapter are further used in the definition of a mechanism governing the development of ice-induced vibrations in Chapter 5. In Chapter 4 results from forced vibration experiments in ice are presented. These results elucidate some of the details of the interaction process between ice and structure when the structure undergoes harmonic oscillation similar to that during frequency lock-in.



# 4

## FORCED VIBRATION EXPERIMENTS IN ICE

### 4.1. INTRODUCTION

A forced vibration experiment is an experiment during which the motion of the structure is controlled kinematically during interaction. Forced vibration experiments are commonly used in offshore engineering for the identification of the added mass and added damping from the fluid load on vibrating submerged bodies. During such experiments rigid bodies (usually cylinders) oscillating with a controlled harmonic motion are pulled through water to study the formation of vortices and the loads on the structure. The obtained load signals are interpreted in terms of added mass and added damping coefficients which give an indication of the energy flow from the water to the structure. An overview of modeling and experiments in the field of fluid-structure interaction containing the general approaches used can be found in Gabbai and Benaroya (2005). Major contributions on forced vibration experiments are those by Sarpkaya (1978) and Gopalkrishnan (1993).

This Chapter covers the results from novel forced vibration experiments in ice which were performed as part of this research. The main aim of these experiments is to study the global and local ice behavior caused by a harmonic motion of an indenter at the ice edge. Harmonic motion of the indenter (structure) closely resembles structural motion in the frequency lock-in regime of ice-induced vibrations as introduced in Chapter 3. Measurements of the local processes in the contact zone for rigid structures and during intermittent crushing have been reported in literature (Sodhi, 2001; Takeuchi et al., 2001; Määttänen et al., 2011), however data in the regime of frequency lock-in is not widely

---

Parts of this chapter have been published in the proceedings of the IAHR International Symposium on Ice, 2012, and in Cold Regions Science and Technology, 2016 (Hendrikse et al., 2012; Hendrikse and Metrikine, 2016a).

available. This is considered to be a result of the current level of understanding of the ice-structure interaction process which has not yet advanced enough to design experiments where frequency lock-in is guaranteed to occur. In a forced vibration setup the motion of the structure can be controlled to be harmonic such that it closely resembles the motion of the structure during frequency lock-in. By application of a tactile sensor at the ice-structure interface the local pressure, contact between ice and structure, and global load are studied.

A secondary goal of the experiments is to obtain an indication of the added mass and added damping during ice-structure interaction. A comparison with added mass and added damping from cylinders oscillating in a fluid can provide some insight in the similarity between frequency lock-in of structures in ice and vortex-induced vibrations of cylinders submerged in water.

## 4

The remainder of this chapter is structured as follows. In Section 4.2 the forced vibration experiments are introduced. A description of the test setup and performed experiments is given. In Section 4.3 observations with respect to global and local ice behavior during the experiments are presented. The results for the added mass and added damping of ice are given in Section 4.4. Section 4.5 summarizes and concludes this chapter.

## 4.2. DESIGN OF THE EXPERIMENT

The experiments were carried out in the Large Ice Tank at the Hamburg Ship Model Basin (HSVA) testing facility in August 2011 as part of the 'Deciphering Ice-Induced Vibrations' (DIIV) test campaign. An overview of the experimental campaign as well as detailed technical drawings of the test setup can be found in Määttänen et al. (2012).

### 4.2.1. EXPERIMENTAL SETUP

The test setup, of which a schematic representation and picture are shown in Figure 4.1, consisted of a rigid beam with a cylindrical indenter with a diameter of 220 mm at the ice level. The beam was equipped with a Tekscan® tactile sensor #5513 at the ice level with a resolution of 0.035 Sensels mm<sup>-2</sup>, a pressure range of 0 to 175 MPa and a sampling frequency of 100 Hz. The sensor was protected from direct ice abrasion by a 0.5 mm thick aluminum foil, and made waterproof by application of silicone sealant. The tactile sensor was used to measure the global load, contact area and local pressure on the structure. The process of calibration of the sensor is described in detail by Metrikin (2011). About one third from the top of the structure the beam was rigidly connected to an EXLAR GSX50 electric linear actuator which controlled the displacement of the structure. Displacements of the structure were measured with two lasers at a sampling frequency of 100 Hz.

All experiments were performed on a single day within a single columnar grained ice sheet which was produced in NaCl-doped water with a salinity of 6.8 ‰ by means of seeding. During the growth process the air temperature in the ice tank was -22 °C. The crystal size of the ice was controlled by scraping the ice from underneath. Air bubbles

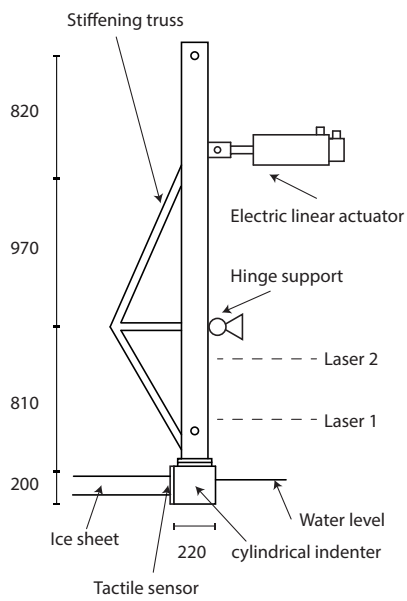


Figure 4.1: Test setup used in forced vibration experiments. The setup consisted of a vertical rigid beam with a cylindrical indenter at the ice level. An electric linear actuator was installed in order to control the motion of the structure. Displacements were measured by two lasers and the contact area, local pressures, and global ice load were measured by a tactile sensor. All measures are in mm.

with 200 – 500  $\mu\text{m}$  diameter were embedded in the growing ice sheet to ensure the brittle behavior of the ice as described in (Evers and Jochmann, 1993). Subsequent to the ice growth process the temperature was raised in order to hit the target ice thickness of 60 mm and target ice properties. During the experiments the temperature of the ice was approximately  $-2\text{ }^\circ\text{C}$ . After the experiments samples of the ice sheet were collected from the sides and middle of the ice sheet at intervals of 10 m along its length for determination of relevant ice sheet properties. Tests on these samples showed an average ice density of  $830\text{ kg m}^{-3}$ , average salinity of 3.3 ‰, and average uniaxial compressive strength of 270 kPa at a strain rate of  $10^{-3}\text{ s}^{-1}$ . At the locations where the samples were taken flexural strength tests were performed which showed an average flexural strength of 150 kPa.

## 4

#### 4.2.2. EXPERIMENTAL PROCEDURE AND TEST MATRIX

The indentation distance of the structure into the ice during a single test is defined as the result of a constant indentation velocity  $v_{ice}$ , which is controlled by the main carriage in the ice basin, the superimposed controlled harmonic motion of the structure, and a deflection of the test structure from the straight equilibrium due to the ice load:

$$u_f(t) = v_{ice}t + A_f \sin \omega_f t + \delta_s(t) \quad (4.1)$$

where  $u_f$  is the displacement of the structure which equals the indentation distance [m],  $t$  is time [s],  $A_f$  is the controlled amplitude of oscillation of the structure [m],  $\omega_f$  is the controlled frequency of oscillation of the structure [ $\text{rad s}^{-1}$ ], and  $\delta_s$  is the structural deflection as a result of ice loading [m].

For an ideal forced vibration test the contribution of  $\delta_s$  should be zero. This requires a rigid structure which is difficult to obtain in a laboratory setting. In case of the experiments considered a small effect of structural deflection can be seen in the measured displacement at the location of laser 1 as illustrated in Figure 4.2. The structural deflection shows to play a role around the time at which the structure changes its direction of motion. It is chosen to neglect the contribution of this structural deflection in the analysis. The high frequency and low amplitude oscillations caused by this structural deflection are considered to be of minor importance for the global interaction behavior presented here. It is noted, however, that for a detailed analysis of individual fracture events during a single cycle of interaction it is necessary to take the contribution of the structural deflection into account.

A total of 51 individual tests were performed in which the amplitude of oscillation of the structure, the indentation velocity, and the frequency of oscillation were varied. The amplitude of oscillation was varied from 11 mm up to 66 mm which corresponds to  $0.05D$  up to  $0.3D$ , with  $D$  the diameter of the cylindrical indenter. The velocity of indentation was chosen to vary from  $0.01\text{ m s}^{-1}$  up to  $0.1\text{ m s}^{-1}$  which contains velocities at which frequency lock-in has been observed in past small-scale free vibration experiments (Huang et al., 2007; Toyama et al., 1983). It is noted however that this range of indentation velocities does not reflect the full range over which the frequency lock-in might occur and is somewhat arbitrary as differences in ice type and ice properties are likely to have a large influence on the range of velocities over which the frequency lock-in can develop.

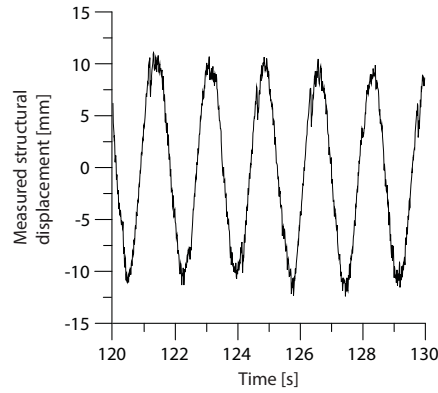


Figure 4.2: Measured structural displacement at the ice action point during a typical forced vibration test.  $v_{ice} = 40 \text{ mm s}^{-1}$ ,  $A_f = 11 \text{ mm}$ ,  $\omega_f = 3.6 \text{ s}^{-1}$ . The displacement signal is obtained at the location of laser 1 (see Figure 4.1) and corrected for the distance to the ice action point.

The frequency of oscillation was chosen based on the requirement that contact between ice and structure should exist at all times during the test. This requirement is met when the relative velocity between ice and structure never becomes negative; which is guaranteed by the following inequality (provided that deflection of the structure is negligible):

$$\omega_f \leq \frac{v_{ice}}{A_f} \quad (4.2)$$

It was chosen to set  $\omega_f$  equal to  $\frac{v_{ice}}{A_f}$  resulting in a zero minimum relative velocity during the tests. This choice was made based on the observation that during frequency lock-in the minimum relative velocity between ice and structure is often close to zero or slightly negative (Toyama et al., 1983).

The overall test matrix is shown in Table 4.1. Combinations marked with an asterisk were tested two or three times. During most of the higher amplitude tests contact was lost around the time of lowest relative velocity. Therefore straightforward comparison of the results of these tests with the results obtained for the lower amplitude experiments is not possible. The tests during which contact was maintained during the entire cycle are shown in bold in Table 4.1. Each test covered an indentation distance of roughly 1 meter to make optimal use of the entire ice sheet.

### 4.3. RESULTS ON GLOBAL AND LOCAL ICE BEHAVIOR

Results of the experiments are presented in three subsections. First the general observations during a typical cycle of forced vibration are introduced. This is followed by an explanation of the observed increase in global load after a period of ductile ice deformation. The third subsection shows the dependence of this increase in global load on the duration of the period of ductile behavior of the ice. Unless stated otherwise, results of



Table 4.1: Test matrix of the forced vibration experiment. Combinations marked with an asterisk were tested two or three times. Tests during which contact was maintained at all times during a cycle of interaction are indicated in bold.

$A_f$ [mm]	11	22	44	66
$v_{ice}$ [mm s <sup>-1</sup> ]	$\omega_f$ [s <sup>-1</sup> ]	$\omega_f$ [s <sup>-1</sup> ]	$\omega_f$ [s <sup>-1</sup> ]	$\omega_f$ [s <sup>-1</sup> ]
10	<b>0.9</b>	-	-	-
20	<b>1.8</b>	0.9	0.45	0.3
30	<b>2.7</b>	1.35	0.68	0.45
40	<b>3.6*</b>	1.8*	0.9*	0.6*
50	<b>4.5*</b>	2.25*	1.13*	0.75*
60	<b>5.4</b>	2.7	1.35	0.9
70	<b>6.3*</b>	3.15*	1.58*	1.05
80	<b>7.2</b>	3.6	1.8	1.2
90	<b>8.1</b>	4.05	2.03	1.35
100	<b>9.0</b>	4.5	2.25	1.5

only those tests are considered in which contact was maintained at all times. Application of the results to the case of frequency lock-in for free vibrating structures is discussed in subsection 4. The obtained tactile sensor measurements were post-processed in order to remove noise and obtain a better view of the dynamic processes at the ice-structure interface. The procedure of post-processing is described in Appendix A.

#### 4.3.1. GENERAL OBSERVATIONS DURING A CYCLE OF FORCED VIBRATION

A typical time trace of the global ice load and the relative velocity between ice and structure during a single forced vibration test are shown in Figure 4.3. The load signal shown in this figure is periodic with the period of forced oscillation of 1.75 s. Each period can be considered to consist of two separate parts. During part of the cycle where the relative velocity is high, namely between the time moments indicated by A and B, the ice behaves in a brittle manner showing uncorrelated local forces resulting in a quasi-random global load pattern. During part of the cycle where the relative velocity is low, i.e. between the time moments indicated by B and C, the ice behaves in a ductile manner showing a higher degree of correlation between local forces resulting in a higher global load level.

The changes in global load during a single cycle of forced vibration are shown in greater detail in Figure 4.4 for two different experiments. The left graph shows a cycle of the experiment presented in Figure 4.3. The right graph shows the results from an experiment with a longer period of oscillation and higher indentation velocity where contact is lost during the time interval at which ductile ice behavior should be observed. Nevertheless the graph clearly illustrates how the ice behavior changes from brittle behavior at a relative velocity of 160 mm s<sup>-1</sup> to transitional behavior at a relative velocity below roughly 60 mm s<sup>-1</sup>. Transitional behavior is defined as the response of ice to loading during which the deformation occurs partly in a visco-elastic or visco-plastic manner, but for which fracture still occurs in a brittle manner in a local contact zone. As the transitional behavior occurs the global load starts to increase with decreasing relative velocity and the time

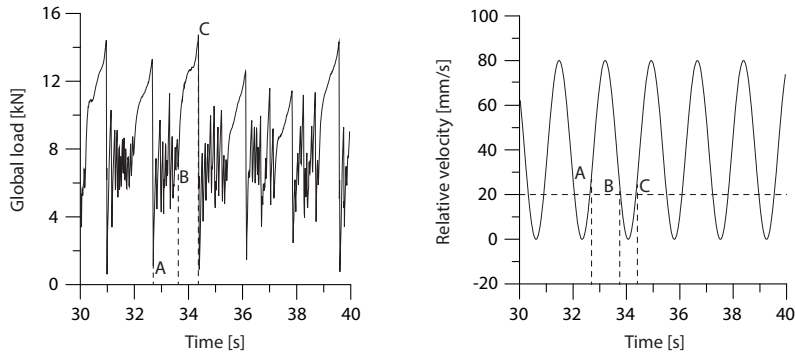


Figure 4.3: Measured global ice load and relative velocity according to Eq. (1) during a typical forced vibration test.  $v_{ice} = 40 \text{ mm s}^{-1}$ ,  $A_f = 11 \text{ mm}$ ,  $\omega_f = 3.6 \text{ s}^{-1}$ . Brittle ice behavior occurs between the time moments indicated by A and B. Ductile ice behavior occurs between the time moments indicated by B and C.

4

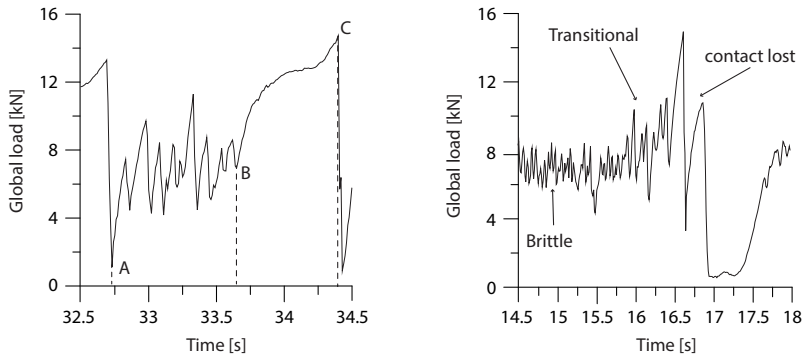


Figure 4.4: Global load during a cycle of forced vibration. Left:  $v_{ice} = 40 \text{ mm s}^{-1}$ ,  $A_f = 11 \text{ mm}$ ,  $\omega_f = 3.6 \text{ s}^{-1}$ . Right:  $v_{ice} = 80 \text{ mm s}^{-1}$ ,  $A_f = 44 \text{ mm}$ ,  $\omega_f = 1.81 \text{ s}^{-1}$ .

between subsequent moments of fracture shows a slight increase as well. The change from brittle to transitional behavior is less apparent in the left graph. The main reason for this is that the higher frequency of oscillation and lower indentation velocity result in a relative velocity which is only for a very short time in the purely brittle regime above  $60 \text{ mm s}^{-1}$ . The behavior between A and B should therefore be considered as transitional behavior.

The brittle and transitional behavior of the ice shown in Figure 4.4 resemble what is observed in experiments dedicated to ice action on rigid structures (Takeuchi et al., 2001). An aperiodic load signal is obtained as long as the relative velocity stays above roughly  $0.06 \text{ m s}^{-1}$ . The mean global load is in the order of  $7 \text{ kN}$  and the maximum global load is on average  $8 \text{ kN}$  in this particular test. The brittle process repeats itself each cycle with roughly the same magnitudes, only the periodicity in the fracture events varies from cycle to cycle. As the relative velocity decreases below roughly  $0.06 \text{ m s}^{-1}$  transitional be-

havior is observed. The load signal remains aperiodic, but the maximum global load increases to about 11.5 kN as the relative velocity and periodicity of ice fracture reduce.

When the relative velocity drops below approximately  $0.02 \text{ m s}^{-1}$  the brittle fracture process stops and the ice starts to deform in a ductile manner. The global load grows during the time the relative velocity stays below the threshold value and reaches peak values between 12 kN and 14 kN. This is roughly a factor 1.75 higher than the average peak load which occurs during brittle crushing at high relative velocities. Fracture of ice occurs when the load-carrying capacity of the ice is reached after sufficient local deformation. The obtained increase in global load is dependent on the time during which the relative velocity remains low enough to maintain ductile behavior of the ice without inducing local fracture.

## 4

### 4.3.2. INCREASE IN GLOBAL LOAD RESULTING FROM AN INCREASE IN CONTACT AREA

The observed increase in global load can be explained in terms of an increase of the contact area between ice and structure and an increase in the mean contact pressure, both as a result of ductile behavior of the ice. The development of the contact area and mean pressure for the experiment shown in Figure 4.3 are shown in Figure 4.5. An increase in the contact area is observed to occur during the interaction phase at which the relative velocity is below  $0.02 \text{ m s}^{-1}$ . This corresponds to ice behavior observed for rigid structures in the ductile regime (Takeuchi et al., 2001). The increase in contact area is on average a factor 1.3 with respect to the maximum contact area when transitional behavior is observed. Additionally an increase in mean contact pressure of about 1.1 is observed. Multiplication of the increase in contact area and the increase in mean contact pressure results in a global load after ductile behavior which is roughly a factor 1.45 larger than the global load during transitional behavior. This corresponds to what is shown in Figure 4.3. The maximum contact area is roughly  $5000 \text{ mm}^2$  which is 25 % of the total area of  $20000 \text{ mm}^2$  defined by the ice thickness and circumference of the cylindrical indenter.

Changes in local pressure contribute to the increased global load after a period of ductile ice behavior. Excerpts of the local pressure distribution at the time moments indicated by A, B, C and D in Figure 4.5 are shown in Figure 4.6. Directly after a major fracture event the contact between ice and structure is local with a few zones of medium pressure (A). At the start of the interval where ductile behavior occurs the contact area has already developed and local hot-spots can be seen (B). Fracture in these hot-spots is delayed though as the overall pressure increases together with the area of contact as a result of ductile ice behavior (C). Comparison of the histogram data of a brittle fracture event (D) and a fracture event after a period of ductile behavior (C) shows clearly the effect of the increase in contact area and mean contact pressure.

The low saturation pressure of 4.5 MPa of the tactile sensor does not allow for a quantification of the maximum local pressure in the ductile and brittle regime. It is expected that the maximum pressure in the high pressure zones which occur when the ice behaves in a brittle manner exceeded the value of 4.5 MPa as well as the maximum value observed after a period of ductile ice behavior. Comparison with earlier experiments by

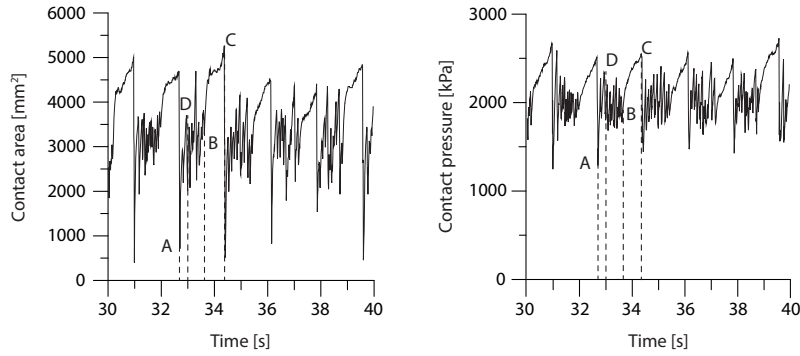


Figure 4.5: Contact area and mean contact pressure during a typical forced vibration experiment.  $v_{ice} = 40 \text{ mm s}^{-1}$ ,  $A_f = 11 \text{ mm}$ ,  $\omega_f = 3.6 \text{ s}^{-1}$ .

4

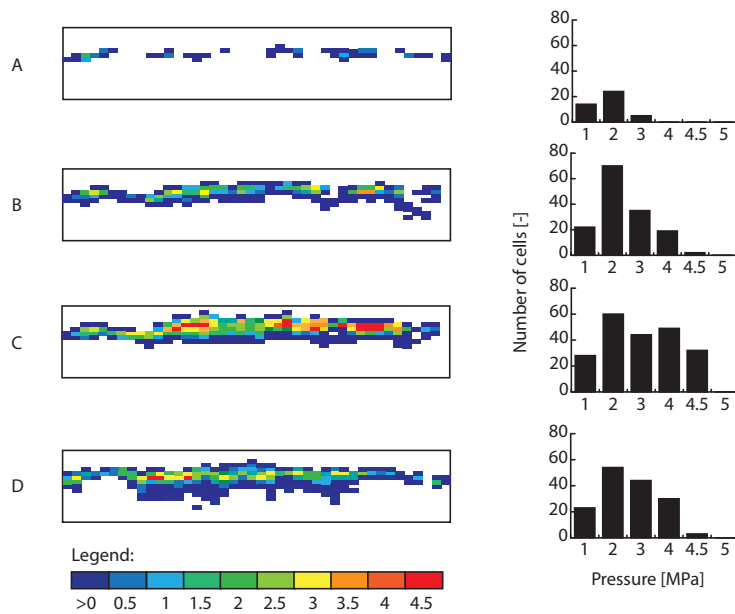


Figure 4.6: Contact area and local pressure at time moments indicated by A, B, C, and D, in Figure 4.5. A – Pressure distribution at the start of a new cycle directly after a large fracture has occurred in the ice. B – Pressure distribution at the start of ductile ice behavior. C – Pressure distribution after a period of ductile ice behavior just before fracture. D – Pressure distribution just before a brittle fracture event. As a result of calibration of the tactile sensor the maximum measured pressure is 4.5 MPa, the true maximum pressure in the high pressure zones in plot D is however likely to exceed this value.

Sodhi (2001) shows that an increase in maximum pressure of about 50% might be expected. Such an increase to 6 MPa in the zones of highest pressure would result in an additional increase of the global load of 7.5%. This amount is relatively small compared to the increase of 45% which can be explained by changes in the contact area and mean contact pressure. Therefore the effect of not capturing the true maximum pressure on the presented results is considered to be small.

#### 4.3.3. DEPENDENCE OF THE INCREASE IN GLOBAL LOAD ON THE DURATION OF DUCTILE ICE BEHAVIOR

The observed increases in contact area and mean pressure during a single cycle of interaction are found to depend on the time period during which the relative velocity is small enough to cause ductile behavior of the ice. The dependence of the maximum contact area, global load, and mean contact pressure on the time period ( $t_{duct}$ ) during which the relative velocity is below  $0.02 \text{ m s}^{-1}$ , the threshold for ductile behavior of ice in this particular test series, is shown in Figure 4.7.  $t_{duct}$  used in the figures is given by:

$$t_{duct} = \frac{1}{\omega_f} \left( 2 \arcsin \left( \frac{0.02}{v_{ice}} \right) + \pi \right) \quad (4.3)$$

The obtained increase in global load, contact area and contact pressure are found to increase with increasing  $t_{duct}$ . In order to reach the roughly maximum contact area of  $6000 \text{ mm}^2$  a minimum time period of 0.6 seconds seems to be required. The value of  $6000 \text{ mm}^2$  corresponds to roughly 30% of the total area which could indicate contact over the full thickness of the wedge front of the ice. The mean contact pressure shows a similar trend. A difference is observed for longer times of ductile behavior. While the increase in contact area seems to level off, the mean contact pressure keeps on increasing at a lower gradient. It is interesting to note that a doubling of the maximum global load observed during crushing at high relative velocities can already be attained within 0.6 seconds as a result of an 75% increase in contact area and a 25% increase in mean pressure.

#### 4.3.4. APPLICATION OF THE RESULTS TO FREQUENCY LOCK-IN

The results presented in the previous three sections are now discussed in light of the frequency lock-in regime of vibrations which can occur for flexible structures interacting with level ice as introduced in Chapter 3. The forced displacement of the structure in the presented experiments closely, but not entirely, resembles the structural displacement observed during frequency lock-in vibrations. During frequency lock-in the structural displacement is not purely harmonic as can for example be seen in Kärnä et al. (1999). Furthermore, a short period of unloading of the ice is often observed during each cycle as the relative velocity between ice and structure becomes negative, i.e. the structure moves away from the ice. In the presented experiments the relative velocity is controlled to never become negative and hence the unloading does not take place. Nevertheless,

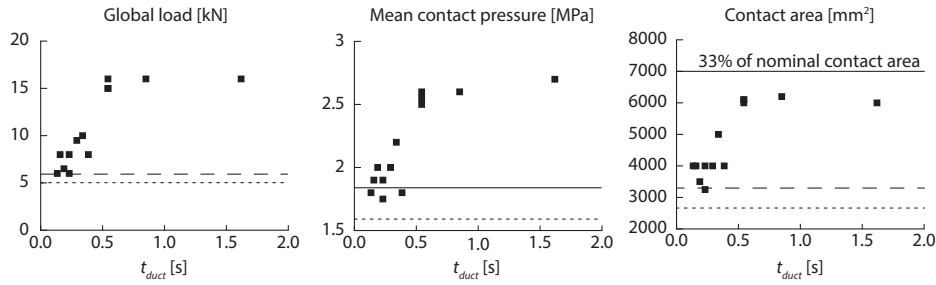


Figure 4.7: Dependence of maximum global load, maximum contact area, and mean contact pressure during a single cycle of interaction (point C in Figure 4.3) on the time period of ductile behavior  $t_{duct}$  (Interval B-C in Figure 4.3). Results are average values for each experiment. Dashed lines indicate the maximum values in the brittle regime and dotted lines indicate mean values in the brittle regime obtained as an average over all experiments.

the obtained results do provide insight in the mechanism causing frequency lock-in vibrations as an increase in global load is observed to occur when the relative velocity between ice and structure is small, and positive.

For sustained frequency lock-in vibrations to occur, it is necessary that the ice provides the structure with an amount of energy that is equal to the energy dissipated by present mechanisms of damping during each cycle. An introduction of energy to the structure can only occur during the time when ice and structure move in the same direction (only in this case ice load and structural velocity at the location of ice loading can be co-directed). The larger the global load during this time, the more energy is introduced. As the maximum global ice load is limited by fracture of the ice, a limit to the energy which can be introduced to the structure exists. As a result of this limit, frequency lock-in is often not observed for structures with relatively high damping.

It is here postulated that the mechanism responsible for the energy flow from ice to structure is the increase in global load as a result of ductile ice behavior in part of the cycle which is observed in the presented results. This point of view corresponds to the classical interpretations by Blenkarn (1970) and Määttänen (1999). They however introduce a dependence of the strength of ice on rate of loading as the source of the increase in global ice load based upon results from small-scale experiments by, for example, Michel and Toussaint (1977). On the basis of the observations presented here it is suggested that the increase in global load is caused by an increase in contact area and mean contact pressure rather than an increase in local ice strength. Nevertheless, the observed trend in the global load remains, irrespective of the chosen theory, and can be considered to be the source of energy during frequency lock-in vibrations.

Provided that the energy introduced by the ice is assumed to be dependent on the increase in global load after a time period of ductile interaction, Equation 4.3, can be used to shed some light on the effects of natural frequency of the structure and ice sheet velocity on the occurrence of frequency lock-in. For a free vibration experiment, in which the displacement of the structure is not controlled,  $\omega_f$  is changed into  $\omega_n$ , being the nat-

ural frequency of the structure. An increase in natural frequency or ice sheet velocity results in a decrease of  $t_{duct}$  and, as can be seen in Figure 4.7, a decrease in maximum global load. A minimum time period exists below which no increase in global load occurs, which in the presented experiments is roughly 0.1 seconds. If it is assumed that frequency lock-in cannot occur for ice velocities below the ductile-to-brittle transition velocity a maximum natural frequency exists above which frequency lock-in can never occur. This could explain why frequency lock-in is almost never observed for natural frequencies above 10 Hz (ISO19906, 2010). It must be noted that the value of 0.1 for the minimum time required for an increase in global load to be observed is typical for the ice used in these experiments and further tests should indicate how this value varies for different types and conditions of ice.

#### 4

Equation 4.3 allows to provide an explanation for the observations by Huang et al. (2007) on the changes in the range of ice sheet velocities for which frequency lock-in occurs when structural properties are varied. From their results it can be seen that for structures with higher natural frequencies the lock-in regime shifts to lower velocities. Based on the results presented here this can be expected as the time during which ductile behavior occurs, which determines the increase in global load, reduces with increasing natural frequency. In other words, the energy the ice can provide to the structure reduces with increasing natural frequency provided that the ice velocity is kept constant. A lower ice velocity results in an increase in energy which compensates for the change in natural frequency.

Based on the results presented here five parameters can be defined which play an important role in determining the possibility for frequency lock-in to occur. The first two, the natural frequency of the structure and ice sheet velocity, have been discussed above. The global ice load level in the brittle regime is the third parameter of importance. It is expected that the increase in global load as a result of ductile ice behavior is proportional to this global load level in the brittle regime. The last two parameters are specific ice properties namely the minimum amount of time required to obtain an increase in global load  $t_{duct,min}$  (0.1 s in this set of experiments) and the relative velocity below which ductile behavior of the ice occurs  $v_{duct}$  (about  $0.02 \text{ m s}^{-1}$  in this set of experiments). These two parameters describe the specific behavior of different ice types and are likely to vary between full-scale and model-scale experiments. Obviously other parameters of importance exist, such as the damping ratio, however it is suggested that the five parameters described here should at least be considered when comparing different observations of frequency lock-in or designing model-scale experiments.

#### 4.4. ADDED MASS AND ADDED DAMPING FROM ICE

The performed experiments resulted in simultaneous measurements of global ice load and structural displacement, which can be used to determine the added mass and added damping of ice in interaction with a harmonically oscillating structure. As a result of several problems which were encountered during and after the experiments steps had to be taken to prepare the results for analysis. These problems and the attempted solutions are discussed in more detail in Appendix B. A method to determine the added mass and

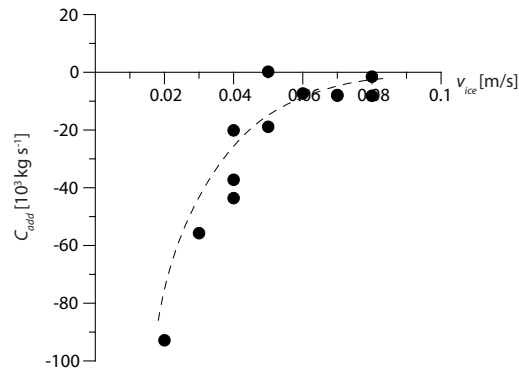


Figure 4.8: Added damping versus indentation velocity for an amplitude of structural oscillation of 11 mm.

added damping is also described there. Although it is impossible to extract quantitatively correct values for the added mass and added damping using the data obtained from the experiments presented here it is considered possible to identify trends for both parameters.

#### 4.4.1. EXPERIMENTAL RESULTS

Results for the added damping from experiments with an amplitude of oscillation of 11 mm are shown in Figure 4.8. The added damping is negative as can be expected in the regime when the ice velocity is equal to the maximum velocity of the structure at the ice level. A trend of increasing added damping values with increasing velocity of indentation can be observed, although there is a large scatter in the results. It is noted here that during the experiments the ratio between  $\omega_f$  and  $v_{ice}$  was kept constant so it is not possible to state whether or not this increase results from the change in velocity, forced vibration frequency, or both. For low velocities the added damping seems to become increasingly negative. For high velocities the value seems to approach zero. The latter would be the expected value for the added damping in case a random load is acting on the structure. This is approximately the case during forced vibration at high velocities and frequencies of oscillation as the duration of the load build-up phase reduces and crushing occurs during most of the cycle. Additional measurements are needed to find the trend in added damping for low velocities around the transition from creep to crushing as well as very high velocities. The observed trend indicates that a larger amount of energy can be transferred from the ice to the structure at lower velocities and natural frequencies in case of a constant  $\frac{v_{ice}}{\omega_n}$  ratio.

Results for the added mass for a constant amplitude of oscillation of 11 mm are shown in Figure 4.9. Values for the added mass are positive at low velocities and become slightly negative at higher velocities. The change takes place around  $40 \text{ mm s}^{-1}$ . Negative added mass values indicate that the structure is perceived as lighter when interacting with the ice. Quantitative values cannot be obtained but, theoretically, a divergence-type insta-



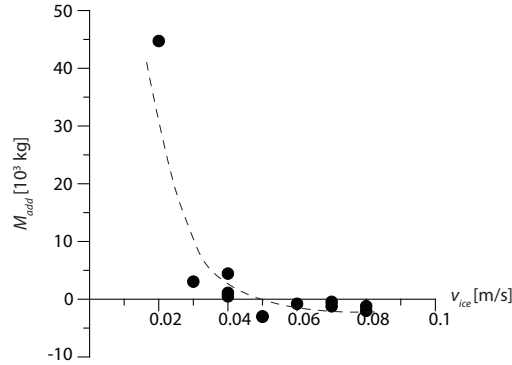


Figure 4.9: Added mass versus indentation velocity for an amplitude of structural oscillation of 11 mm.

4

bility could occur when the negative added mass exceeds the real structural mass. At high velocities the added mass is expected to approach zero as the load signal becomes dominated by crushing. It cannot be excluded that the negative added mass values obtained from these experiments are the result of interaction. At most it can be stated that there is a trend of reducing added mass with increasing indentation velocity.

The presented results indicate a change in the interaction load when changing from low velocities towards high velocities. A possible explanation for this observation could be that for the low velocities the ice behaves more ductile during interaction and as a result more energy can be provided to the structure. This would suggest that the transition boundary from creep to crushing in ice is of importance for the interaction between ice and structures. Unfortunately no experiments were carried out at velocities below  $0.02 \text{ m s}^{-1}$  and for varying frequencies of oscillation at similar velocities of indentation and therefore it is impossible to draw generally applicable conclusions.

#### 4.4.2. COMPARISON WITH FLUID-STRUCTURE INTERACTION

Frequency lock-in which can occur for flexible structures in level ice is sometimes compared to vortex-induced vibrations of cylinders submerged in water (Palmer et al., 2010). The latter problem is a synchronization problem where the frequency of vortex generation synchronizes with one of the natural frequencies of the structure. In the case of ice-induced vibrations a clear global frequency of ice failure is not observed to occur in the brittle regime as shown in Chapter 2. The interaction therefore seems to be different from that during fluid-structure interaction for which periodic vortex shedding is observed on rigid structures as well. It is interesting to compare the observed trends in added damping for ice-structure and fluid-structure interaction, which should show similar characteristics in case the mechanisms are comparable.

In case of fluid-structure interaction the added damping can be determined from:

$$C_{fluid}^{add} = -\frac{1}{2}\rho DLv^2 \frac{1}{A_f \omega_f} \frac{2}{T_f} \int_{t_0}^{t_0+T_f} \tilde{F}(t) \sin(\omega_f t) dt \quad (4.4)$$

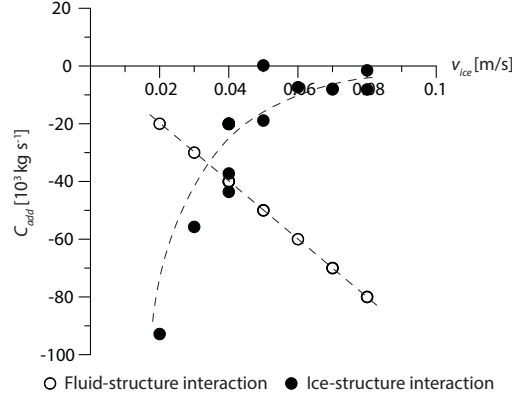


Figure 4.10: Comparison of load in phase with velocity in ice-structure and fluid-structure interaction for an assumed  $A = -1 \times 10^6$  in case of fluid-structure interaction and the experimental results in case of ice-structure interaction.

with  $\rho$  the mass density of water [ $\text{kg m}^{-3}$ ],  $D$  the diameter of the submerged cylinder [m],  $L$  the length of the submerged cylinder [m],  $v$  the fluid flow velocity [ $\text{m s}^{-1}$ ], and  $\tilde{F}(t)$  the non-dimensional fluid force [-]. For a cylinder with fixed dimensions and a constant reduced amplitude  $\frac{A_f}{D}$  and a constant reduced velocity  $\frac{v}{\omega_f D}$  Equation 4.4 can be rewritten into:

$$C_{fluid}^{add} = Av \quad (4.5)$$

where  $A$  is a constant. As quantitative comparison is not possible, an arbitrary negative value:  $A = -1 \times 10^6$ , is chosen here.

In Figure 4.10 the added damping is shown for both ice-structure and fluid-structure interaction for a constant  $\frac{v_{ice}}{\omega_n}$  ratio and constant reduced amplitude. In the case of fluid-structure interaction the trend is quite different from ice-structure interaction. For fluid-structure interaction the added damping becomes increasingly negative with increasing flow velocity. A linear dependence is observed. In case of ice-structure interaction a trend of increasingly negative values with decreasing velocity is observed, most likely due to the nature of the ductile-to-brittle transition as discussed in the previous Section.

Comparing the trends in added damping between ice-structure and fluid-structure interaction it can be concluded that they are not equal, and to some extent are opposite. This suggests that the physical mechanism driving vortex-induced vibrations is different from that driving frequency lock-in. The different trends could explain why for vortex-induced vibrations lock-in is observed to occur at higher flow velocities for structures with higher natural frequencies, while in case of ice-induced vibrations frequency lock-in shows to occur at lower velocities for structures with higher natural frequencies (Huang et al., 2007).

## 4.5. CONCLUSION

Indentation tests were performed with a cylindrical structure subject to a controlled harmonic oscillation. The aim of the tests has been to study ice behavior when loaded at a varying rate of indentation resembling the rate of indentation during frequency lock-in. During the experiments the development of the global load, local pressure and contact area were measured.

Results of the experiments show that ice behavior changes according to the relative velocity between ice and structure. As soon as the relative velocity becomes small enough a change from brittle to transitional or ductile behavior of the ice is observed. Both transitional and ductile behavior result in an increase of the global load which can be explained by an increase in contact area combined with an increase in mean contact pressure. The magnitude of the increase in contact area and mean contact pressure depends on the time period during which the relative velocity between ice and structure is small enough to cause ductile deformation of the ice. The longer the duration, the larger the contact area and mean pressure increase, resulting in a higher global load upon fracture of the ice.

The obtained results indicate a maximum natural frequency to exist above which frequency lock-in cannot occur. This maximum natural frequency varies for different types and conditions of the ice. The results provide an explanation for the fact that the velocities for which frequency lock-in occurs decrease when the natural frequency of the structure is increased. Five parameters of importance with respect to frequency lock-in are defined based on the forced vibration experiments. These are the natural frequency of the structure, ice sheet velocity, mean global ice load in the brittle regime, minimum time period of ductile behavior above which an increase of global load occurs, and the relative velocity below which ductile behavior of the ice starts. It is suggested that these parameters are to be considered when comparing different observations on frequency lock-in or designing model-scale experiments.

Indications of the trends in added mass and added damping of ice in interaction with a harmonically oscillating structure have been obtained. For low velocities the added damping is negative becoming less negative with increasing velocity. A comparison with the trend in added damping for fluid-structure interaction shows that the trends are opposite, indicating that the mechanism causing vortex-induced vibrations to arise is physically different from the mechanism causing frequency lock-in. The added mass in frequency lock-in is positive at low velocities but decreases and becomes negative for higher velocities. At high velocities the added mass is however expected to approach zero and these negative values need further validation.

In the next chapter the results obtained from these experiments, combined with the observations on ice action on rigid structures in Chapter 2 and ice-induced vibrations as described in Chapter 3, are unified in a theory on the basis of which a phenomenological model for the simulation of ice-induced vibrations is developed.

# 5

## PHYSICAL MECHANISM AND DEVELOPED MODEL FOR ICE-INDUCED VIBRATIONS

### 5.1. INTRODUCTION

What physical mechanism can explain the development of ice-induced vibrations and is consistent with observations of ice action on rigid structures as well as observations from forced vibration experiments? The definition of such governing mechanism is required in order to develop models for the prediction of ice-induced vibrations which are applicable over a wide range of ice conditions and for different types of structures. In this Chapter the aim is to define a governing theory which encompasses the experimental and full-scale observations presented in the preceding Chapters.

Several theories exist in literature for explanation of the development of ice-induced vibrations. Traditionally two main schools of thought can be distinguished. The first ascribes ice-induced vibrations to occur as a result of a negative gradient in the dependence of global load on loading velocity (the so-called negative damping). The second defines a characteristic failure length in the ice, which results in ice failure having a distinct frequency for a given velocity of indentation, often referred to as spalling frequency (Gagnon, 2012). When this frequency is close to one of the natural frequencies of the structure resonance or synchronization can occur. What follows is a short discussion of both theories.

The first common approach states that sustained intermittent crushing and frequency lock-in can be explained to occur as a result of negative damping. As mentioned above, this negative damping is merely a result of the decrease of global ice load with increasing

---

Parts of this chapter have been published in International Journal of Solids and Structures (Hendrikse and Metrikine, 2015) and Cold Regions Science and Technology (Hendrikse and Metrikine, 2016b).

ice velocity as introduced in Chapter 2. For edge indentation of ice by rigid structures such dependence of the maximum global ice load on ice velocity has been reported in several studies (Singh et al., 1990; Sodhi and Morris, 1984; Takeuchi et al., 2001). As an explanation for this observation it is often stated that the strength of ice depends on the rate by which it is loaded, referring to the observed negative gradient in the dependence of uniaxial compressive strength of ice on the loading rate in small-scale experiments (Michel and Toussaint, 1977). Models which rely on the dependence of ice strength on loading velocity (Blenkarn, 1970; Huang and Liu, 2009; Kärnä et al., 1999; Määttänen, 1999) directly link the negative gradient in the global load to the negative gradient in compressive strength.

The direct relation between the dependence of ice strength on loading rate and the observed trend in global load is however not fully supported by experimental and full-scale observations (see for details Chapter 2). A negative gradient in the dependence of the compressive strength of ice on loading velocity is not always identified in field observations on warm ice (Schwarz, 1971), whereas frequency lock-in and intermittent crushing are commonly observed during the spring months, when the ice can be considered as warm. From a modeling point of view, the velocity at which the negative gradient occurs has to be changed in order to obtain good predictions for structures with varying degrees of flexibility (Kärnä, 1992; Määttänen, 1999). This effectively results in ice behavior dependent on structural properties. The latter unphysical consequence of the adopted assumptions limits the applicability of the models significantly, and, as a matter of fact, proves that the models do not capture the physics of the phenomenon correctly.

The second common approach is to assume a characteristic failure length in the ice (Gagnon, 2012; Matlock et al., 1969; Palmer et al., 2010; Sodhi, 1995). Evidence for such a characteristic failure length to exist is reported by Gagnon (1999). The occurrence of ice-induced vibrations is either explained as a resonance condition between a periodic load and structure with a distinct natural frequency, or a synchronization between two systems with distinct natural frequencies. As illustrated in detail in Chapter 2, the ice load in the brittle regime has no apparent periodicity on a global scale. On a local scale, the scale of a single zone of high pressure, evidence of such characteristic failure length does exist, which can explain the peaks observed in the spectrum of the global load on a rigid structure at high indentation velocities.

It is often explained that these local failure processes synchronize when a flexible structure is implemented (Palmer and Bjerkas, 2013). This is however not supported by observations on intermittent crushing and frequency lock-in where the ice shows to fail several times during a single cycle of interaction. In case of a synchronized failure there should be only a single failure event per cycle, such as is, for example, the case for vortex-induced vibrations. Additionally, theories based on a characteristic failure length predict that frequency lock-in for structures with a high natural frequency should occur at high ice velocities, compared to structures with a low natural frequency in similar ice conditions. This trend is opposite to that observed in experiments (Huang et al., 2007). The results from forced vibration experiments show that during a cycle of interaction synchronized failure occurs only once after a period of ductile behavior and there is no synchronization with a local brittle fracture frequency.

What can be concluded is that neither of the two above discussed approaches provides a consistent theory for level ice action on vertically sided structures. The developed models based on these theories can mimic the dynamic ice-structure interaction, however their predictions often do not match experimental data over a large range of conditions as pointed out in several earlier studies (Jeong and Baddour, 2010; Muhonen, 1996).

In this Chapter a governing mechanism is introduced in which the changes in the contact area between ice and structure are defined as the source of ice-induced vibrations. The contact area is known to vary between cases where ice is loaded slowly, resulting in ductile deformation and failure behavior, and when ice is loaded at a higher speed, resulting in brittle deformation and failure behavior. Ductile deformation and failure lead to a larger contact area and hence a larger maximum global load on the structure. When flexible structures are subject to level ice, the loading rate varies during interaction which can result in large variations in contact area and thereby an increase in global load during parts of the interaction cycle, the latter being a requirement for sustained ice-induced vibrations to develop.

The remainder of this chapter is structured as follows. In Section 5.2 the governing mechanism is introduced. A phenomenological model which reproduces the main aspects of this mechanism is defined in Section 5.3. Subsections deal with the mathematical description of the model and definition of model parameters. In Section 5.4 the model is applied for simulation of ice action on rigid structures, ice-induced vibrations, and forced vibration in ice in order to demonstrate the consistency of the approach. Steps required for validation and further development of the model are defined in short in Section 5.5. Main conclusions are collected in Section 5.6.

## 5.2. CONTACT AREA VARIATION AS A SOURCE OF ICE-INDUCED VIBRATIONS

In this section a theory is introduced which can explain the main observations for ice action on rigid structures, ice-induced vibrations, and forced vibration experiments. It is stated that it is the variation in contact area between ice and structure, which can develop when the deformation and failure behavior of the ice changes as a result of a changing relative velocity between ice and structure which governs the dynamic ice-structure interaction. First the action of ice on rigid structures is described. Then it is explained how ice-induced vibrations develop when ice interacts with a flexible structure. In the last part the observations from forced vibration experiments are explained in the defined framework. Only the indentation range is considered for which the ice fails either by creep or crushing and global failure by bending or buckling does not occur.

Ice action on rigid structures at low aspect ratios is characterized by a global load and contact area dependence on velocity as illustrated in Figure 5.1. The sketch assumes that the ice edge is tapered by spalling in both the creep and crushing regime. In the creep regime this does not necessarily occur and a contact over the full thickness of the ice can be established. In such case the global load and contact area would be signifi-

cantly higher. In the crushing regime spalling causes a tapered ice edge to form automatically for aspect ratios, the ratio between structure width and ice thickness, above approximately one.

In the creep regime the contact between ice and structure develops over the full width of the structure and thickness of the tapered front of the ice with a more or less uniform pressure. Strain rate hardening of the ice causes the maximum global load to increase with increasing indentation velocity (Ponter et al., 1983). In the crushing regime the contact between ice and structure occurs in specific zones of high pressure on a line roughly in the middle of the ice sheet. Zones of high pressure appear at locations of local contact and disappear upon local fracture of the ice, causing an aperiodic loading pattern to be observed, and forming a rough ice edge. In the crushing regime at high velocities ice deformation is almost purely elastic and the number of high pressure zones in contact with the structure varies around a mean value resulting in a maximum and mean global load more or less independent of indentation velocity (Sodhi and Morris, 1984). For further details with respect to ice action on rigid structures in both regimes the reader is referred to Chapter 2.

## 5

Close to the transition from creep to crushing, marked by the transition velocity  $v_{trans}$ , a transition regime can be defined. In this region the maximum and mean global ice load show a decrease with increasing indentation velocity. The decrease is explained to result from a decrease in maximum and mean contact area in this range as observed in the tests by Takeuchi et al. (2001). Around the transition velocity the deformation process in the ice is not purely elastic yet and ductile deformations of the ice, visco-elastic or visco-plastic deformations, delay failure in local contact zones allowing for a larger contact area to develop, and hence a larger global load to be observed. Ductile deformation is different from creep as it develops at the same time-scale as elastic deformations, whereas creep deformation develops over much longer time intervals. As individual zones do still fail locally the load is aperiodic like at high velocities in the crushing regime. The upper velocity of the transition regime is difficult to define, but can be considered to lie around a velocity where the mean and maximum global load levels off, which indicates that ductile deformation of the ice no longer results in a significant increase in contact area. The change in the contact area between ice and structure as a result of the different deformation components at a time moment of failure is illustrated in Figure 5.1.

In case a flexible structure is placed in the level ice conditions the relative velocity between ice and structure changes during interaction. When the relative velocity becomes small enough such that ductile deformation of the ice can result in an increase of the contact between ice and structure, the global load on a structure can become much higher than when the relative velocity always remains in the range where brittle crushing after almost purely elastic deformation of the ice is observed. Both during intermittent crushing as well as frequency lock-in such increase in contact area develops during part of the cycle causing an increase in global load, which is driving the vibrations. In case of continuous brittle crushing the relative velocity remains too high to cause any increase in contact area, and hence no significant increase in global load is observed. Results from free vibration experiments shown in Chapter 3 illustrate that the contact area be-

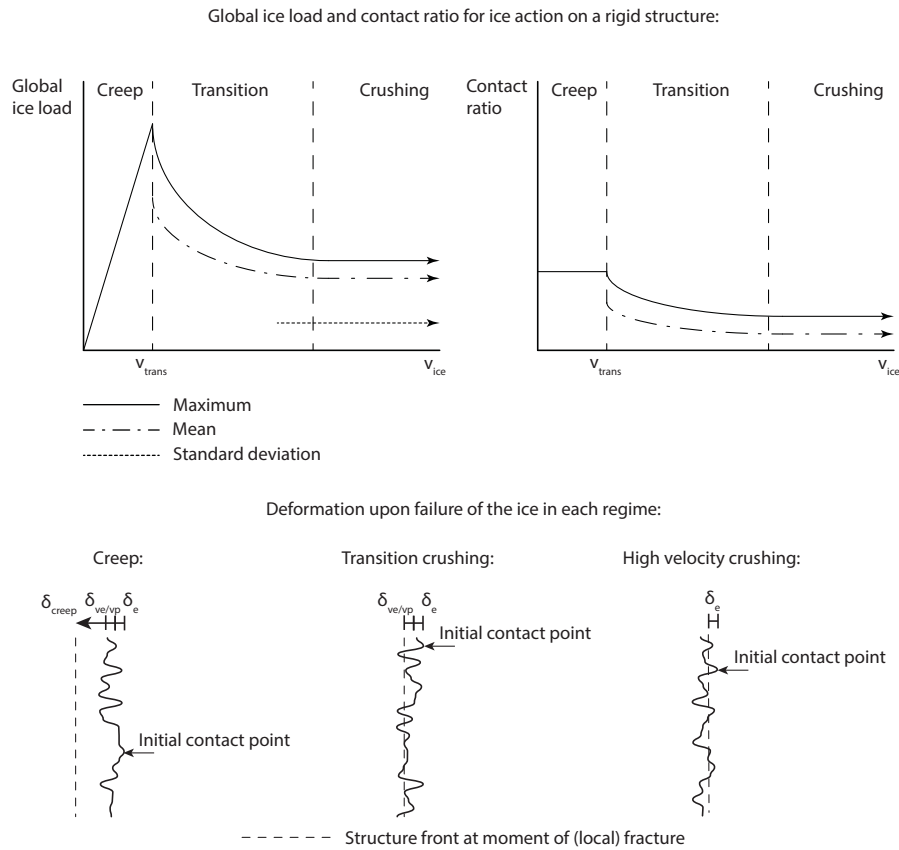


Figure 5.1: Top left: Illustration of maximum, mean, and standard deviation of the global ice load dependence on velocity for ice action on a rigid structure in the creep, transition, and crushing regime based on experimental observations described in detail in Chapter 2. Top right: Illustration of the dependence of the contact area between ice and structure on velocity for ice action on a rigid structure. The contact area reflecting the moment when the maximum global load occurs is shown in the creep regime, the mean contact area is shown in the other regimes. Bottom: Illustration of the deformation and failure processes at different velocities resulting in the changes in contact area at the moment of failure.  $\delta_e$  = elastic deformation,  $\delta_{ve/vp}$  = visco-elastic and visco-plastic (ductile) deformation,  $\delta_{creep}$  = creep deformation.



tween ice and structure increases significantly during the time period where the relative velocity between ice and structure is low during intermittent crushing.

Looking in more detail into the case of frequency lock-in based on the here defined mechanism it is required that during a single cycle of oscillation there must be a time interval in which the relative velocity is low and of which the duration is sufficient for an increase in contact area to develop, resulting in a larger global resistance of the ice. This can explain why frequency lock-in is most commonly observed for structures with low natural frequencies. Indeed, the higher the natural frequency, the less time for such development of the contact area and, therefore, the smaller increase in global load can be achieved. Additionally, it explains why damping has a large effect. As the process is limited by the duration of loading at a low relative velocity, the maximum increase in global load, and therefore the energy input for sustained vibration, is governed by the natural frequency of the structure. Therefore, frequency lock-in can never develop if the structure is capable of dissipating sufficient energy.

## 5

The theory that the contact area governs the interaction process is consistent with the observations from forced vibration experiments shown in Chapter 4. During the forced vibration experiments it has been observed that an increase in global load only occurs when sufficient time is allowed for the development of an increase in contact area at low loading rates. The trend observed in negative added damping shows increasing negative added damping with decreasing velocity and natural frequency. For these cases the time of loading in the range where the contact area can increase, increases significantly compared to high velocity cases with high natural frequencies. Hence the area grows significantly in the former cases resulting in a large increase in global load during part of the cycle when ice and structure move in the same direction, and thereby resulting in negative damping.

The mechanism defined here is based on the difference between creep, ductile and brittle deformation and failure behavior of ice observed for different indentation velocities on rigid structures. These different types of behavior result in a decreasing trend in maximum global load with increasing indentation velocity. This approach shows some similarity to the classical negative damping approach as described in the introduction of this Chapter. The origin of the dependence of the global load on indentation velocity is however fundamentally different from that applied in the existing theories, as here it is ascribed to deformation processes in the ice leading to changes in the contact area, and in the existing theories it is ascribed to the ice strength being velocity dependent. In order to further illustrate that a mechanism based on changes in the contact area between ice and structure can capture the majority of experimental and full-scale observations presented in Chapters 2 to 4 a phenomenological model for the simulation of dynamic ice-structure interaction based on the theory described here is developed and applied for different interaction scenarios in the next Sections.

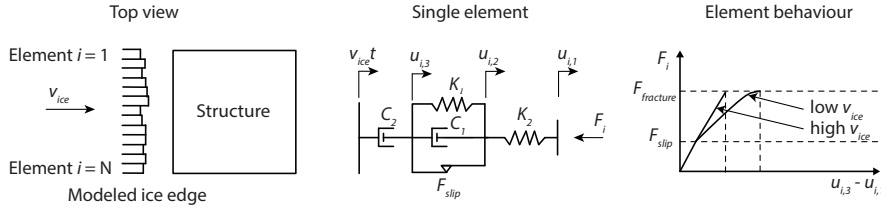


Figure 5.2: Left: Top view of modeled ice edge divided into  $N$  individual elements. Center: Representation of a single ice element in the contact zone. Right: Load – displacement curve of a single ice element for different ice sheet velocities.  $F_{fracture}$  is the load upon which fracture occurs in the front spring element defined by the failure condition in Equation 5.4.

### 5.3. PHENOMENOLOGICAL MODEL OF ICE-STRUCTURE INTERACTION

5

In this section a phenomenological model is introduced which captures and reproduces the main parts of the mechanism introduced in the previous Section. Such model requires to include local contact between ice and structure, elastic deformation of ice, crushing failure, global creep, and visco-elastic or visco-plastic deformation resulting in an increase of contact at low loading rates at least in a simplified manner. The first subsection contains the mathematical model description. The definition of the model input parameters is given in the second subsection.

#### 5.3.1. MODEL DESCRIPTION

In order to take into account a varying contact area the ice sheet is split up in  $N$  zones along the ice-structure interface as shown in Figure 5.2. The elements represent the area of contact between the structure and intact ice, where it is assumed that the load from broken ice pieces in contact with the structure is small and can be neglected. The aim of this approach is not to model the exact contact area variation, but rather to enable the model to capture the main statistical characteristics of this variation (the mean, maximum and standard deviation for different velocities). Each individual zone  $i$  is represented by an element as shown in Figure 5.2. The chosen element represents an elastic-viscoplastic material with strain hardening known as the Bingham element. Elastic deformations of the ice are captured by the front spring element. The spring-dashpot-slider combination takes into account the ductile deformation occurring in the ice at low velocities. The rear dashpot is included to model global creep of ice at very low velocities in a simplified manner.

It is assumed that the total inertia of the ice is sufficiently high such that the ice sheet velocity can be taken to be constant. Under this assumption the environmental driving forces on the ice sheet as well as the loss of mass during the interaction process can be neglected. The equations of motion for a single ice element are then given by:

$$\begin{aligned}
u_{i,1}(t) &= \begin{cases} u_{i,2}(t) & \text{no contact} \\ u_s(t) & \text{contact} \end{cases} \\
\dot{u}_{i,2}(t) &= \begin{cases} v_{ice} & \text{no contact} \\ \frac{K_2}{C_2}(u_s(t) - u_{i,2}(t)) + v_{ice} & \text{contact stick} \\ \left(\frac{K_2}{C_1} + \frac{K_2}{C_2}\right)(u_s(t) - u_{i,2}(t)) + \frac{K_1}{C_1}(u_{i,3}(t) - u_{i,2}(t)) & \\ + v_{ice} + \frac{F_{slip}}{C_1} & \text{contact slip} \end{cases} \quad (5.1) \\
\dot{u}_{i,3}(t) &= \begin{cases} v_{ice} & \text{no contact} \\ \frac{K_2}{C_2}(u_s(t) - u_{i,2}(t)) + v_{ice} & \text{contact} \end{cases}
\end{aligned}$$

where  $u_{i,1}$ ,  $u_{i,2}$ , and  $u_{i,3}$  are displacements of characteristic points of element  $i$  as illustrated in Figure 5.2 [m],  $u_s$  is the displacement of the structure [m],  $v_{ice}$  is the constant velocity of the ice sheet far from the contact zone [ $\text{m s}^{-1}$ ],  $K_2$  is the elastic stiffness of the ice [ $\text{kg s}^{-2}$ ],  $K_1$  is the stiffness of the center spring of the element [ $\text{kg s}^{-2}$ ],  $C_1$  is the damping coefficient of the center dashpot of the element [ $\text{kg s}^{-1}$ ],  $C_2$  is the damping coefficient of the rear dashpot of the element [ $\text{kg s}^{-1}$ ],  $F_{slip}$  is the activation force of the sliding element (maximum force that it can hold at stick) [N], and  $t$  is time [s]. Over-dots represent derivatives with respect to time. Situations of no contact, contact where the sliding element sticks, and contact where the sliding element slides are distinguished. The ice load  $F_i$  a single element exerts on the structure is given by:

$$F_i(t, u_s, \dot{u}_s) = K_2(u_{i,2}(t, u_s, \dot{u}_s) - u_{i,1}(t, u_s, \dot{u}_s)) \quad (5.2)$$

As a representation for the structure a single degree of freedom oscillator is used. This is the simplest way of representing one mode of vibration of a structure which is deemed sufficient to model the fundamentals of the interaction process. The equation of motion for the structure is given by:

$$\begin{aligned}
M_s \ddot{u}_s + C_s \dot{u}_s + K_s u_s &= F_{ice}(t, u_s, \dot{u}_s) \\
F_{ice}(t, u_s, \dot{u}_s) &= \sum_{i=1}^N F_i(t, u_s, \dot{u}_s) \quad (5.3)
\end{aligned}$$

where  $M_s$  is the mass of the structure [kg],  $C_s$  is the structural damping [ $\text{kg s}^{-1}$ ],  $K_s$  is the structural stiffness [ $\text{kg s}^{-2}$ ], and  $F_{ice}$  is the global ice force acting on the structure [N].

Local brittle fracture of ice is set to occur when a critical value of deformation is reached in the elastic spring with stiffness  $K_2$ . The condition for fracture is given by:

$$u_{i,2}(t) - u_{i,1}(t) = \delta_{crit} \quad (5.4)$$

where  $\delta_{crit}$  is the maximum admissible deformation of an element. Upon fracture of the ice the original element is replaced by a new element with the new ice edge position drawn from a uniform distribution  $U(u_s - r_{max}, u_s)$ , where  $r_{max}$  is a value for the maximum offset of an element with respect to the position of the structure [m].

The initial conditions for the structure are given by  $u_s(0)$  and  $\dot{u}_s(0)$ . The initial conditions of the ice sheet are given by the initial position of each element. In order to have the initial apparent roughness of the ice edge comparable to that during interaction, the initial position of the front of each element is compensated for the elastic deformation of the ice and drawn from the distribution  $U(u_s - r_{max} - \delta_{crit}, u_s)$ .

The presented model is capable of describing the ice action on vertically sided structures in the creep, transitional, and brittle regime in a simplified manner. Secondary and tertiary creep effects are not included in the creep behavior. Fracture in each zone is modeled as a simple load drop and the actual physics are not introduced in the model. Only the contact with intact ice capable of carrying a significant pressure is modeled, the extrusion of- and contact with broken ice pieces or rubble is not taken into consideration.

### 5.3.2. DEFINITION OF MODEL INPUT PARAMETERS

The presented model has twelve input parameters of which the three parameters governing the structure behavior  $M_s$ ,  $C_s$ , and  $K_s$  as well as the indentation velocity  $v_{ice}$  are assumed to be clearly defined and known. The remaining eight parameters:  $K_1$ ,  $K_2$ ,  $C_1$ ,  $C_2$ ,  $F_{slip}$ ,  $\delta_{crit}$ ,  $r_{max}$ , and  $N$  define the ice behavior in the model. Currently it is not possible to define these input parameters based on physical ice properties such as for example temperature, salinity, and grain size. A method of defining the input parameters has been developed which relies on existing measurement data, hereafter referred to as reference measurements. Under the assumption that the deformation and fracture behavior of ice does not change significantly with changes in structural properties and ice thickness the model can be used to simulate different interaction scenarios based on the reference ice behavior. The limitation of this approach is that the model can only be applied for ice conditions for which reference measurements are available.

By using reference measurements the model is fixed to predict certain behavior for a specified reference case where ice acts against a rigid structure. This introduces a loop in the approach where the model predicts certain behavior which has been defined as input. However, if based on this implementation of pure ice behavior on rigid structures, the observations on ice-induced vibrations and from forced vibration experiments can be recovered, the model and theory can still be shown to be consistent. The next step in development is to study the definition of the input parameters of the model such that the interaction can be predicted based on measurements of physical ice properties. This step requires significant experimental effort and is not part of the work in this thesis.

The eight input parameters can be defined based on eight reference measurements obtained from a condition where an ice sheet of thickness  $h_{ref}$  acts on a rigid structure of width  $d_{ref}$  with a low aspect ratio such that no buckling occurs. The eight reference measurements are illustrated in Figure 5.3. The value for the transition velocity which marks the transition between global creep and brittle ice behavior  $v_{ref,trans}$  is the first reference value required [ $\text{m s}^{-1}$ ]. Four reference values for the global load are needed to describe the curve shown in Figure 5.3 being the maximum global load at the transition velocity  $F_{ref,max}$ , the mean global load at high indentation velocities  $F_{ref,mean}$ ,

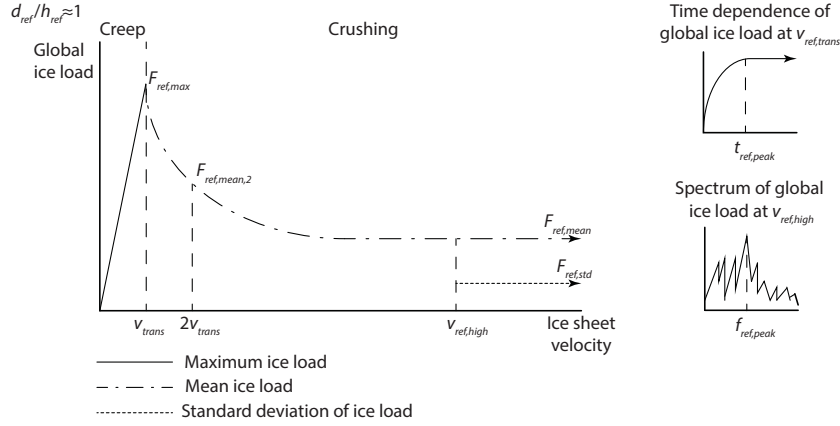


Figure 5.3: Example illustration of input curve used to define the parameters of the creep-crushing elements in the model. The curve should be obtained from measurements with rigid indenters for the specific ice conditions investigated. The horizontal axis is not to scale.

5

the standard deviation of the global load at high indentation velocities  $F_{ref,std}$ , and the mean global load at an indentation velocity twice the transition velocity  $F_{ref,mean,2}$  [N]. Local deformation of the ice is defined based on a reference value for the time moment  $t_{ref,peak}$  at which the global peak load occurs in creep at the transition velocity [s], a value for the peak frequency in the spectrum of the load  $f_{ref,peak}$  [ $s^{-1}$ ] at a high indentation velocity  $v_{ref,high}$  [ $m s^{-1}$ ] in the regime where the ice deformation is almost purely elastic, and a fraction of the critical deformation of the ice up to which the ice behaves purely elastic  $c_{ref}$  [-]. The latter is not shown in Figure 5.3, but links directly to observations on first crack formation in compression of ice as described in Schulson and Duval (2009).

The parameters of the phenomenological model can be chosen such that the model reproduces the exact behavior as defined by the reference measurements and illustrated in Figure 5.3. In order to define the relations between the input parameters and the reference measurements equations for the arithmetic mean and standard deviation of the global ice load from the model, as well as the peak frequency in the spectrum of the global load predicted by the model are defined:

$$\begin{aligned}
 F_{mean}(v_{ice}) &= N \frac{K_2 \int_0^{t_{fail}} u_{i,2} dt}{\frac{0.5r_{max}}{v_{ice}} + t_{fail}} \\
 F_{std}(v_{ice}) &= \sqrt{N \left( \frac{K_2^2 \int_0^{t_{fail}} u_{i,2}^2 dt}{\frac{0.5r_{max}}{v_{ice}} + t_{fail}} - F_{mean}^2(v_{ice}) \right)} \\
 f_{peak}(v_{ice}) &= \frac{0.5r_{max} + \delta_{crit}}{v_{ice}}
 \end{aligned} \tag{5.5}$$

, where  $t_{fail}$  [s] is the time moment at which an individual element fails against a rigid

structure when the ice is moving at a velocity  $v_{ice}$  which can be obtained by solving the differential equation governing the motion of an ice element in the model. The equation for the peak frequency assumes the total deformation of the ice elements to be equal to  $\delta_{crit}$  upon failure, which is an approximation valid only at high ice velocities. By using these three equations and additionally the equation for the maximum ice load in the model:

$$F_{max} = NK_2\delta_{crit} \quad (5.6)$$

, the input parameters  $N, \delta_{crit}, r_{max}, K_2$  can be expressed in terms of reference measurements as:

$$\begin{aligned} \delta_{crit} &= 2 \frac{F_{mean}}{F_{ref,max}} \frac{v_{ref}}{f_{peak}} \\ r_{max} &= \frac{2v_{ref,high}}{f_{ref,peak}} - 2\delta_{crit} \\ N_{ref} &= \frac{\frac{2}{3}F_{ref,max}F_{ref,mean} - F_{ref,mean}^2}{F_{ref,std}^2} \\ K_2 &= \frac{hF_{ref,max}}{h_{ref}N_{ref}\delta_{crit}} \end{aligned} \quad (5.7)$$

, where the approximation is made that at high velocities the deformation  $u_{i,2}(t)$  is given by  $v_{ice}t$ . The value for  $K_2$  is scaled with the ice thickness such that the global load scales linearly with variations in ice thickness in the model based on observations by (Timco, 2007).  $N_{ref}$  is the amount of elements which is needed to reproduce the statistics of the global load for a structure with a reference width  $d_{ref}$ . To incorporate the dependence of global load on structure width the number of elements in the model is defined as:

$$N = \frac{d_s}{d_{ref}} N_{ref} \quad (5.8)$$

This results in a linear dependence of the maximum and mean global load on structure width, and a decrease of the standard deviation as a fraction of the mean load with increasing structure width.

The next two input parameters of the model, the damping coefficient  $C_2$  and coefficient  $c$ , can be directly derived from two additional equations. Global creep of ice occurs below  $v_{ref,trans}$  which in the model is reflected by the condition that no creep-crushing element should fail for indentation velocities below or equal to  $v_{ref,trans}$ . From this requirement the value for the rear damping coefficient  $C_2$  follows as:

$$C_2 = \frac{K_2\delta_{crit}}{v_{ref,trans}} \quad (5.9)$$

In the model it is assumed that the transition velocity does not vary with changes in ice thickness and structure width. Coefficient  $c$  determines the onset of slip in the sliding element which defines the load level up to which the ice behaves elastically in the model [-]. During indentation first cracks and damage start to form at a load level equal to approximately 30% of the failure load (Nakazawa and Sodhi, 1990; Schulson and Duval,

2009) which is considered to be the threshold for the start of the ductile deformation and therefore it is chosen as  $c = c_{ref} = 0.3$ .

The final two input parameters of the model, the spring stiffness  $K_1$  and damping coefficient  $C_1$ , can only be determined by an iterative procedure solving two additional equations to match the remaining two reference measurements  $F_{ref,mean,2}$  and  $t_{ref,peak}$ :

$$F_{ref,mean,2} = N_{ref} \frac{K_2 \int_0^{t_{fail}} u_{i,2}(t, 2v_{ref,trans}) dt}{\frac{0.5r_{max}}{2v_{ref,trans}} + t_{fail}} \quad (5.10)$$

$$t_{ref,peak} = \frac{0.5r_{max}}{v_{trans}} + t_{f1}$$

$$u_{i,2}(t_{f1}, v_{trans}) = f_1 \delta_{crit}$$

The time moment at which the peak load occurs in the model at a velocity  $v_{ref,trans}$  is equal to infinity. An approximation is therefore made setting the time moment of peak load equal to  $f_1 \delta_{crit}$  [m] with  $f_1$  chosen as 0.95.

## 5

#### 5.4. CONSISTENCY OF THE MODEL AND PHYSICAL MECHANISM

Consistency of the defined theory and developed model with respect to experimental and full-scale observations as described in Chapters 2 to 4 is demonstrated in three steps. The first step considers verification of the model capability to describe ice action on a rigid structure in the creep, transition, and crushing regimes and is presented in Section 5.4.1. In the second step in Section 5.4.2. a flexible structure is introduced without changing the description of the ice. This results in intermittent crushing and frequency lock-in to be observed. In the third step in Section 5.4.3. forced vibration experiments are simulated to demonstrate that similar trends in added mass and added damping are recovered with the model as observed in the experiments described in Chapter 4.

For all three consistency checks a single set of ice parameters is used to show that the model and theory capture ice action on vertically sided structures in general without the need of changing any of the ice related parameters. The input parameters are defined in Table 5.1 and based on data from several indentation tests with structures in freshwater ice (Nakazawa and Sodhi, 1990; Sodhi, 1998, 2001) as no single test campaign reported in literature contains all required reference measurements. The transition velocity is chosen based on Nakazawa and Sodhi (1990) who performed low velocity indentation experiments with rigid vertically sided cylinders. The time moment of peak load around the transition velocity is obtained from this report as well, and corrected for the difference between a prepared ice sheet with a flat surface used in the experiments and the initial rough surface used in the model. Values for the brittle mean ice load and standard deviation as well as the peak frequency are obtained from Sodhi (1998) where a relatively stiff structure was used during indentation at high velocities. The maximum global load is estimated based on Sodhi (2001) where it is shown that the maximum global pressure can be about five times the mean brittle pressure during severe intermittent crushing with flexible structures. The mean value of the ice load at a velocity of twice the transition velocity is estimated as three times the mean value at high velocities based on the

Table 5.1: Input parameters for laboratory grown freshwater ice based on values reported in Nakazawa and Sodhi (1990); Sodhi (1998, 2001).

Parameter:	Input value:	Dimension:
$d_{ref}$	0.2	[m]
$h_{ref}$	0.05	[m]
$v_{ref,high}$	0.1	[m s <sup>-1</sup> ]
$f_{ref,peak}$	20	[Hz]
$v_{trans}$	0.001	[m s <sup>-1</sup> ]
$F_{ref,max}$	25000	[N]
$F_{ref,std}$	800	[N]
$F_{ref,mean}$	5000	[N]
$F_{ref,mean,2}$	15000	[N]
$t_{ref,peak}$	60	[s]
$c$	0.3	[-]

observation that the mean contact area increases by roughly this factor (Takeuchi et al., 2001) in medium-scale indentation experiments.

5

#### 5.4.1. ICE ACTION ON A RIGID STRUCTURE

The capability of the model to capture ice action on a rigid structure defined by the reference values in Table 5.1 is verified. Each simulation presented in this section lasted for 50 failure events per ice element. Statistical values are determined considering only the second half of the obtained signals to minimize the influence of initial conditions. Figure 5.4 shows the simulated maximum global load in the creep regime, as well as the maximum, mean, and standard deviation of the global load in the transition and crushing regime. The trends in global load follow those observed for rigid structures in general and, as should be the case, the trend defined by the input data given in Table 5.1. Note that the horizontal axis in Figure 5.4 is a log-scale.

The statistical measures of the contact ratio are shown as well in Figure 5.4. The contact ratio defines the number of elements in contact with the structure and is a measure for the actual contact area in the model:

$$C_r = \frac{N_c}{N} \quad (5.11)$$

where  $N_c$  is the number of elements in contact with the structure at a given time [-]. An estimate of the true contact area is then given by:

$$A_c = C_r d_s \frac{h}{3} \quad (5.12)$$

where the assumption is made that the height of the wedge front of the ice is roughly equal to  $\frac{h}{3}$  and that each individual contact zone covers this height in total.

The mean global load clearly follows the trend in mean contact ratio. The mean global load levels off to the input value of 5 kN for high velocities. The maximum global load



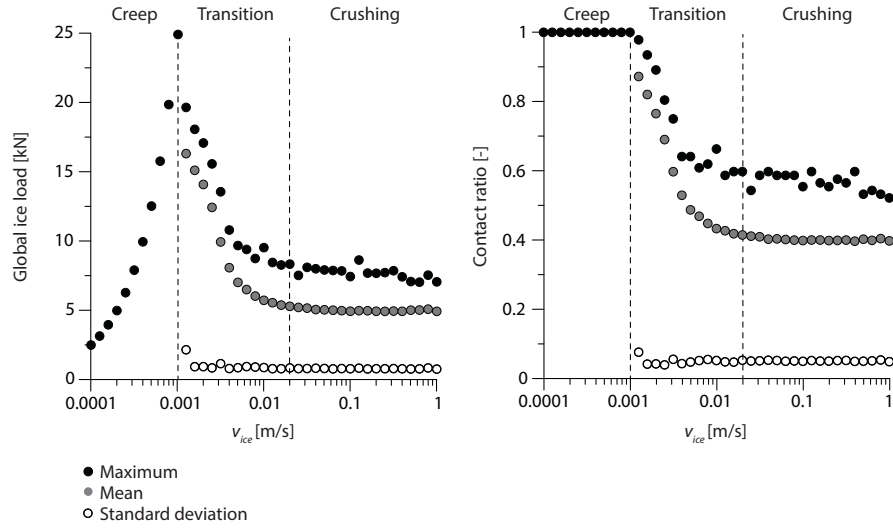


Figure 5.4: Left: Maximum, mean, and standard deviation of the global ice load as a function of ice sheet velocity for simulated ice action on a rigid structure. Right: Maximum, mean, and standard deviation of the contact ratio (Equation 5.11) as a function of ice sheet velocity for the same simulation.

is 25 kN at the transition velocity as defined. The maximum contact ratio is 1 for all simulated velocities in the creep range where full contact develops as expected. In the crushing regime the maximum contact ratio decreases to a value of 0.6 which is about 1.5 times the mean contact ratio and similar to the ratio between maximum global force and mean global force in this range. The standard deviation of the global load is approximately 800 N as defined by the input.

Figure 5.5 shows the time dependencies of the global ice load obtained for velocities equal to  $v_{trans}$  and  $v_{ref,high}$  as well as the amplitude spectrum of the global load at a velocity  $v_{ref,high}$ . The difference between creep and crushing in the model can clearly be seen. In creep the load gradually approaches a peak value as all elements come in contact and are loaded up to their limit. At a time moment  $t_{ref,peak}$  of 60 seconds the load is about 0.95 times the maximum load as defined by the input. In crushing an aperiodic load signal is obtained. The peak frequency in the spectrum is shown to be around 20 Hz which corresponds to the input value defined at  $v_{ref,high}$ .

The obtained results show that the model can describe the main features of ice action on rigid structures. The creep regime, transition regime, and crushing regime are recovered. In the creep regime the maximum global load increases with increasing loading rate. In the transition regime there is a reduction in the mean and maximum global ice load for velocities increasing with respect to the transition velocity reaching a steady value as the crushing regime is entered. This results from a change in contact between ice and structure which occurs as deformations in the center spring-dashpot-slider element are reduced with increasing loading rate. In crushing the load is aperiodic. The magnitudes of global load values match those defined by the reference measurements in Table 5.1.

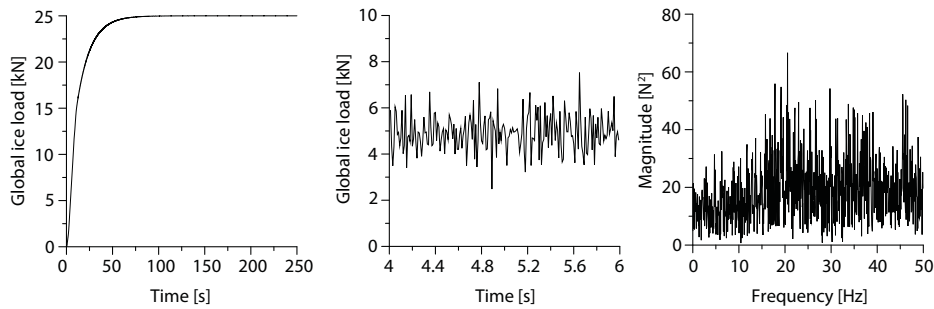


Figure 5.5: Left: Global ice load signal on a rigid structure for an ice velocity of  $0.001 \text{ m s}^{-1}$  ( $v_{trans}$ ). Middle: Global ice load signal on a rigid structure for an ice velocity of  $0.1 \text{ m s}^{-1}$  ( $v_{ref}$ ). Right: The spectrum of the global load at a velocity of  $0.1 \text{ m s}^{-1}$  showing a peak around 20 Hz.

### 5.4.2. ICE-INDUCED VIBRATIONS

An arbitrary flexible structure is introduced in the model with a width of 0.2 m, low damping characterized by  $\zeta = 0.01$ , a natural frequency of 2 Hz, and a low stiffness  $K_s = 25 \times 10^5 \text{ kg s}^{-2}$  such that its deflection under the maximum global ice load is in the same order of magnitude as the deformation of the ice. Simulations with such flexible structure demonstrate how ice-induced vibrations can develop. Properties of the ice are unchanged with respect to the rigid case described in the previous Section and defined by the reference values given in Table 5.1. Each simulation presented in this Section lasted for at least 80 cycles of structural oscillation or 50 failure events per ice element whichever greater. Statistical values are determined considering only the second half of the obtained signals to minimize the influence of initial conditions.

The general trends for the statistical measures of the global load and contact area in the different regimes of interaction are shown in Figure 5.6. Intermittent crushing and frequency lock-in develop over a range of velocities as indicated. Comparing Figure 5.6 with Figure 5.4 for a rigid structure the influence of the flexibility of the structure on the obtained results can be seen. In the intermittent crushing regime the maximum, mean, and standard deviation of the global load as well as the mean and standard deviation of the contact area are larger as a result of interaction. Frequency lock-in does not show a significant change in contact area and global load compared to the rigid scenario at similar velocities. Some slight increase in maximum and mean global load seems to occur, which can be explained to result from the time moments where the global load increases due to interaction. During continuous brittle crushing the statistical measures for the flexible structure are the same as for the rigid structure as no significant interaction between ice and structure is taking place. Detailed results for each of the regimes of ice-induced vibrations are presented next.

#### INTERMITTENT CRUSHING

In Figure 5.7 the simulated global ice load and structural displacement signal are shown for a velocity of  $0.005 \text{ m s}^{-1}$  at which intermittent crushing occurs. A characteristic saw-

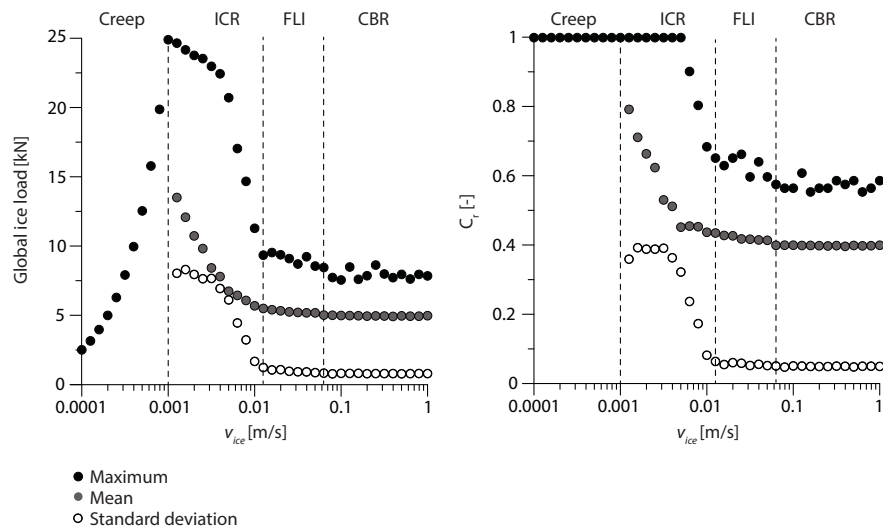


Figure 5.6: Left: Maximum, mean, and standard deviation of the global ice load as a function of ice sheet velocity for simulated ice-structure interaction. Right: Maximum, mean, and standard deviation of the contact ratio (Equation 5.11) as a function of ice sheet velocity. ICR = Intermittent crushing, FLI = Frequency lock-in, CBR = Continuous brittle crushing.

tooth global load and displacement signal are obtained with a saw-tooth frequency lower than the natural frequency of the structure. The development of the contact ratio and relative velocity between ice and structure are shown in Figure 5.7 as well. During the load build-up phase the contact area gradually increases as the relative velocity between ice and structure becomes small. As soon as a single element fails after almost full contact has been reached a cascade of failure is triggered over the entire width of the structure. This causes a significant reduction in contact area and an increase in relative velocity as the structure starts to move towards the ice. Once the transient structural oscillation as a result of the large load drop has decayed sufficiently such that the relative velocity becomes small again the contact area starts to grow and the whole process repeats itself. In this particular example with a very flexible structure, moments of loss of contact can be observed, these do not necessarily occur for structures with a larger stiffness or mass.

Figure 5.8 shows the dominant frequency in the spectrum of the global ice load and structural displacement in the intermittent crushing regime. As a result of the interaction the dominant frequency is the same for both the structural displacement and global ice load in this regime. A trend of linear increase in frequency with velocity can be observed for the lower velocities, where full-contact is approximately obtained as shown in Figure 5.6. When the transition towards frequency lock-in is made the increase in frequency deviates from the linear trend. In this range the saw-tooth behavior becomes less apparent from the time dependencies of global ice load and structural displacement.

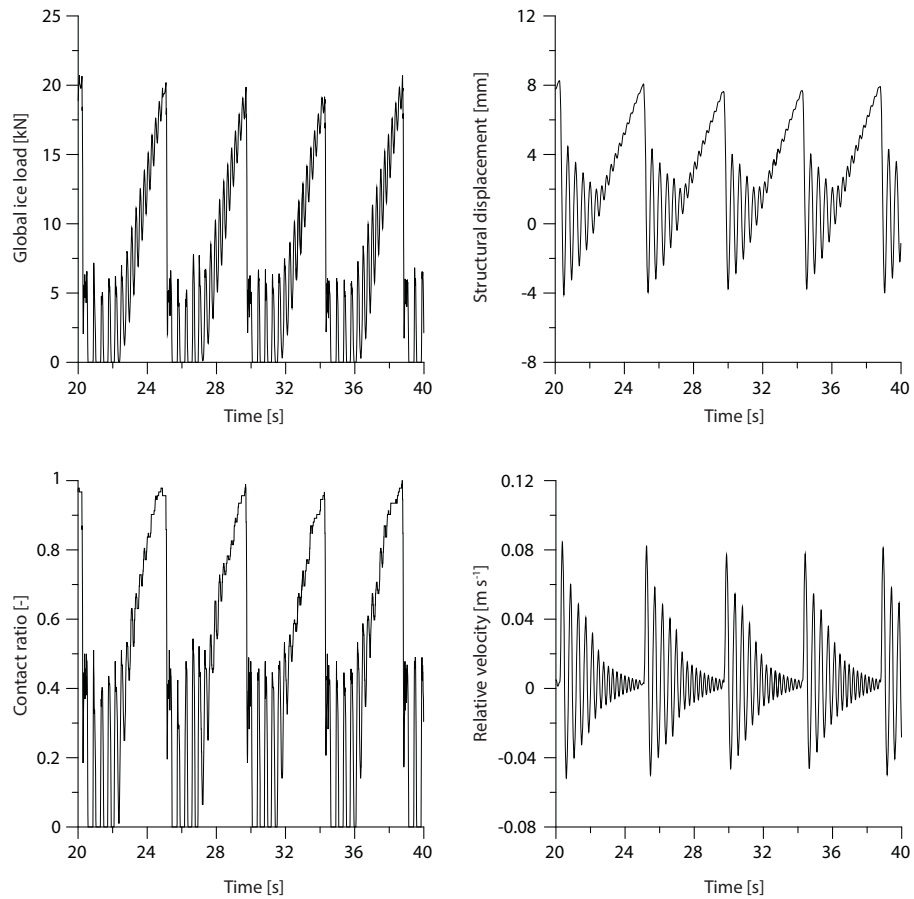


Figure 5.7: Top: Obtained time traces for the global ice load and structural displacement in the intermittent crushing regime for an ice velocity of  $0.005 \text{ m s}^{-1}$ . Bottom: Time dependencies of contact ratio and relative velocity for the same simulation.

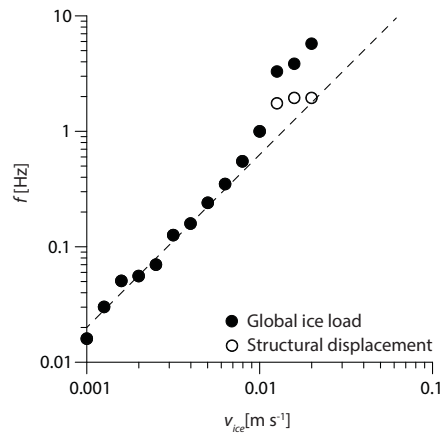


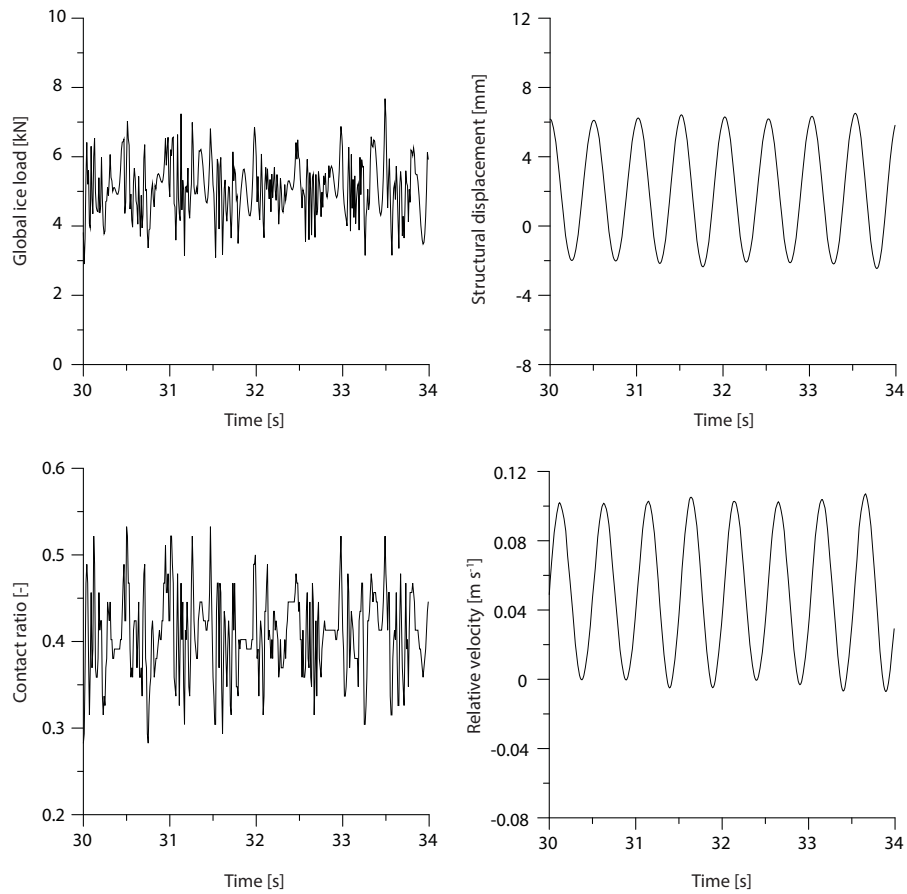
Figure 5.8: Frequency in spectrum of the global ice load and structural displacement with the most energy associated to it as a function of velocity. The trend illustrates the almost linear increase of frequency of saw-tooth oscillation with velocity during intermittent crushing.

5

#### FREQUENCY LOCK-IN

An example of the obtained displacement and load signal during frequency lock-in at an ice velocity of  $0.05 \text{ m s}^{-1}$  is shown in Figure 5.9. The contact area development and relative velocity between ice and structure are shown as well. The structural displacement is nearly sinusoidal at a frequency close to the natural frequency of 2 Hz. The global ice load signal shows periods of crushing followed by periods of load build-up towards a peak value. Peak loads occur synchronized with the structural motion around the time moment the structure starts to move back towards the ice. During the time period of low relative velocity between ice and structure, the contact area is generally larger compared to the periods of high relative velocity, and shows to either grow or stay constant allowing for the high peak loads to develop. For sustained frequency lock-in to develop it is not necessary that full synchronization, or contact over the entire width of the structure develops. During the periods of negative relative velocity between ice and structure the ice is unloaded as can be observed in the global load signal.

One key experimental observation is that during frequency lock-in an almost linear relation between the maximum structural velocity and ice sheet velocity exists (Toyama et al., 1983). A similar trend is observed in the results from the model as shown in Figure 5.10. The value for  $\beta$  is obtained as the average value over 10 cycles of lock-in vibration as the value shows some variation from cycle to cycle. The value for  $\beta$  lies between 1.0 and 1.5 for these simulations and varies for different velocities. The larger the value for  $\beta$  the longer the time of unloading of the ice as the relative velocity becomes more negative. This results in less energy transferred from the ice to the structure. A value of  $\beta$  much smaller than one would indicate that the relative velocity between ice and structure stays large and positive all the time. In such case the processes driving the increase in contact area cannot take place. The actual value for  $\beta$  is expected to be such that the



5

Figure 5.9: Top: Obtained time traces for the global ice load and structural displacement in the frequency lock-in regime for an ice velocity of  $0.05 \text{ m s}^{-1}$ . Bottom: Time dependencies of contact ratio and relative velocity for the same simulation.

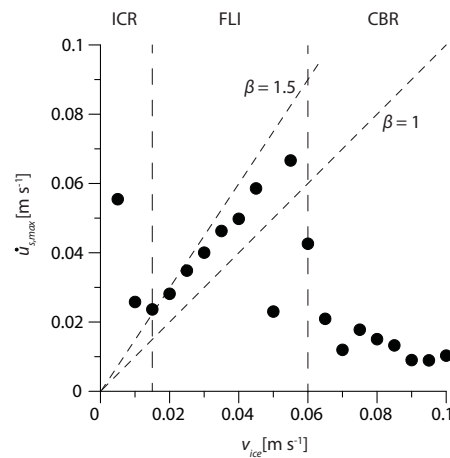


Figure 5.10: Obtained maximum structural velocity plotted against ice sheet velocity in the frequency lock-in regime. ICR = Intermittent crushing, FLI = Frequency lock-in, CBR = Continuous brittle crushing.

5

energy introduced by the ice per cycle of oscillation equals the energy dissipated by the damping mechanisms. Variations per cycle then occur to balance out the randomness of the process.

Another key observation is that the frequency of oscillation of the structure often is equal or lies slightly below the natural frequency of the structure not in contact with ice during frequency lock-in. Figure 5.11 shows the frequency of the response of the structure containing the largest amount of energy as a function of ice sheet velocity. For the simulations in the lock-in regime at low velocities the frequency is indeed slightly below the natural frequency, but for the simulations at higher velocities it is equal to the natural frequency. The reduction is mainly caused by the ice resisting the motion of the structure at the time when the structure turns to move towards the ice. The longer this resistance, the lower the observed frequency of oscillation. This resistance time shows to decrease for larger ice sheet velocities in the model.

#### CONTINUOUS BRITTLE CRUSHING

At ice sheet velocities above approximately  $0.06 \text{ m s}^{-1}$  the interaction regime is continuous brittle crushing. An example of the obtained displacement and load signal for continuous brittle crushing at a velocity of  $0.15 \text{ m s}^{-1}$  is shown in Figure 5.12. In this regime the dependence of global ice load on time shows no apparent periodicity and the response of the structure is characterized by small oscillations around an equilibrium position. As the relative velocity stays at a high value all the time the contact ratio changes around a mean value but does not show any significant build-up over a long period of time.

The obtained results for each individual regime of ice-induced vibrations presented in the previous Subsections show that the model predictions are consistent with experi-

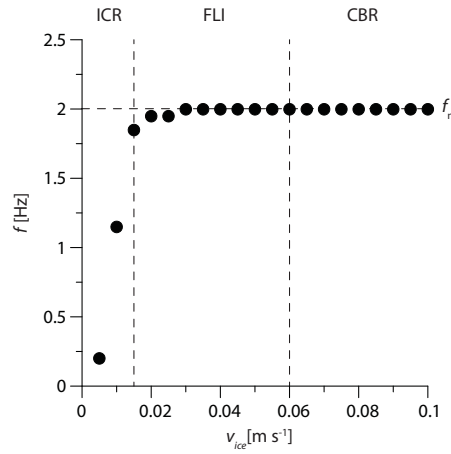


Figure 5.11: Frequency of structural response plotted against the ice sheet velocity. The natural frequency of the structure of 2 Hz is indicated. ICR = Intermittent crushing, FLI = Frequency lock-in, CBR = Continuous brittle crushing.

mental and full-scale observations on ice-induced vibrations. When a flexible structure with low damping is introduced in the simulated ice conditions all three regimes of ice-induced vibrations are recovered. Within the frequency lock-in regime the trends with respect to maximum structure velocity and frequency of oscillation as presented in Chapter 3 are recovered. The simulation results illustrate how ice-induced vibrations can develop as a result of changes in the contact area between ice and structure. In the next subsection a short study into the effect of changes in structural properties on the predictions is given with the focus on the frequency lock-in regime.

#### EFFECT OF CHANGES IN STRUCTURAL PROPERTIES ON PREDICTIONS

Changes in structural properties result in a change of the interaction process and development of ice-induced vibrations. For example for rigid structures, structures with relatively high stiffness and mass, only continuous brittle crushing is observed. In order to develop some basic insight on the effects of changes in structural properties on the interaction process these are discussed here treating the natural frequency, mass, and damping ratio separately on the basis of the following simplified equation:

$$\ddot{u}_s + 2\zeta\omega_n\dot{u}_s + \omega_n^2 u_s = \frac{F_{ice}(t, u_s, \dot{u}_s)}{M_s} \quad (5.13)$$

Only the range where frequency lock-in vibrations occur is considered here, where the effect of changes in the three structural parameters is illustrated on the basis of plots of maximum structural velocity versus ice sheet velocity from which the frequency lock-in range can straightforwardly be deduced. In continuous brittle crushing changes in structural properties result in different structural behavior, but considering that no interaction between ice and structure takes place the effect of changes in structural prop-



5

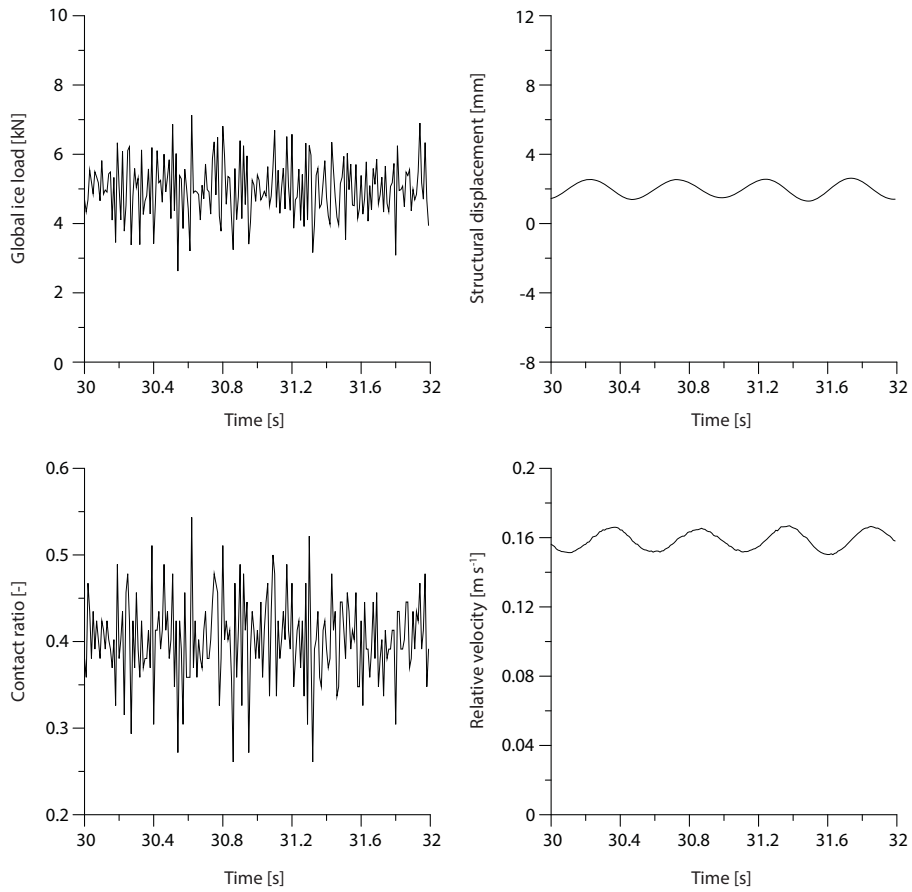


Figure 5.12: Top: Obtained time traces for the global ice load and structural displacement in the continuous brittle crushing regime for an ice velocity of  $0.15 \text{ m s}^{-1}$ . Bottom: Time dependencies of contact ratio and relative velocity for the same simulation.

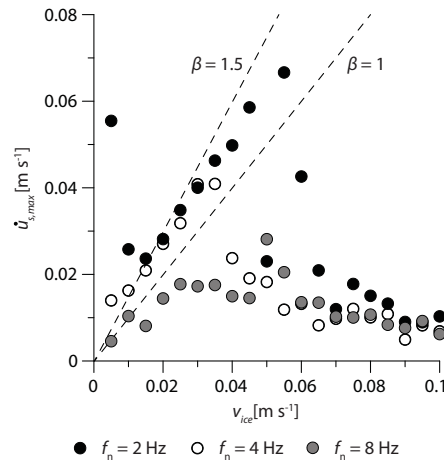


Figure 5.13: Effect of changes in natural frequency as a result of a change in structural stiffness on the range of velocities for which frequency lock-in develops.

erties are straightforward. In the intermittent crushing regime the interaction is in general quasi-static where an increase in stiffness of the structure results in a decrease in the saw-tooth frequency and decrease of the peak displacement of the structure.

A change in natural frequency can be made by changing either the stiffness of the structure or the mass of the structure. From Equation 5.13 it can be seen that these changes have a different effect. Changing the stiffness only changes the coefficients on the left hand side of the equation, while changing the mass additionally changes the right hand side of the equation. Therefore different effects can be expected. Effects of changes in the natural frequency by varying the stiffness of the structure while keeping the mass and damping ratio constant are shown in Figure 5.13. The natural frequency is varied from 2 Hz to 4 Hz and 8 Hz. The increase in natural frequency from 2 Hz to 4 Hz by changing the structural stiffness causes the lock-in range to shift to lower velocities. At higher frequencies there is less time for an increase in contact area to develop and hence less energy is obtained from the ice at similar velocities. For the natural frequency of 8 Hz the lock-in range is almost fully lost as shown by the maximum structural velocity which does not come close to the ice velocity any longer except for a velocity of  $0.01 \text{ m s}^{-1}$ . The latter structure could be qualified as a rigid structure.

Changes in the natural frequency as a result of a change in the mass of the structure are shown in Figure 5.14. The result is an opposite shift of the lock-in range. This is explained by Equation 5.13 from which the right hand side increases with decreasing mass. When the global ice load pattern does not change this results in easier vibration of the structure. In the examples presented here the increase in natural frequency is outbalanced by the decrease in structural mass and the lock-in range shifts to higher velocities.

It is concluded that it is not straightforward to predict what effect a change in natural

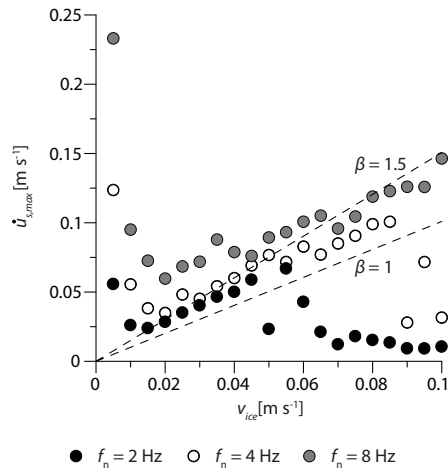


Figure 5.14: Effect of changes in natural frequency as a result of a change in structural mass on the range of velocities for which frequency lock-in develops.

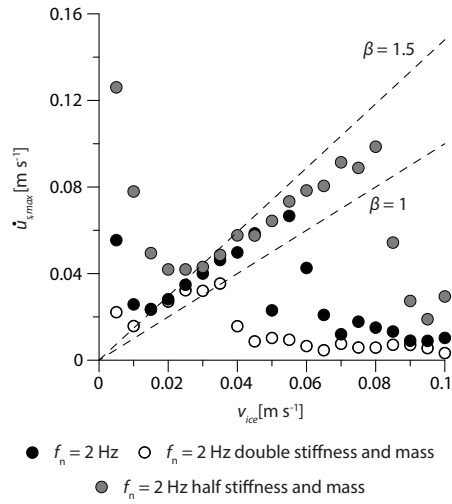
5

frequency will have on the interaction, as it matters how this change is obtained, either by changing the mass, its stiffness or a combination of both. Nevertheless, the observation by Huang et al. (2007) that for increasing stiffness the lock-in range shifts to lower ice sheet velocities is recovered in the model.

The effect of changes in structural mass keeping the damping ratio and natural frequency unchanged are shown in Figure 5.15. It is noted that an unchanged natural frequency can only be obtained by simultaneously changing the structural stiffness with the mass. It is seen that for the stiffer and heavier structures the lock-in range shifts to lower velocities. Simultaneously the maximum velocity in intermittent crushing reduces as well. Further increasing the stiffness and mass of the structures will result in the recovery of ice action on a rigid structure.

The effect of changes in the damping ratio keeping the natural frequency and structure mass constant are shown in Figure 5.16. More damping reduces the range of velocities for which frequency lock-in develops, the effect being more pronounced for the upper boundary than the lower boundary.

The results presented here provide an indication of the effect changes in structural properties have on the interaction. In general the ratio between structural and ice properties governs the interaction process and therefore changes in ice properties will yield different effects than changes in structural properties. For the moment these can be assessed only through simulation. Another aspect to consider are the initial conditions of the structure. In the simulations presented in this thesis the structure is assumed at rest at the start of the simulation. For relatively stiff structures frequency lock-in might not develop from the stable position, but do persist after a significant push out of the equilibrium position when damping and mass are low. An example of such case is shown in Chapter 7 in relation to the practical application of the model.



5

Figure 5.15: Effect of changes in structural mass and stiffness with unchanged natural frequency on the range of velocities for which frequency lock-in develops.

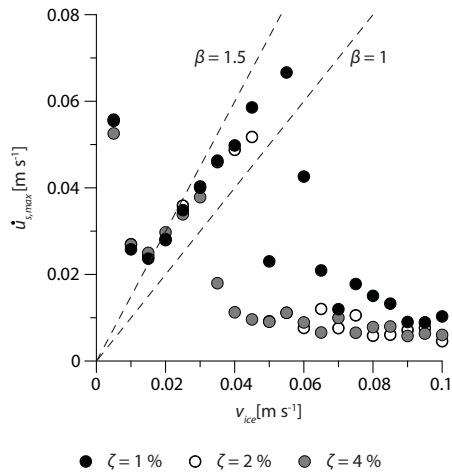


Figure 5.16: Effect of changes in damping ratio on the range of velocities for which frequency lock-in develops.

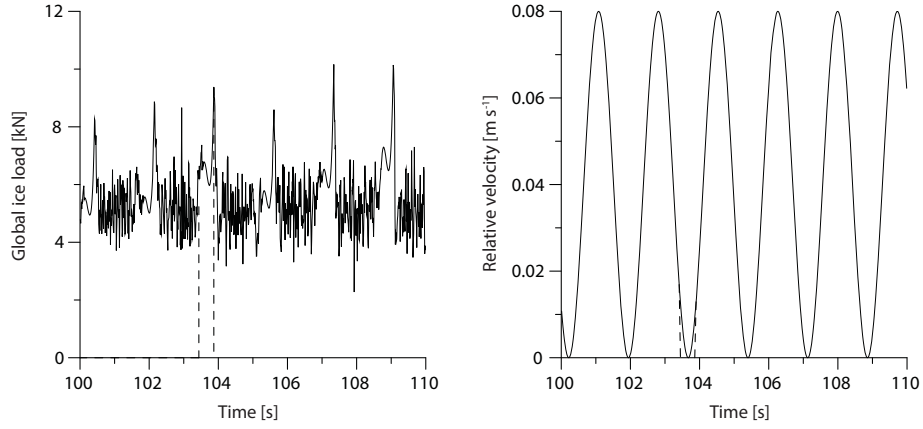


Figure 5.17: Simulated global load and relative velocity for a forced vibration experiment.  $v_{ice} = 40 \text{ mm s}^{-1}$ ,  $A_f = 11 \text{ mm}$ ,  $\omega_f = 3.6 \text{ s}^{-1}$ . Characteristics of the process are comparable to those observed in experiments in Figure 4.3.

5

### 5.4.3. FORCED VIBRATION

Forced vibration experiments are simulated with the model to check if trends in added mass and added damping as obtained from experiments and presented in Chapter 4 can be recovered. To this end a structure with a width of 0.2 m subject to a controlled harmonic oscillation defined by:

$$u_f(t) = v_{ice}t + 0.011 \sin(\omega_f t) \quad (5.14)$$

with:

$$\omega_f = \frac{v_{ice}}{0.011} \quad (5.15)$$

is simulated in the ice conditions defined by the reference values given in Table 5.1. Each simulation presented in this section is ran for at least 200 cycles of structural oscillation. Statistical values are determined considering only the second half of the obtained results to minimize the influence of initial conditions.

In Figure 5.17 the simulated time dependence of the global ice load during a cycle of forced vibration is shown for a velocity of  $40 \text{ mm s}^{-1}$ . The result can be compared to Figure 4.3. During the time when the relative velocity between ice and structure is low an increase in global load is obtained as in the experiments. A difference though is that in the model there is some time of unloading of the ice even though the relative velocity never becomes negative. This results from the choice of the phenomenological element to represent the ice behavior for which the relative velocity is governed by the difference in structural velocity and velocity of the center element rather than structural velocity and constant ice sheet velocity.

Results for the added damping are shown in Figure 5.18. The range of velocities for which experimental results are presented in Chapter 4 is indicated by open dots. Over

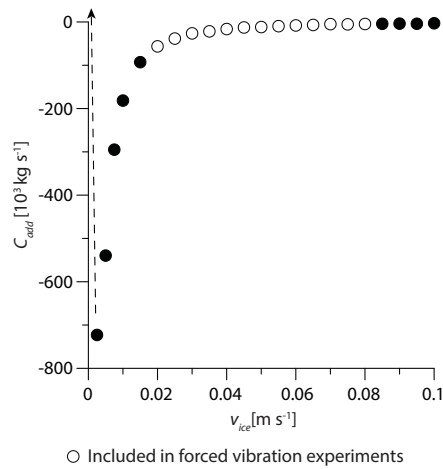


Figure 5.18: Added damping from forced vibration simulations. The range of velocities tested in the experiments presented in Chapter 4 is indicated by open dots. The trend for low velocities below the transition velocity from creep to crushing is indicated by the arrow as the large positive values obtained make it difficult to distinguish the trend in the crushing range when they are plotted all together.

this range the model prediction follows the trend observed in the experiment where the added damping becomes less negative with increasing velocity. The simulated results show that the added damping approaches a value of zero for high velocities for which the duration of loading at low relative velocity becomes increasingly less. At low velocities the added damping becomes increasingly negative as long as the velocity stays well above the transition from creep to crushing. In creep the ice no longer fails during every cycle of oscillation and the added damping is predicted to become positive (indicated by the arrow in Figure 5.18). In future experiments it would be interesting to perform tests at low velocities and in the creep range to confirm this trend.

Results for the added mass are shown in Figure 5.19. The range of velocities for which experimental results are presented in Chapter 4 is indicated by open dots. Over this range the model result follows a similar trend as that observed in the experiment except that the values for added mass do not become negative, but approach zero for high velocities. The latter is what is expected when the interaction between ice and structure vanishes for high velocities. It is not possible to state whether or not some mechanism is missing in the model or whether the experimental results are flawed. Considering that the experimental results have been obtained over only a limited amount of cycles small errors have a large impact on the obtained values. It is expected that a new set of experiments shows that indeed the added mass approaches zero for high velocities.

The model shows to produce similar trends for the added damping and added mass as obtained from the experiments presented in Chapter 4. Results indicate that future tests at low and high velocities and natural frequencies could provide relevant data for model validation. The model is now used to simulate forced vibration experiments for frequencies of oscillation of 1, 2, 4, and 8 Hz to illustrate the change in added mass and added

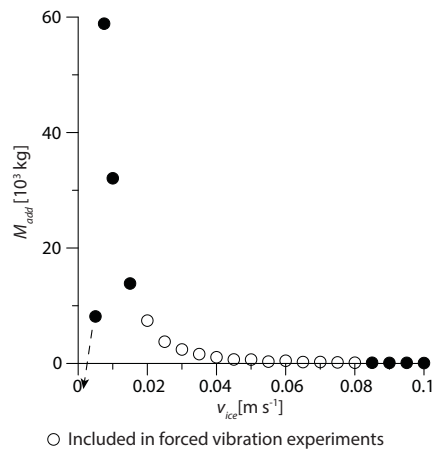


Figure 5.19: Added mass from forced vibration simulations. The range of velocities tested in the experiments presented in Chapter 4 is indicated by open dots. The trend for low velocities below the transition velocity from creep to crushing is indicated by the arrow as the large negative values obtained make it difficult to distinguish the trend in the crushing range when they are plotted all together.

5

damping for different, but constant, frequencies of oscillation as a function of indentation velocity. The amplitude is changed for each run such that the minimum relative velocity is zero during a cycle of forced vibration. Results for the added damping are shown in Figure 5.20. A clear trend of less negative added damping for higher frequencies of oscillation is observed. This shows that less energy can be obtained from the ice at higher frequencies under the assumed harmonic displacement of the structure. Furthermore, the minimum velocity for which the added damping becomes negative shows to shift to higher velocities for higher frequencies of oscillation. Finally, although less obvious for the high frequencies, the negative added damping reduces with increasing velocity.

Results for the added mass are shown in Figure 5.21. A small region of high positive added mass exists around a low velocity, but then it levels off seemingly approaching zero for high velocities. Negative added mass only occurs for the lowest velocities, where intermittent crushing would be expected to develop.

## 5.5. VALIDATION AND FURTHER DEVELOPMENT

The simulation results presented in the previous Section show that based on the theory that the changes in contact area govern the dynamic ice-structure interaction a consistent model can be developed which captures level ice action on vertically sided structures in general. In order to validate the theory and further develop the numerical model detailed measurements of the local contact and deformation processes are needed. Such measurements unfortunately do not exist for both rigid and flexible structures in similar ice conditions over a large range of velocities and structural properties. Once such

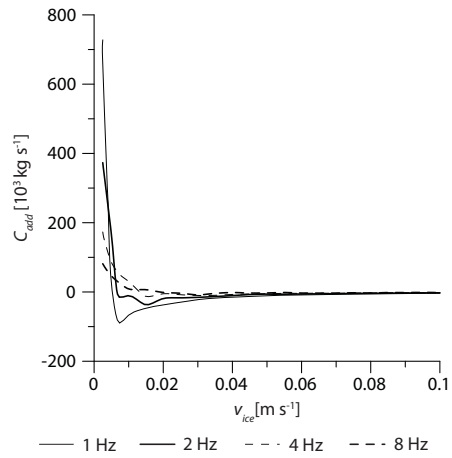


Figure 5.20: Trends in added damping as a function of velocity for constant frequencies of forced oscillation of 1, 2, 4, and 8 Hz.

5

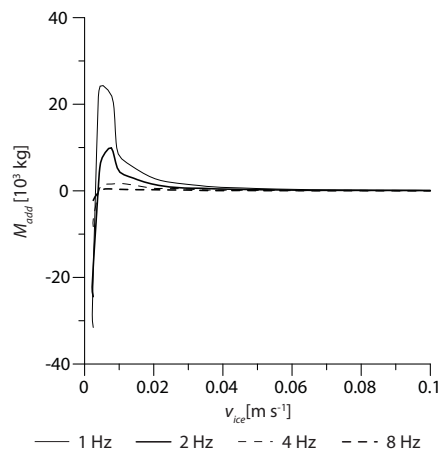


Figure 5.21: Trends in added mass as a function of velocity for constant frequencies of forced oscillation of 1, 2, 4, and 8 Hz.



measurements are obtained quantitative comparison between simulation results and experiments or full-scale observations will become possible.

As a first step in this process of experimental validation and development a campaign with rigid structures is envisaged. For such structures the trends in global load and contact area should be studied, ideally considering some variation in ice thickness and indenter width or diameter. Tests both at high indentation velocity, low velocity in the creep regime, and especially the transition region will give a complete overview of the ice behavior. Using this data the procedure of using reference measurements to define the ice behavior in the here proposed model can be assessed. Once satisfactory results have been obtained, the next step would be to use the model to predict the interaction between ice and flexible structure for the now known ice conditions and validate the predictions with experiments.

At the time of writing of this thesis the IVOS project is ongoing at HSVA, Hamburg in which frequency lock-in is studied with the application of a high sensitivity tactile sensor at the ice structure interface. Results from this project can indicate if the contact area approach defined here is indeed solely governing the development of frequency lock-in or whether additional processes play a significant role and need to be included in both the theoretical description and model.

## 5

### 5.6. CONCLUSION

A theory for explanation of the development of ice-induced vibrations has been presented. The theory is based on the observation that ice action on a vertically sided structure is controlled by the velocity dependent deformation and failure behavior of ice. At low loading rates a large contact between ice and structure can develop as a result of ductile deformations in the ice. This large contact area results in high loads. At high loading rates the ice behaves more or less elastic and contact is only attained in local zones across the ice-structure interface. When a flexible structure is interacting with the ice the loading rate changes continuously and when becoming small enough causes an increased contact area to develop resulting in an increased global load on the structure. Ice-induced vibrations occur when this increase in global load develops sufficiently to provide sufficient energy to the structure.

A phenomenological model has been presented which captures the main aspects of the theory. The model includes, in a simplified manner, local contact between ice and structure, elastic deformation of ice, crushing failure, global creep, and ductile deformation resulting in an increase of contact between ice and structure at low loading rates. A method to define the model input parameters based on reference measurements has been developed. The model is shown to reproduce ice action on a rigid structure consistent with that observed from experiments as described in Chapter 2 and defined by reference measurements. The development of ice-induced vibrations is shown by implementation of a simplified flexible structure with low damping in the model. The regimes of intermittent crushing, frequency lock-in, and continuous brittle crushing are all captured by the model. Specific observations in the frequency lock-in regime such as the

frequency lock-in relation introduced in Chapter 3 are contained in the model. Simulation of forced vibration experiments shows that the trends for the added mass and added damping from ice as obtained in experiments described in Chapter 4 are recovered as well. Based on the simulation results it has been concluded that the defined theory allows for a consistent model to be developed which captures level ice action on vertically sided structures in general.

Further validation of the theory and development of the model requires dedicated experiments to be performed. This is needed in order to make the step towards accurate quantitative comparison between simulation results and experiments or full-scale observations. It has been proposed that first tests with rigid structures focusing purely on the ice behavior during indentation for different velocities are executed.

In the next chapter buckling is introduced in the model to study its limiting effect on ice-induced vibrations. Practical application of the model is treated in Chapter 7 considering the implementation of multi-degree of freedom structural models and design of model-scale tests.



# 6

## ICE-INDUCED VIBRATIONS AND ICE BUCKLING

### 6.1. INTRODUCTION

In the previous chapter a model is introduced for simulation of level ice interaction with vertically sided structures in the case where ice fails either in creep or crushing. Based on experimental and full-scale observations shown in Chapter 2 ice is known to sometimes fail by bending as a result of buckling when the ice is thin, or the structure is relatively wide. This type of failure is referred to here as buckling failure. As buckling limits the development and duration of crushing, it is expected to naturally limit the development of ice-induced vibrations as observed often in model-scale as well as full-scale conditions (Bjerkas et al., 2013; Ziemer and Evers, 2014).

In this chapter buckling as a limiting mechanism for ice-induced vibrations is theoretically investigated by combining the model introduced in Chapter 5 with a model of a wedge beam on elastic foundation to incorporate buckling of the ice. The resulting model incorporates, in a simplified manner, creep, crushing, and flexural ice behavior and captures typical trends observed for ice-induced vibrations. The wedge beam approach has been introduced by Kerr (1978) and is deemed to be a reasonable approximation for the ice buckling problem taking into consideration the radial cracks which form in the ice during its interaction with a structure. Limitations of the wedge beam approach are discussed by Sodhi (1979) in comparison with plate theory. Although the limitations are quite severe, accuracy of the wedge beam model predictions is deemed sufficient for the developed phenomenological model. The model introduced is subsequently applied to study the development of ice-induced vibrations in the regime of mixed crushing and buckling. Such studies on ice-induced vibrations in this regime were not previously available in the literature.

---

This Chapter has been published in Cold Regions Science and Technology, (Hendrikse and Metrikine, 2016b). Parts of the article have been moved to other Chapters in this thesis for consistency.

In Section 6.2 the expanded model is presented and additional input parameters necessary to model ice buckling are defined. Section 6.3 shows the application of the model to study action of a sheet of model-ice on a rigid, vertically sided structure. The obtained results are discussed with reference to model-scale experimental observations. Section 6.4 presents a study of the development of ice-induced vibrations of a flexible structure in the regime of mixed crushing and buckling. The obtained results are discussed in Section 6.5 and main conclusions are collected in Section 6.6.

## 6.2. MODEL DESCRIPTION

An overview of the phenomenological model for combined creep, crushing, and buckling of level ice acting on a vertically sided structure is presented in Figure 6.1. The structure is modeled as a single-degree-of-freedom oscillator defined by its mass  $M_s$  [kg], damping  $C_s$  [kg s<sup>-1</sup>], stiffness  $K_s$  [kg s<sup>-2</sup>], displacement  $u_s(t)$  [m], and structural width  $d_s$  [m]. This simple approximation is considered sufficient for the study presented here. The ice is assumed to have sufficient inertia such that its motion can be characterized by a constant indentation velocity  $v_{ice}$  [m s<sup>-1</sup>]. The ice load on the structure  $F_{ice}(t)$  [N] is the summation of the loads from  $N$  individual creep-crushing elements at the contact zone between ice and structure which are defined in Chapter 5.

6

Out of plane motion of the ice  $w(x, t)$  [m] outside of the creep-crushing zone is modeled by a wedge beam on elastic foundation. The equation of motion of the beam is given by:

$$Dw(x, t)'''' + 2\frac{D}{d(x)}d(x)'w(x, t)''' + \frac{F_{ice}(t)}{d(x)}w(x, t)'' + \kappa w(x, t) + \chi \dot{w}(x, t) + \rho h \ddot{w}(x, t) = 0$$

$$d(x) = d_s + (L - x)2 \tan\left(\frac{\phi}{2}\right)$$

$$D = \frac{Eh^3}{12(1 - \nu^2)}$$
(6.1)

, where primes indicate spatial derivatives with respect to  $x$ , over-dots represent derivatives with respect to time,  $L$  is the beam length [m],  $h$  the ice thickness [m],  $\phi$  the wedge angle [rad],  $\kappa$  the specific weight of water [kg (ms)<sup>-2</sup>],  $\rho$  the mass density of ice [kg m<sup>-3</sup>],  $E$  the Young's modulus of ice [N m<sup>-2</sup>],  $\nu$  the Poisson ratio of ice [-], and  $\chi$  a distributed viscous damping per unit area [kg m<sup>-2</sup> s<sup>-1</sup>]. The beam is considered fixed at a distance  $L$  away from the structure and subject to axial force  $F_{ice}(t)$ , bending moment  $M_{ice}(t)$  [Nm], and vertical force  $F_{v;ice}(t)$  [N] at the ice-structure interface defined in terms of boundary conditions as:

$$w(L, t) = w(x, t)'|_{x=L} = 0$$

$$-Dd(x)w(x, t)''|_{x=L} = M_{ice}(t) = U(0, 0.001)F_{ice}(t)$$

$$-Dd(x)w(x, t)'''|_{x=L} - Dd(x)'w(x, t)''|_{x=L} + F_{ice}(t)w(x, t)'|_{x=L} = F_{v;ice}(t)$$

$$F_{v;ice}(t) = -\text{sgn}(\dot{w}(x, t)|_{x=L})\mu F_{ice}(t)$$
(6.2)

, where the bending moment  $M_{ice}$  is introduced to cause a disturbance of the in-plane equilibrium of the beam such as to allow buckling to develop. The value is chosen small

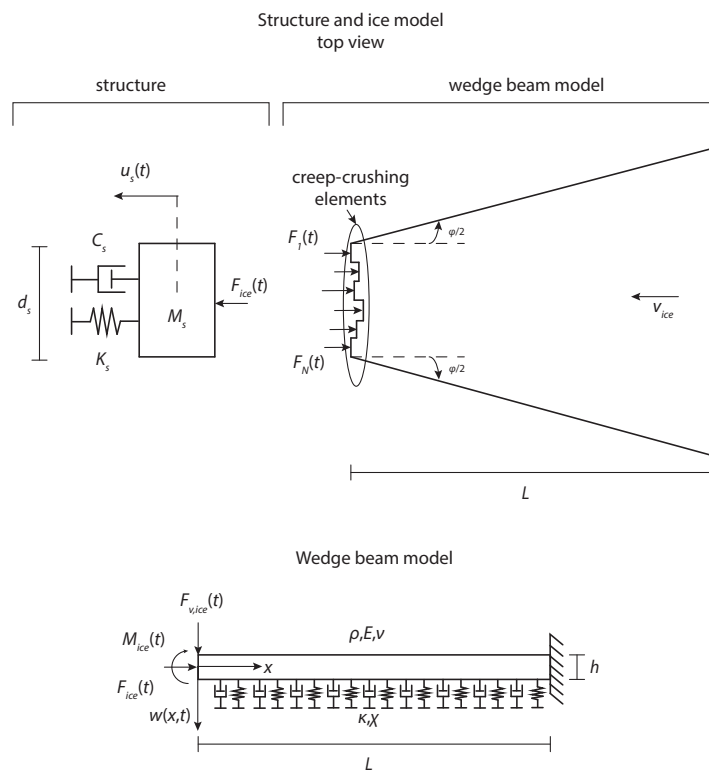


Figure 6.1: Model for combined creep, crushing and buckling of ice acting on a vertically sided offshore structure. The structure is modeled as a single-degree-of-freedom oscillator. The ice model consists of a wedge beam on elastic foundation to model the flexural motion and  $N$  individual creep-crushing elements at the ice-structure interface to model the in-plane deformation and failure of the ice in the contact area.

such that if failure by exceedance of the flexural strength occurs this is a result of buckling instability and not of pure bending of the beam. Upon failure of a creep-crushing element a new value for the eccentricity is drawn from a uniform distribution  $U(0, 0.001)$ . The vertical force  $F_{v,ice}$  is implemented to include frictional sliding in vertical direction along the ice-structure interface characterized by friction coefficient  $\mu$  [-].

Failure is set to occur when the bending stress at one cross-section in the beam,  $x^*$ , exceeds the flexural strength at a certain moment in time:

$$\left| \frac{6D}{h^2} w(x, t)'' \right|_{x=x^*} - \frac{F_{ice}(t)}{hd(x^*)} = \sigma_f \quad (6.3)$$

where  $\sigma_f$  [ $\text{N m}^{-2}$ ] is the flexural strength of the ice. Upon failure the ice beam is removed from the model until the distance over which the ice has broken has been covered and new contact between the ice and structure is established.

The model is studied numerically by application of a central difference scheme with respect to the spatial coordinate to discretize the ice beam into  $N_{beam}$  elements and rewriting the governing set of equations into a system of first order differential equations (state-space representation) which are solved in the time domain by application of the 4th order Runge-Kutta method. Event functions are implemented for the detection of contact, stick-slip behavior of the creep-crushing elements, and failure of the ice by bending or crushing.

## 6

### 6.3. MODEL APPLICATION FOR ICE ACTION ON RIGID STRUCTURES

In this section the predictions of the model for the case of a model-ice sheet acting against a rigid vertically sided structure are described. The results demonstrate the applicability of the model for modeling creep, crushing, and buckling of ice. Input parameters of the model are shown in Table 6.1. The model-scale ice properties are based upon the values for urea ice reported by Sodhi and Morris (1984). In their report results of indentation experiments are shown which contain a large portion of the required reference measurements.

With respect to the creep-crushing elements the values for  $F_{ref,max}$ ,  $F_{ref,mean}$ ,  $F_{ref,std}$ ,  $v_{ref,high}$ , and  $f_{ref,peak}$  for the defined  $d_{ref}$  and  $h_{ref}$  can be obtained from tables in the appendix of the report by Sodhi and Morris (1984), where here the observations from the tests on 25 February 1983 and 3 February 1983 have been averaged. For the transition velocity  $v_{ref,trans}$  an estimate is made of  $1 \text{ mm s}^{-1}$  which is a bit higher than the reported values for small-grained freshwater ice in Nakazawa and Sodhi (1990). The value for  $t_{ref,peak}$  is also estimated based on that report taking into account that the model assumes a rough ice edge at the start and the experiments were carried out with a prepared flat surface of the ice. The value for  $F_{ref,mean,2}$  is estimated based on the ratio between the mean contact area during high velocity crushing and close to the transition from creep to crushing in the experiments by Takeuchi et al. (2001).

For the wedge beam model the values for  $E$ , and  $\sigma_f$  are obtained from Sodhi and Morris (1984). The length of the beam is chosen to be much larger than the ice thickness and set at 9 m and a large wedge angle of  $45^\circ$  is chosen. Values for the Poisson ratio and mass density of urea ice are based on the work by Timco (1980). The distributed spring stiffness is defined by the specific weight of water, and the distributed viscous damping is chosen such that energy reflected from the fixed boundary of the ice beam is limited. The dynamic friction coefficient is chosen based upon reference values for kinetic friction between ice and steel.

The reference measurements used here to define the input of the model are chosen with care to obtain ice behavior in the model which matches model-scale observations. Validation of the proposed method of defining input parameters requires experimental effort and the results from simulations presented hereafter will change when different input parameters are defined. However, as long as the general ice load dependence as sketched in Figure 5.3 is assumed to reflect the trend in ice loads on a rigid structure, changes in parameters will mainly affect the location of the boundaries between creep and crushing, and between the different regimes of ice-induced vibrations when flexible structures are considered in the model. For the wedge beam approach the same is valid. The competition between buckling and crushing remains in the model unless the wedge angle is chosen as 0 degrees, which results in a straight beam for which the ice will either always crush or always buckle.

A failure map for model-scale conditions is generated by varying the indentation velocity between  $1 \times 10^{-4} \text{ m s}^{-1}$  and  $1 \text{ m s}^{-1}$  and the structural width between 0.05 m and 1.7 m in the model. The result is shown in Figure 6.2. Creep, crushing, buckling and mixed crushing and buckling failure are distinguished. Each simulation is run for 10 seconds of the simulated signal, or an indentation distance of 30 failure lengths, whichever longer. Creep is defined to occur when during the simulation no creep-crushing element fails and no buckling failure occurs. Buckling is defined to occur when the ice fails according to Equation 6.3 before a single creep-crushing element has failed. In case only creep-crushing elements fail the failure mode is set to be crushing, whereas a combination of crushing and buckling failure is defined as mixed mode failure.

Comparing the obtained failure map in Figure 6.2 with the one based upon experimental observations shown in Figure 2.1 one can see that the trends are reproduced by the model. For indentation velocities below  $v_{trans}$  the model predicts either creep or buckling failure to occur depending on the aspect ratio. Crushing occurs for velocities above  $v_{trans}$  and a transition to mixed failure or buckling takes place for an aspect ratio between 2 and 10 approximately, depending on the indentation velocity  $v_{ice}$ .

Typical time dependencies of the ice load as predicted by the model for each of the failure modes are also shown in Figure 6.2 and can be compared with the signals given by Timco (1987). Creep shows the load leveling off after some time of loading as all creep-crushing elements come into contact with the structure. Crushing shows a typical random load signal around a mean value. Buckling is characterized by a load build-up phase, followed by a load drop to zero resulting from global failure. Mixed mode failure shows some time of crushing until buckling failure occurs. The time of crushing in this case is governed by



Table 6.1: Input parameters for model-scale urea ice based on values reported in Sodhi and Morris (1984), Timco (1980), Nakazawa and Sodhi (1990), and Takeuchi et al. (2001).

Parameter:	Input value:	Dimension:
$d_{ref}$	0.05	[m]
$h_{ref}$	0.055	[m]
$v_{ref,high}$	0.13	[m s <sup>-1</sup> ]
$v_{ref,trans}$	0.001	[m s <sup>-1</sup> ]
$F_{ref,max}$	5500	[N]
$F_{ref,std}$	500	[N]
$F_{ref,mean}$	1500	[N]
$f_{ref,peak}$	11	[Hz]
$F_{ref,mean,2}$	3750	[N]
$t_{ref,peak}$	150	[s]
$c$	0.3	[-]
$L$	9	[m]
$E$	$1.74 \times 10^8$	[N m <sup>-2</sup> ]
$\nu$	0.33	[-]
$\kappa$	10055	[kg (ms) <sup>-2</sup> ]
$\phi$	$0.5\pi$	[rad]
$\chi$	512.5	[kg m <sup>-2</sup> s <sup>-1</sup> ]
$\rho$	950	[kg m <sup>-3</sup> ]
$\sigma_f$	$1.7 \times 10^5$	[N m <sup>-2</sup> ]
$\mu$	0.03	[-]
$N_{beam}$	180	[-]

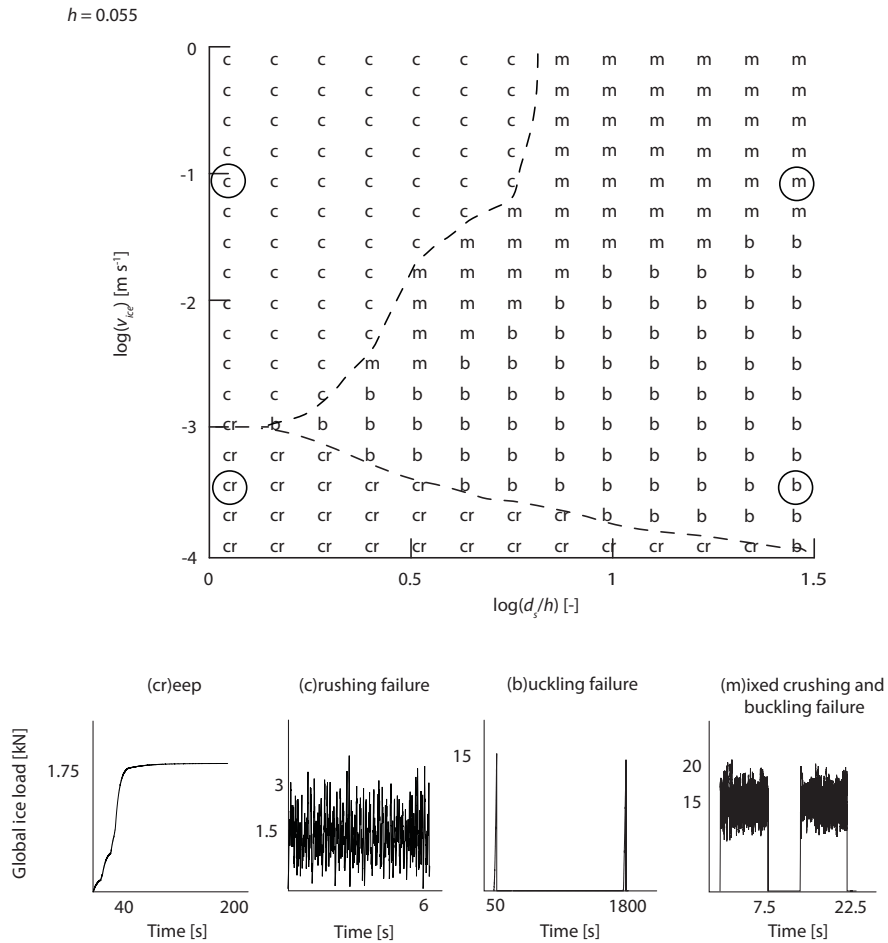


Figure 6.2: Top: Numerically generated failure map for representative urea ice conditions given in Table 6.1 based on ice properties reported in Sodhi and Morris (1984). Bottom: Ice load signals generated with the model for the different types of failure at conditions circled in the failure map are shown at the bottom. Legend: cr – creep, c – crushing failure, b – buckling failure, m – mixed crushing and buckling failure.

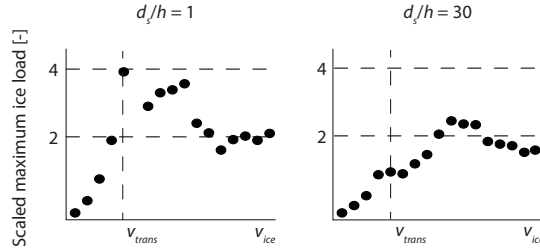


Figure 6.3: Dependence of maximum global ice load on indentation velocity for an aspect ratio of one and thirty. The maximum global load is scaled with respect to the mean load for crushing at high velocities.

the time needed for the ice to reach an out-of-plane deformed state which causes global failure.

The dependence of the maximum global load on velocity for an aspect ratio of one and thirty is shown in Figure 6.3. The ice loads in this figure are scaled with respect to the mean load for crushing at high velocities. The model reproduces the typical trend in the dependence of the global load on indentation velocity in case of creep and crushing at an aspect ratio of one. The maximum ice load is observed around the transition velocity above which the load decreases towards a more or less steady value for increasing velocity. The disappearance of this trend for higher aspect ratios as observed in model-scale experiments (Sodhi and Morris, 1984) is reproduced as shown for an aspect ratio of thirty. The trend of reducing maximum global load from the transition velocity is no longer observed at such high aspect ratio. The latter is a result of buckling failure.

The transition between creep and buckling, or crushing and buckling in the model is governed by the ratio between the global crushing load and the critical buckling load of the wedge beam. This ratio can be approximated by:

$$\frac{F_{crush}(v_{ice}) \frac{hd_s}{h_{ref}d_{ref}}}{P} = 1 \quad (6.4)$$

where  $F_{crush}(v_{ice})$  [N] is the dependence of the global load on indentation velocity for the reference case for crushing as defined in Chapter 5, and  $P$  [N] is the critical buckling load of the wedge beam. In order to gain some insight in the dependence of the critical buckling load in the model on the different input parameters the static critical buckling load based upon is determined based on Equation 6.1 and Equation 6.2 by solving the generalized eigenvalue problem applying the finite difference method. This analysis does not include the velocity and inertia effects which are included in the results from model simulations presented in this Chapter. The result in terms of the three dimensionless parameters governing the problem is shown in Figure 6.4. The result presented here is valid only for boundary conditions defined by Equation 6.2 where the external bending moment  $M_{ice}$  is not taken into consideration. For different boundary conditions similar maps can be straightforwardly reproduced. An analytical solution for buckling of a semi-infinite wedge can be found in Nevel (1980).

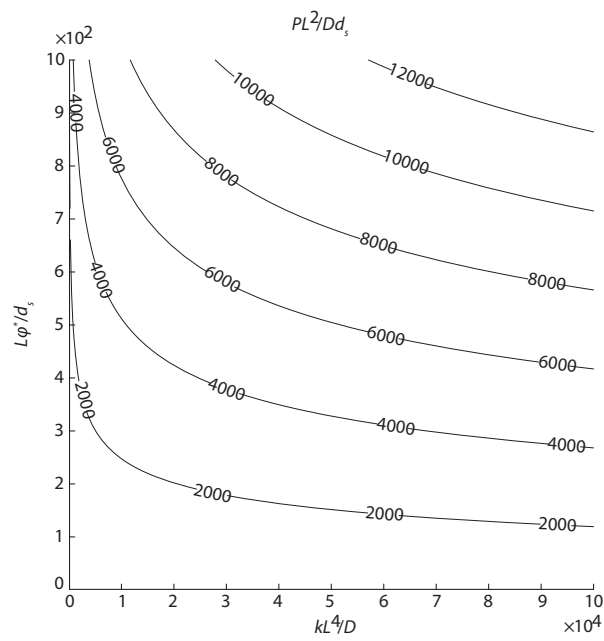


Figure 6.4: Critical buckling load of a wedge beam on elastic foundation in a fixed-free configuration defined by Equation 6.1 and Equation 6.2.

Figure 6.4 shows that the critical buckling load  $P$  does not increase proportionally with an increase in structural width  $d_s$ , whereas the global load due to creep and crushing increases proportionally with  $d_s$ , as given by Equation 6.4. As a result a transition from crushing to buckling occurs for large structural width  $d_s$  provided that all other parameters are kept constant. As the crushing load depends on velocity the transition does not occur at a single value of  $d_s$  for all indentation velocities, as can be observed from the failure map in Figure 6.2. The actual value of  $d_s$  for which the transition occurs increases with increasing  $\kappa$ ,  $D$ ,  $\phi^*$ , and  $h$  and decreases for increasing  $F_{crush}(v_{ice})$ , where  $\phi^*$  is defined by:

$$\phi^* = 2 \tan\left(\frac{\phi}{2}\right) \quad (6.5)$$

The length of the beam has only a small effect on the results as buckling occurs near the ice-structure interface, but should not be too short in relation to the structure width and ice thickness.

The results obtained with the model for the case of level ice action on a rigid vertically sided structure shown in this section illustrate that the model qualitatively captures the different failure modes of ice which may occur, and generates representative load signals and trends in statistical properties of the ice load. In the next Section the model is applied to study the development of ice-induced vibrations in cases associated with ice failure by mixed crushing and buckling.

## 6

### 6.4. ICE-INDUCED VIBRATIONS AND ICE BUCKLING

In this section the results of a study into the development of ice-induced vibrations in cases associated with ice failure by mixed crushing and buckling are presented. All simulations are performed with ice defined by the properties given in Table 6.1. In Section 6.4.1 the development of ice-induced vibrations for a structure with various widths, of which the dynamic properties are scaled with respect to the ice load, is shown. Results obtained with this configuration illustrate the effect of changes in the failure mode of ice on the development of ice-induced vibrations and the effect of flexibility of the structure on the occurring failure mode. In Section 6.4.2 one particular case is treated for which the flexibility of the structure results in intermittent crushing that prevents buckling failure from occurring under the conditions that lead to buckling for indentation on a rigid structure. In Section 6.4.3 the development of ice-induced vibrations for a structure with fixed properties for different values of ice thickness is shown. This is a general case which is applicable for real structures which encounter varying ice conditions over their lifetime.

#### 6.4.1. A STRUCTURE WITH SCALED DYNAMIC PROPERTIES

Simulations were ran for a flexible structure with low damping in ice conditions defined by the parameters given in Table 6.1, for which the occurring failure mode of ice as a function of structure width and velocity is shown in the failure map in Figure 6.2. The structural properties are chosen arbitrarily such that for an aspect ratio of one intermittent crushing and frequency lock-in occur over a range of velocities. A natural frequency

of 2.5 Hz, damping ratio of 3% of critical, and structural stiffness:

$$K_s = 0.5K_2N_{ref} \frac{d_s}{d_{ref}} \quad (6.6)$$

are defined. This choice of the structural properties assures that the dynamic interaction scales with changing width of the structure. The results obtained thereby elucidate the effect of mixed crushing and buckling failure on the development of ice-induced vibrations and the effect of flexibility of the structure on the observed failure mode.

With respect to the results for ice-induced vibrations obtained with the model intermittent crushing, frequency lock-in, and continuous brittle crushing are distinguished. Intermittent crushing is said to occur in the model if a quasi-periodic saw-tooth pattern with a period greater than the natural period of the structure is observed in the time dependence of both the ice load and structural displacement. Frequency lock-in is defined to occur in the model, based on observations by Toyama et al. (1983), in the case when a periodic motion of the structure occurs with a period close to its natural period (observed in the absence of the ice loading) and with the maximum velocity equal to or slightly higher than the indentation velocity.

Figure 6.5 shows the occurring types of ice-induced vibrations in the plane of velocity and width of the structure. For an aspect ratio of one, intermittent crushing (icr) is predicted at velocities between  $0.001 \text{ m s}^{-1}$  and  $0.025 \text{ m s}^{-1}$  approximately. From  $0.025 \text{ m s}^{-1}$  up to  $0.075 \text{ m s}^{-1}$  frequency lock-in (fli) is predicted and above  $0.075 \text{ m s}^{-1}$  brittle crushing (cbr) is observed corresponding to a random response of the structure. As the structural properties are scaled with the increasing ice load following Equation 6.6 the range of velocities for which ice-induced vibrations occur does not vary with changing width of the structure unless buckling failure occurs, limiting the development of ice-induced vibrations.

Ice-induced vibrations which develop for a limited interval of time followed by buckling are indicated with an asterisk. Such vibrations mainly develop for the failure conditions in which mixed mode failure would be expected based on the failure map shown in Figure 6.2. These cases sometimes include only one or two cycles of vibration before buckling failure occurs. When buckling occurs without crushing, or the duration of mixed mode failure is too short, ice-induced vibrations are no longer observed.

Examples of time-dependencies corresponding to intermittent crushing and frequency lock-in during crushing and mixed failure circled in Figure 6.5 are shown in Figure 6.6. With respect to intermittent crushing at a velocity of  $0.002 \text{ m s}^{-1}$  the results show that the maximum displacement and saw-tooth period are not affected by the flexural motion of the beam, whereas the vibrations are limited in duration for the higher aspect ratio due to buckling failure. For frequency lock-in at a velocity of  $0.04 \text{ m s}^{-1}$  oscillations of the structure are similar at low and high aspect ratios, and also in this case the number of cycles is limited by the occurrence of buckling failure. Effects of upward and downward motion of the ice sheet on the crushing process are not included in the model, except for global failure in bending resulting in a loss of contact, and are not available from literature, but are expected to be small given that crushing is a very local process. The

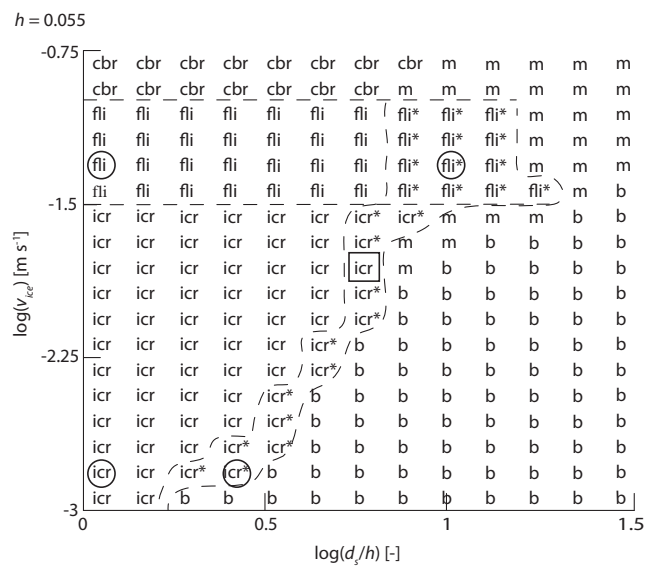


Figure 6.5: Predicted types of ice-induced vibrations for a structure whose dynamic properties are scaled according to Equation 6.6. Time dependencies of displacement of the structure and ice load of the circled cases are shown in Figure 6.6. The case indicated by the rectangle is discussed in more detail in Section 6.4.2. Legend: icr – intermittent crushing, fli – frequency lock-in, cbr – continuous brittle crushing, b – buckling, m – mixed crushing and buckling failure, icr\* intermittent crushing followed by buckling failure, fli\* frequency lock-in followed by buckling failure.

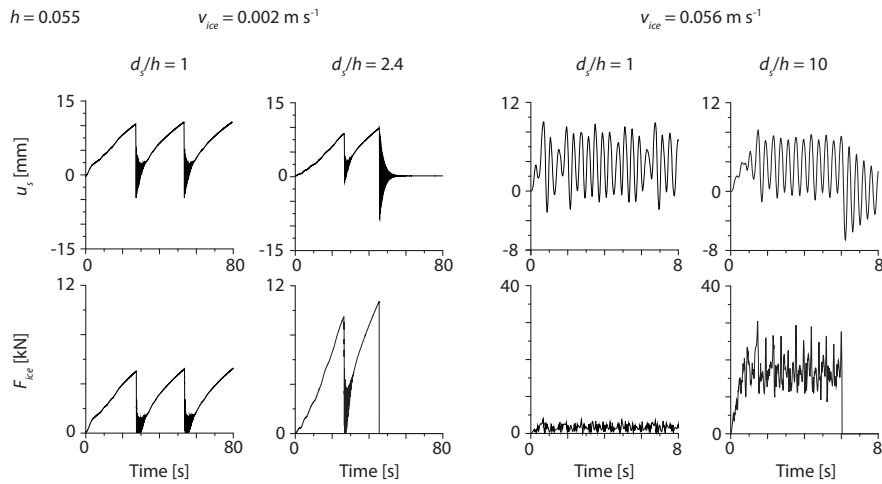


Figure 6.6: Examples of structural displacement and global ice load during intermittent crushing and frequency lock-in in conditions of continuous crushing at an aspect ratio of 1, and mixed crushing and buckling failure at aspect ratios of 2.4 and 10, respectively. The conditions for which the signals are obtained are circled in Figure 6.5.

results show that the development of ice-induced vibrations in cases of mixed buckling and crushing is primarily dependent on the ratio between the time required for buckling to result in failure, the buckling period, and the period of intermittent crushing or frequency lock-in.

Figure 6.7 shows this buckling period as a function of velocity and width of the structure for indentation on a rigid structure as used to obtain the failure map in Figure 6.2. The buckling period shows a general decreasing trend for increasing velocity and increasing width. A limit value is reached for high velocity indentation. This is a result of the axial load no longer decreasing with increasing velocity, and the load build-up time becoming shorter such that its contribution to the buckling period diminishes. An interesting region is obtained for aspect ratios between 3 and 30 roughly where with increasing velocity from the transition velocity the buckling period first reduces and then slightly increases again. This effect is caused by the dependence of the axial load on indentation velocity in relation to the critical buckling load as described in Section 6.3. Additionally, the frictional sliding at the ice-structure interface and randomness in the model have a large effect on the obtained buckling period for cases where the global ice load is close to the critical buckling load. Due to these effects it is difficult to predict the actual buckling period and the possibility for ice-induced vibrations to develop without simulating the interaction.

One effect which is observed is that the introduction of a flexible structure can cause the buckling period to increase with respect to the values shown in Figure 6.7. This happens mostly for cases in which intermittent crushing develops such as shown in Figure 6.6 for an aspect ratio of 2.4. During intermittent crushing the global ice load generally in-



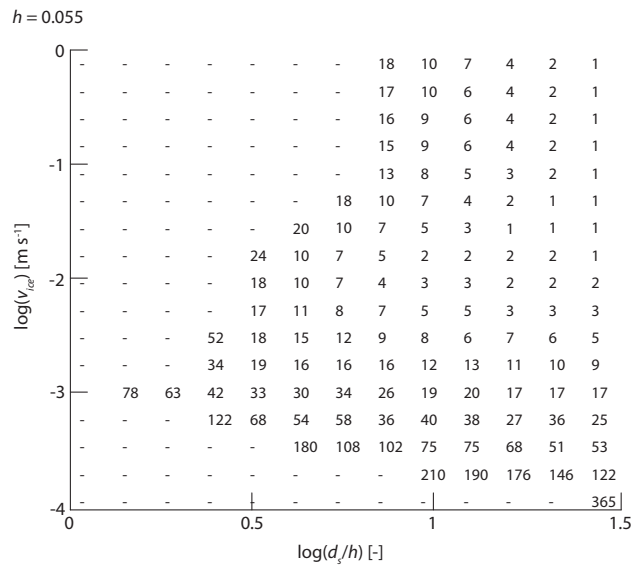


Figure 6.7: Buckling period [s] for modeled ice as a function of indentation velocity and width of the structure. The period shows a general trend of decrease with increasing structural width and ice velocity.

## 6

creases to a higher value than would be observed for the same conditions with a rigid structure. This might lead to the expectation that buckling would occur sooner. However, the large load drops which occur during intermittent crushing can result in the build-up of the out-of-plane deformation of the ice, ultimately causing the buckling failure, to diminish in between saw-tooth events thereby causing the buckling failure to be delayed, or not occur at all. In the next section this effect is further illustrated based on a simulation for which buckling failure was found to be prevented by continuous intermittent crushing.

### 6.4.2. INTERMITTENT CRUSHING LIMITING THE DEVELOPMENT OF BUCKLING FAILURE

In this section it is shown how ice-induced vibrations may prevent buckling failure from occurring instead of buckling failure limiting the duration of ice-induced vibrations. A case clearly illustrating the effect of structural motion on the development of buckling failure is indicated by the rectangle in Figure 6.5. For this case the ice is expected to fail in mixed crushing and buckling when looking at the failure map in Figure 6.2. The buckling period is expected to be approximately 7 seconds as shown in Figure 6.7. However, as illustrated in Figure 6.8, sustained intermittent crushing occurs for at least 16 seconds, the duration of the particular simulation. The vertical displacement of the front of the wedge beam is also shown in Figure 6.8, which for the given boundary conditions is a representative measure of the bending of the beam. Comparing the displacement of the front of the beam for the case in which ice acts on a rigid structure with the indentation

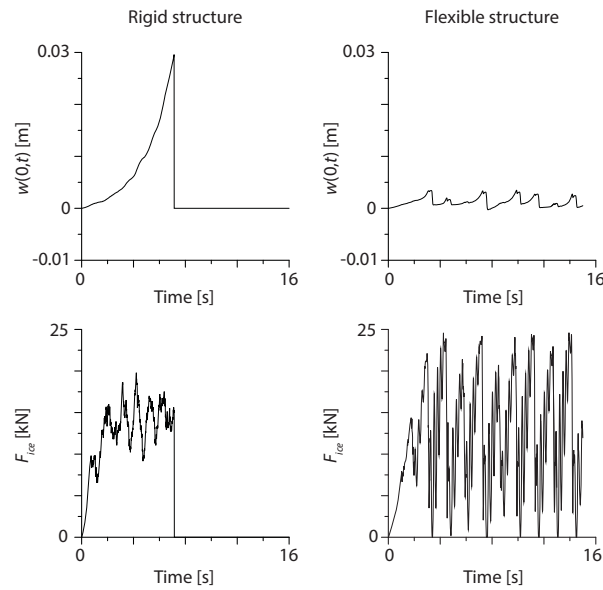


Figure 6.8: Vertical displacement of the ice edge in contact with the structure and global ice load for a velocity of  $0.018 \text{ m s}^{-1}$ , aspect ratio of 5.6 and ice thickness of 0.055 m. Left: a rigid structure showing buckling failure to occur after 7 seconds of crushing. Right: Intermittent crushing on a flexible structure preventing the buckling failure.

on a flexible structure shows the reason for the buckling failure to be prevented.

For the rigid structure the ice load builds up to, and then oscillates around, an average value which exceeds the buckling limit of the beam causing the beam to become unstable and deform until buckling failure occurs. For the flexible structure the ice load builds up to a higher level, far exceeding the critical buckling load, however before the beam can sufficiently deform to cause buckling failure the ice load drops to a close to zero value allowing the beam to return to its equilibrium position. In such particular case of the intermittent crushing period being smaller than the buckling period the development of ice-induced vibrations thus prevents buckling failure from happening.

The result shown in Figure 6.8 is highly dependent on boundary conditions, which determine how fast the beam can move back to the equilibrium position and on the randomness in the ice properties taken into account. Theoretically a similar result could be obtained for frequency lock-in as the ice load also oscillates periodically, and could oscillate around the critical buckling load, however this was not observed in any of the simulations.

### 6.4.3. A STRUCTURE IN CONDITIONS OF DIFFERENT ICE THICKNESS

Now a structure with fixed properties in conditions with different ice thickness is considered. This situation resembles an offshore structure which encounters varying ice con-

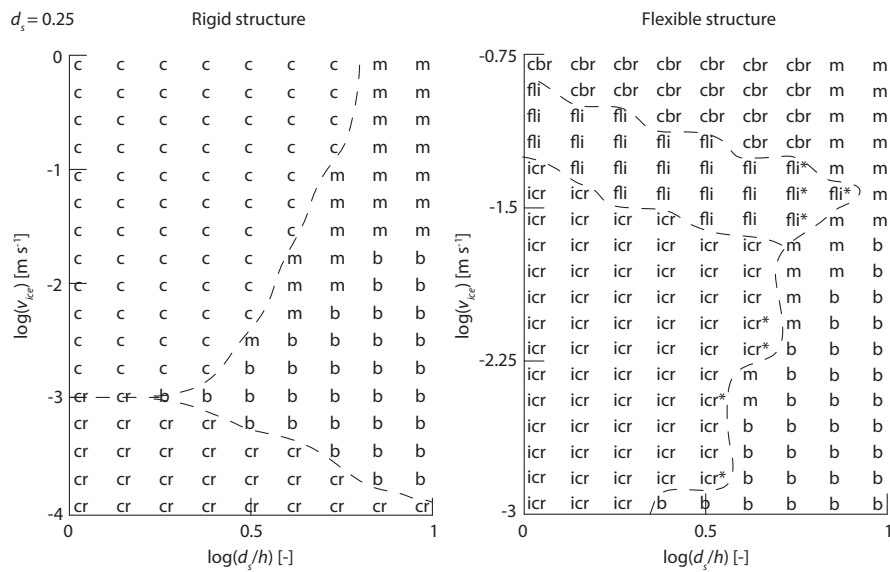


Figure 6.9: Left: failure map for rigid structure of 0.25 m width for different ice thickness and velocity. Right: Occurrence of ice-induced vibrations for a flexible structure with a width of 0.25 m, 2.5 Hz natural frequency, and 3% damping as a percentage of critical, for varying ice thickness and velocity. Legend: cr – creep, c – crushing failure, b – buckling failure, m – mixed crushing and buckling failure, icr – intermittent crushing, fli – frequency lock-in, cbr - continuous brittle crushing, icr\* intermittent crushing followed by buckling failure, fli\* frequency lock-in followed by buckling failure.

## 6

ditions over its lifetime, however we ran the situation for the model-scale ice properties given in Table 6.1. The structural properties are fixed to the following values: structural width of 0.25 m, natural frequency of 2.5 Hz, damping ratio of 3%, and structural stiffness of  $2.5K_2N_{ref}$ , with  $K_2$  fixed to the value for an ice thickness of 0.025 m. The ice thickness is varied from 0.025 m up to 0.25 m resulting in an aspect ratio varying between one and ten. Results of the simulation are shown in Figure 6.9 including a failure map generated with a rigid structure of 0.25 m width for the same ice conditions. Note that the vertical axis differs between plots as for ice-induced vibrations the range of velocities below the transition velocity is not simulated, nor the highest velocities for which continuous brittle crushing occurs.

The maximum velocity for which intermittent crushing and frequency lock-in occur generally decreases with decreasing ice thickness as a result of reduction of the global ice load. This can result in two situations when it comes to ice-induced vibrations in mixed failure conditions. First, the ice thickness for which mixed failure conditions occur might yield a too low global load level for ice-induced vibrations to develop. In this case there is no influence of buckling on the development of ice-induced vibrations or vice versa. The second case is that for which the global ice load is still large enough to cause ice-induced vibrations. In this case the criteria and conditions are the same as those discussed in the previous subsections. An analysis which considers pure crushing over the whole range of

ice thicknesses would provide an upper bound for the aspect ratio for which ice-induced vibrations may develop for a given structure. If this upper bound aspect ratio is higher than the aspect ratio for which mixed failure is expected an integrated analysis taking into account all failure modes might give more realistic load signals for the design of such structure, provided that the model used for simulation of the ice load is validated to predict realistic ice load signals.

## 6.5. DISCUSSION

The results presented in Section 6.4 show that three conditions should be met in order for ice-induced vibrations to develop in situations when the ice fails in the regime of mixed crushing and buckling. First, the ice crushing load and critical buckling load should belong in the range that allows for the mixed crushing and buckling mode to occur. Second, the time required for buckling failure to develop, referred to as the buckling period here, must be significantly greater than the period of frequency lock-in or period of intermittent crushing. And third, ice-induced vibrations must be admissible for the given structural and ice properties. The first two conditions are briefly discussed, followed by a discussion on failure maps for thick ice. The third condition depends on the mechanism governing the development of ice-induced vibrations which is described in detail in Chapter 5.

The condition for ice to fail in mixed crushing and buckling is defined by ice properties, boundary conditions, structural size, and structural shape. Each of these, having an effect on the critical buckling load and crushing load level, thereby affect the transition condition given by Equation 6.4. For specific ice conditions the critical buckling load dependence on ice and structural properties can be assessed by developing a map as shown in Figure 6.4. Boundary conditions play a significant role as, for example, the presence of large piles of rubble on top and below the ice would increase the critical buckling load significantly and hence crushing might be expected for conditions in which level ice without rubble would experience buckling failure. This example has already been mentioned by Blanchet et al. (1988) in discussion of the observations made on the Molikpaq structure in the Beaufort Sea. With respect to structural shape the development of radial cracks plays a role as well as the orientation of the load with respect to the formed wedges. The difference between a rectangular structure and cylindrical structure is illustrated in Figure 6.10. For a cylindrical structure the wedges have a smaller angle, resulting in lower buckling resistance, however the load on each wedge is reduced when compared to the rectangular structure of same width. Therefore the transition between crushing and mixed failure might occur at higher aspect ratios (Kerr, 1978). For large circumferential buckling failure the wedge beam approach is not applicable and plate theory is perhaps a better choice.

The buckling period has been shown to depend on indentation velocity, aspect ratio and ice properties in general in Section 6.4. Further study is needed to quantify the dependence of the buckling period on these properties. Specifically, the applicability of the wedge beam model for quantitative modeling of this type of interaction needs to be considered first. The observed trends are however expected to remain as the problem does

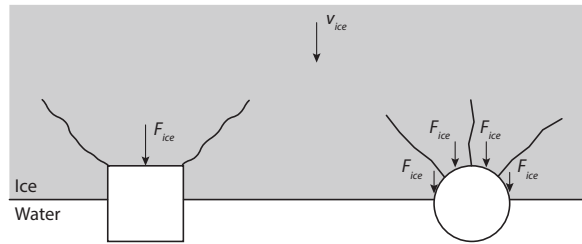


Figure 6.10: Effect of the shape of the structure on development of radial cracks in the ice and global ice load distribution amongst different wedges of ice in contact with the structure.

not change significantly when more complex models for buckling are introduced as long as the buckling is considered in an elastic manner. The period of frequency lock-in, if it occurs, is well known to be around the natural frequency or slightly below the natural frequency of the structure. The period of saw-tooth oscillation during intermittent crushing is in general greater and decreases with increasing indentation velocity (Sodhi, 1991). No general rule of thumb is yet available to estimate those periods based on given ice properties, so one has to rely on numerical simulations to obtain an indication for those.

## 6

The failure maps and ice conditions in this Chapter reflect model-scale conditions. In Full-scale conditions where the ice is often much thicker these failure maps change significantly as pointed out by Blanchet et al. (1988). For thick ice buckling will ultimately disappear from the failure maps as the critical buckling load increases roughly with the third power of the ice thickness, while the axial crushing or creep load increases more or less linearly. Figure 6.11 shows the failure map for an ice thickness of 1 meter, all other properties given in Table 6.1. Here it can already be seen that the aspect ratio for which buckling starts to occur shifts to higher values when compared to Figure 6.2, illustrating the expected change. In Full-scale also the Elastic modulus of ice is generally much larger than the model-scale value used for the simulations here which additionally increases the critical buckling load.

## 6.6. CONCLUSION

A model for prediction of the transient ice-structure dynamic interaction has been developed. The model is applicable to the ice interaction with vertically sided structures and accounts for creep and crushing in the contact zone as well as for the dynamic buckling caused by varying in time in-plane compressive force originated at the contact area. The creep and crushing are modeled by distributed along the contact area phenomenological lumped elements, whereas a wedge beam on elastic foundation is employed to account for flexural ice failure. Special attention has been paid to the conditions in the regime of mixed crushing and buckling-induced bending failure.

First, the model has been applied under the assumption that the structure is rigid and immovable. It has been shown that the model qualitatively reproduces the transitions

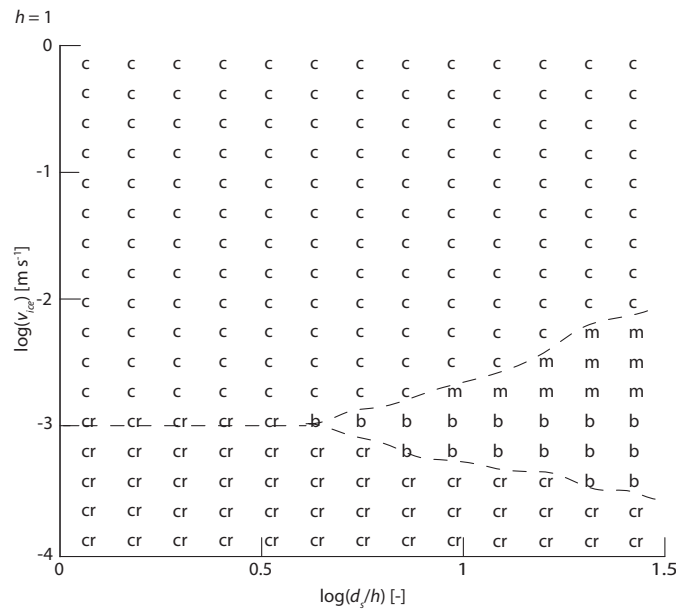


Figure 6.11: Numerically generated failure map for 1 meter thick model-ice based on the input values given in Table 6.1.

between the failure modes of creep, crushing, buckling and mixed crushing and buckling as observed experimentally in laboratory conditions. The dependence of global ice load on velocity for low and high aspect ratios also matches with trends observed in laboratory conditions. Also, the ice load time dependencies predicted by the model have shown to be qualitatively similar to those observed experimentally. Next, the model has been applied to study ice-induced vibrations in the regime of mixed crushing and buckling of the ice. Results of the study have shown that ice-induced vibrations can develop in such cases as long as the buckling failure does not occur within a period of intermittent crushing or frequency lock-in vibration. This buckling period is predicted to decrease with increasing velocity of the ice and width of the structure.

A combination of parameters of the model has been discovered which predicts the buckling failure of ice on a rigid structure but results in long period of sustained intermittent crushing on a flexible structure of the same size. This is understood as a consequence of the drops in ice load during intermittent crushing which allow the beam to bend back to the equilibrium in-plane position before the critical bending stress in the beam resulting in bending failure could be reached. Although it is challenging to predict conditions under which such scenario might occur, the obtained result clearly shows that buckling does not necessarily prevent the occurrence of ice-induced vibrations. The model developed in this Chapter predicts even that the opposite can happen, namely that ice-induced vibrations may occur under the conditions which would result in buckling should the structure be rigid.

In the next chapter practical application of the model is treated where the here presented model for creep-crushing and buckling is used in the discussion of design of model-scale tests for ice-induced vibrations.

# 7

## PRACTICAL APPLICATION

### 7.1. INTRODUCTION

In this chapter the focus is on the practical application of the theory and developed numerical model introduced in Chapters 5 and 6. On the basis of examples and discussion some directions for further research are identified, aimed at the development of a practical model for the prediction of the behavior of vertically sided structures in level ice conditions.

In Section 7.1 the implementation of Multi-Degree-Of-Freedom (MDOF) structural models is treated. A simplified Euler-Bernoulli beam model of an offshore wind turbine is implemented to illustrate the development of frequency lock-in at higher structural modes and the effect of additional, besides the ice load, external loads on the structure on the ice-structure interaction process. Implementation of two-dimensional structural models is discussed on the basis of a cylindrically shaped structure. Aspects to be considered in the modeling of multi-legged structures are briefly summarized.

In Section 7.2 variation of ice properties is treated. Two examples are given. The first example considers an ice sheet with finite mass acting against a large structure for which the interaction regime changes from continuous brittle crushing to intermittent crushing as the ice sheet loses its momentum and slows down. The second example shows how an inclusion of thick ice can briefly trigger frequency lock-in vibrations in ice conditions which otherwise result in continuous brittle crushing. This example serves to underline the importance of initial conditions for the development of frequency lock-in.

Finally in Section 7.3 the topic of design of model-scale experiments for ice-induced vibrations is covered. Current practice to scale according to keeping the Froude-number and Cauchy-number constant is consistent with the mechanism defined in this work. However, practical challenges arise in scaling the time and rate dependent deformation

---

Parts of this chapter have been published in the proceedings of the International Conference on Ocean, Offshore and Arctic Engineering, 2014 (Hendrikse et al., 2014).



processes in the ice making it very challenging to exactly scale the problem. An alternative option where only the geometrical parameters are scaled is introduced.

Summarizing conclusions are given in Section 7.4.

## 7.2. IMPLEMENTATION OF MDOF STRUCTURAL MODELS

In the previous Chapters of this thesis the structure is modeled as a single-degree-of-freedom oscillator. Such simplification is advantageous for research purposes and can be considered a reasonable simplification in case of model-scale experiments for which structures are often designed such that only the first natural mode plays a role during the ice-structure interaction. For studying the behavior of offshore structures more detailed structural models are required. In this Section application of the developed phenomenological model in combination with such detailed models is treated.

### 7.2.1. A SIMPLIFIED 1D BEAM MODEL OF AN OFFSHORE WIND TURBINE

A one-dimensional model of an offshore wind turbine is considered to illustrate the development of frequency lock-in at higher structural modes and the effect of additional, besides the ice load, external loads on the structure on the ice-structure interaction process. The in-plane motion is analyzed taking into account, in a simplified manner, various properties of the foundation, transition piece, and tower. A schematic overview of the model is given in Figure 7.1, whose main element is an Euler-Bernoulli beam for which the bending motion is governed by the following equation:

$$EI \frac{\partial^4 u_i(z, t)}{\partial z^4} + \frac{\partial}{\partial z} \left( T_i(z) \frac{\partial u_i(z, t)}{\partial z} \right) + K_i u_i(z, t) + (\rho_i A + \mu_i) \frac{\partial^2 u_i(z, t)}{\partial t^2} = F_i(t, u_i, \dot{u}_i) \quad (7.1)$$

where  $u_i(z, t)$  is the horizontal displacement of part  $i$  of the wind turbine [m],  $EI$  is the bending stiffness [ $\text{N m}^2$ ],  $\rho_i$  is the mass density of the wind turbine material [ $\text{kg m}^{-3}$ ],  $A$  is the cross-sectional area [ $\text{m}^2$ ],  $K_i$  is a linear soil stiffness acting on part 1 only [ $\text{N m}^{-2}$ ],  $\mu_i$  is the added mass of the submerged parts of the structure [ $\text{kg m}^{-1}$ ],  $F_i$  is the total non-linear external load acting on the structure [ $\text{N m}^{-1}$ ], and  $T_i(z)$  is the axial compressive force acting over the length of the beam, given by:

$$T_i(z) = g \left( M_{top} - A \rho_i \left( -z_i + \sum_{j=1}^i L_j \right) + A \sum_{j=i}^5 \rho_j L_j \right) \quad (7.2)$$

with  $M_{top}$  the mass of the rotor nacelle assembly [kg],  $g$  the gravitational constant, and  $z$  the coordinate along the length of the structure [m]. A detailed description of the governing equations is further given in Appendix C.

Input parameters for the structure are given in Table 7.1. These parameters result in the first four natural frequencies of 0.31, 2.21, 5.33, and 10.72 Hz. Figure 7.2 shows the first four modes of the structure. The ice action point is indicated in the Figure showing that modes 2 and 3 can extract energy relatively easily from the ice. Ice properties are given

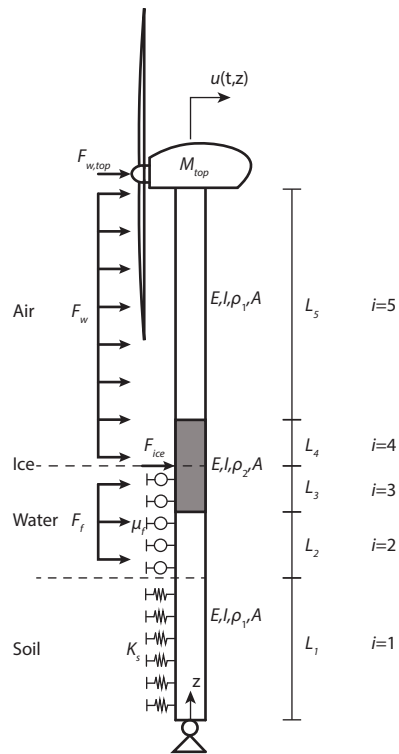


Figure 7.1: One-dimensional beam model of an offshore wind turbine in level ice conditions. The rotor-nacelle assembly is modeled as a point mass and the interaction between blades and wind is taken into account using the blade element theory in combination with momentum theory.

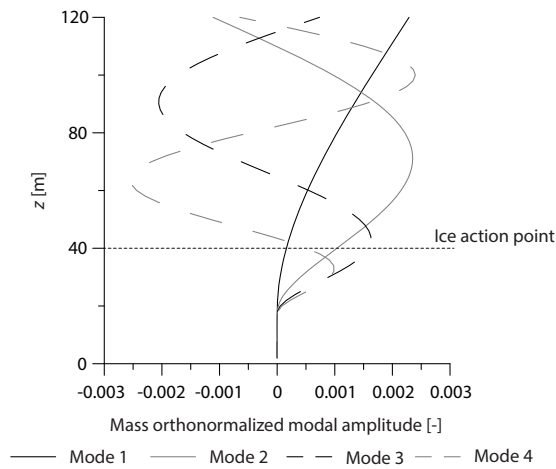


Figure 7.2: First four natural modes of the offshore wind turbine model. The mass-orthonormalized modal amplitudes are shown.

in Table 7.2 and are chosen similar to the freshwater ice used in Chapter 5, but with the standard deviation of the load taken higher to avoid the use of a large amount of ice elements in the simulation. The problem is solved in the time domain by application of the 4th order Runge-Kutta method. The beam is discretized using a central difference scheme.

## 7

In the first simulation only ice loads are considered and the wind speed and current velocity are taken equal to zero. Figure 7.3 shows the obtained structural displacement signals for ice sheet velocities of 0.01, 0.06, and 0.1  $\text{m s}^{-1}$ . Proportional damping is chosen resulting in the damping of the first four modes of 1, 1.5, 3.4, 6.7 % of critical. The low velocity shows intermittent crushing type of behavior however the low first natural frequency influences the sawtooth pattern quite significantly. For a velocity of 0.1  $\text{m s}^{-1}$  clearly continuous brittle crushing occurs and the displacement signal contains components of the lowest modes of the structure. For the velocity of 0.06  $\text{m s}^{-1}$  frequency lock-in occurs in the second mode of the structure. Although the first mode has lower damping, the second mode gets into lock-in more easily as the mass-orthonormalized modal amplitude is much higher at the location of ice action as shown in Figure 7.2. In this case the higher damping and natural frequency of mode 2, which normally would make frequency lock-in more difficult to develop in mode 2 compared to mode 1, are offset by the larger modal amplitude. Furthermore, frequency lock-in in mode 1 cannot develop as the second mode interferes by changing the relative velocity during a cycle of oscillation and thereby disturbing the process of contact area development in the ice.

Figure 7.2 shows that mode 3 is also easily excited by the ice and hence lock-in in mode 3 could be possible. The higher natural frequency and damping in the previous simulation did not allow it, but changing the damping values such that they become 1, 0.29, 0.43, 0.77 % of critical results in the displacement signals shown in Figure 7.4. Here frequency

Table 7.1: Input parameters for the offshore wind turbine model.

Parameter:	Input value:	Dimension:
$h$	0.4	[m]
$M_{top}$	$2.3 \times 10^5$	[kg]
$\rho_a$	1.225	[kg m <sup>-3</sup> ]
$\rho_f$	1025	[kg m <sup>-3</sup> ]
$\rho_1$	7850	[kg m <sup>-3</sup> ]
$\rho_2$	10350	[kg m <sup>-3</sup> ]
$\mu_f$	$4 \times 10^4$	[kg m <sup>-1</sup> ]
$K_s$	$2 \times 10^{10}$	[N m <sup>-2</sup> ]
$L_1, L_2, L_3, L_4, L_5$	20,10,10,10,70	[m]
$E$	$2.1 \times 10^{11}$	[N m <sup>2</sup> ]
$D$	5	[m]
$I$	2.38	[m <sup>4</sup> ]
$C_{D,f}$	1	[-]
$C_{D,a}$	0.8	[-]

Table 7.2: Input parameters for the ice used for the offshore wind turbine simulation.

Parameter:	Input value:	Dimension:
$d_{ref}$	5	[m]
$h_{ref}$	0.4	[m]
$v_{ref,high}$	0.1	[m s <sup>-1</sup> ]
$f_{ref,peak}$	20	[Hz]
$v_{trans}$	0.001	[m s <sup>-1</sup> ]
$F_{ref,max}$	$5 \times 10^6$	[N]
$F_{ref,std}$	$1 \times 10^5$	[N]
$F_{ref,mean}$	$1 \times 10^6$	[N]
$F_{ref,mean,2}$	$3 \times 10^6$	[N]
$t_{ref,peak}$	60	[s]
$c$	0.3	[-]

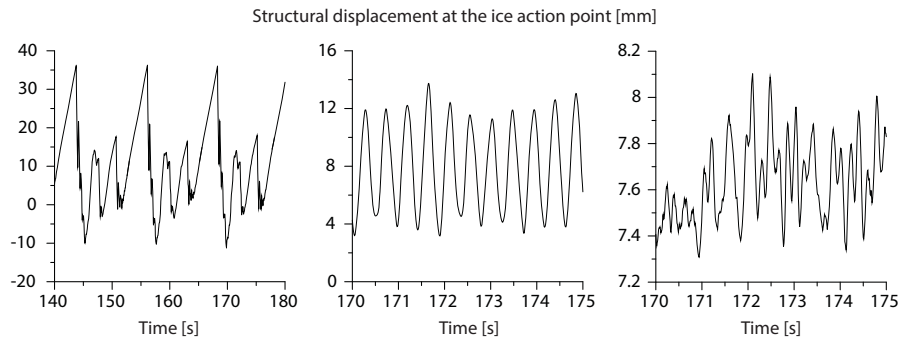


Figure 7.3: Displacement of the offshore wind turbine at the ice action point for ice velocities of 0.01, 0.06, and  $0.1 \text{ m s}^{-1}$ .

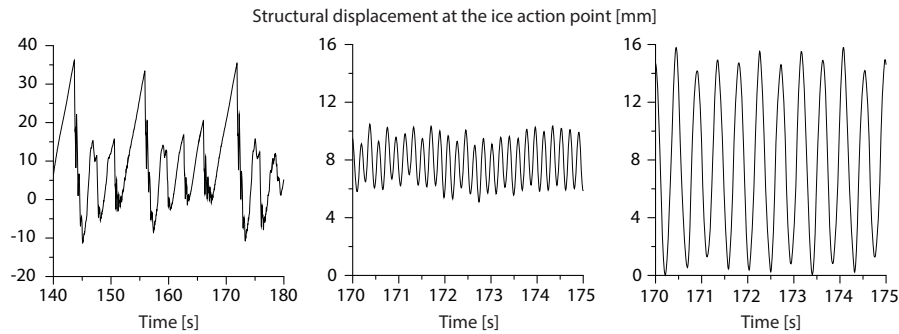


Figure 7.4: Displacement of the offshore wind turbine at the ice action point for ice velocities of 0.01, 0.06, and  $0.1 \text{ m s}^{-1}$  with lower damping in modes 2 and 3.

7

lock-in in mode 3 is first encountered at a velocity of  $0.06 \text{ m s}^{-1}$  and at  $0.1 \text{ m s}^{-1}$  lock-in in mode 2 occurs. Mode three is expected to lock at lower velocities as explained on the basis of parameter changes in Chapter 5. For the velocity of  $0.1 \text{ m s}^{-1}$  lock-in in mode 3 can no longer develop, but mode 2 having a lower natural frequency and low damping can still extract enough energy from the ice for sustained frequency lock-in to develop.

Figure 7.5 shows the resulting structural displacement signals at the ice action point when wind and current loading are included in the simulation. The mean wind speed is set at  $12 \text{ m s}^{-1}$  and the current speed equal to the ice velocity. The structural damping is the same as for the simulations shown in Figure 7.3. It can be clearly seen that the wind loading is active in this scenario from the changes in mean displacement in the signals for  $0.06$  and  $0.1 \text{ m s}^{-1}$  ice velocity. The second mode is interacting with the ice resulting in frequency lock-in type vibrations on top of the oscillations in mode one. It is interesting to see that frequency lock-in in this case develops in the second mode at a velocity of  $0.1 \text{ m s}^{-1}$ , while without wind no frequency lock-in is observed (Figure 7.3). This illustrates the importance of including all external actions on the structure when determining the

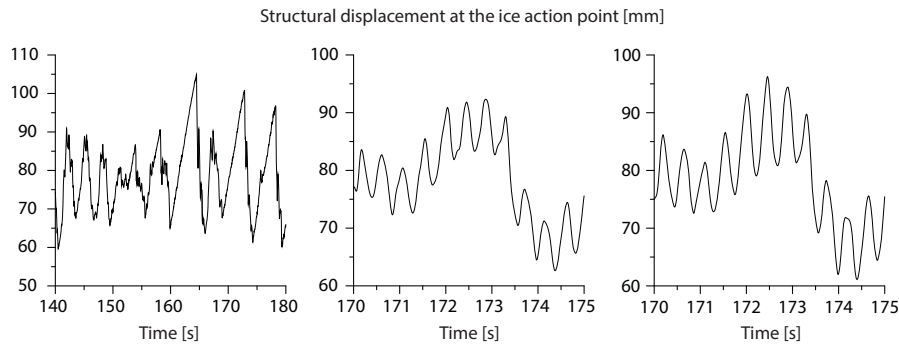


Figure 7.5: Displacement of the offshore wind turbine at the ice action point for ice velocities of 0.01, 0.06, and  $0.1 \text{ m s}^{-1}$  including wind and current loading.

structural response to ice loads.

### 7.2.2. STRUCTURAL SHAPE

Offshore structures often have either a cylindrical or rectangular cross-sectional shape at the waterline. In Chapter 5 and 6 a rectangular cross-section has been assumed for which the ice acts perpendicular to one of the faces. Under the assumption that the major component of structural motion only occurs in the direction of ice motion this allows to simplify the structure into a single-degree-of-freedom oscillator. For cylindrical structures or rectangular structures for which the ice does not approach the structure perpendicular to one of its sides, the approach presented in Chapter 5 can be used consistently provided the assumption is made that the major component of structural motion is in the direction of ice drift and when the reference measurements used to define the input of the model are consistent with the structural shape and angle of ice attack. In this way the effect of the shape is incorporated directly into the reference measurements.

When two dimensional in-plane motion is considered the phenomenological approach can no longer be applied straightforwardly. During interaction frictional sliding, confinement, formation of radial cracks, and in general the two dimensional deformation of- and stress in the ice play a role. The effect of these on the crushing process is difficult to assess. From panel measurements on the Norströmsgrund lighthouse it can be seen that the normal loads on the side panels during interaction are much less than those on panels facing the direction of ice motion (Bjerkas et al., 2013). Korzhavin's equation suggests that the load on a cylinder is about 90% of the load on a rectangle given by the shape factor introduced (Korzhavin, 1971). Solution of the two dimensional indentation problem is not attempted here. A simplified method to consider the side-side interaction simultaneously with the in-line action is presented. This should be considered as a first step in the development of a model that can be used to take side resistance of the ice into account during simulations.

The following approach is taken for a cylindrical structure, free to move in  $x$  and  $y$  di-

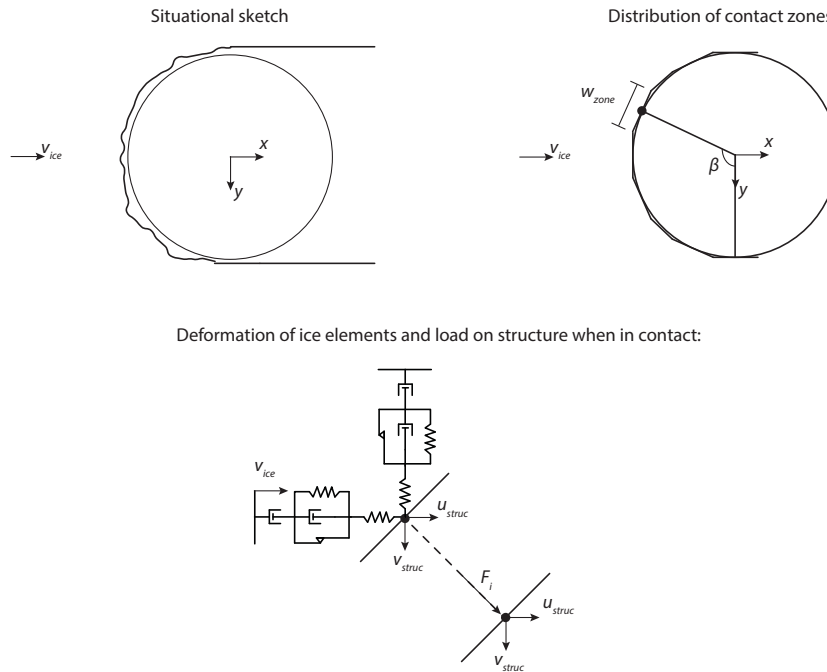


Figure 7.6: Overview of first step towards a two-dimensional model for ice action on vertically sided structures.

## 7

rection, interacting with an ice floe as shown in Figure 7.6. The circumference of the cylinder is split up into  $N$  interaction zones with a width  $w_{zone}$  equal to the width of an interaction zone obtained from reference measurements as defined in Chapter 5. For each zone two ice elements are introduced, one acting in the direction of the ice drift which is chosen to coincide with the global  $x$  direction, and one in the cross-wise direction, or the global  $y$  direction. Both elements only give compression resistance and the element in  $x$  direction is pushed forward with the ice velocity. Contact occurs when either the  $x$  offset or  $y$  offset is crossed at which point both elements are simultaneously in contact with the structure in that contact zone. The elements are not coupled and each of them results in a normal load on the structure as shown in Figure 7.6. Failure is set to occur when the total deformation equals the critical deformation, upon which point a normal offset is drawn. The frictional load is not taken into account and sliding is not considered. A detailed description of the governing equations can be found in Appendix C.

Figure 7.7 shows the dependence of the statistical measures of the ice load for a cylindrical structure modeled according to the approach defined, with the ice properties equal to those used for the consistency check in Chapter 5 and a diameter of 0.2 m. The results for a rectangular structure with a width of 0.2 m are also shown for comparison. The mean and maximum load in the direction of motion of the ice, the  $x$ -direction, are about 80 to 85 % of the load on the rectangular structure. In  $y$ -direction the mean load in

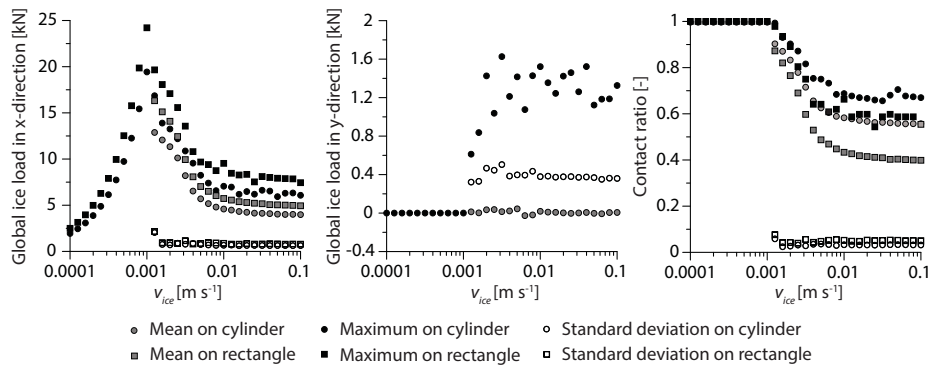


Figure 7.7: Left: Maximum, mean, and standard deviation of the global ice load as a function of ice sheet velocity for simulated ice action on a rigid cylindrical structure. Right: Maximum, mean, and standard deviation of the contact ratio (Equation 5.7) as a function of ice sheet velocity for the same simulation. The measures for a rectangular structure in the same ice conditions with a width equal to the diameter of the cylinder are also shown.

the crushing regime as well as the maximum load in the creep regime is approximately zero as expected. The mean and maximum contact ratio are higher for the cylindrical structure, indicating that a larger percentage of the elements is in general in contact, but these are mainly the side elements which do not contribute much to the global load in x-direction.

In Figure 7.8 the displacements of an arbitrary flexible structure with a diameter of 0.2 m, low damping  $\zeta = 0.01$ , a natural frequency of 2 Hz, and a low stiffness  $K_s = 2.5 \times 10^6$  [kg  $s^{-2}$ ] in the x-y plane are shown for intermittent crushing at 5  $mm s^{-1}$  velocity, frequency lock-in at 0.025  $m s^{-1}$  velocity, and continuous brittle crushing at 0.1  $m s^{-1}$  velocity. It can be seen that during intermittent crushing the majority of displacement is in global x-direction. During frequency lock-in the oscillations occur mainly in x-direction but some motion in y direction is observed as well resulting in a bit oval shaped displacement patterns. In continuous brittle crushing the displacements are generally smaller, but approximately equal in both directions in terms of magnitude.

The approach shown here should be considered as a first step towards the development of a two-dimensional model for level-ice vertically sided structure interaction where the ice does not act perpendicular to the structure surface. Further development should follow after the general method of definition of input parameters and theory have been validated. An experimental test campaign including a rigid cylinder and rectangular structure in the same ice conditions can provide the necessary data to progress towards a two dimensional model.

### 7.2.3. MULTI-LEGGED STRUCTURES

Implementation of the developed phenomenological model for the simulation of interaction between level ice and multi-legged structures can straightforwardly be done



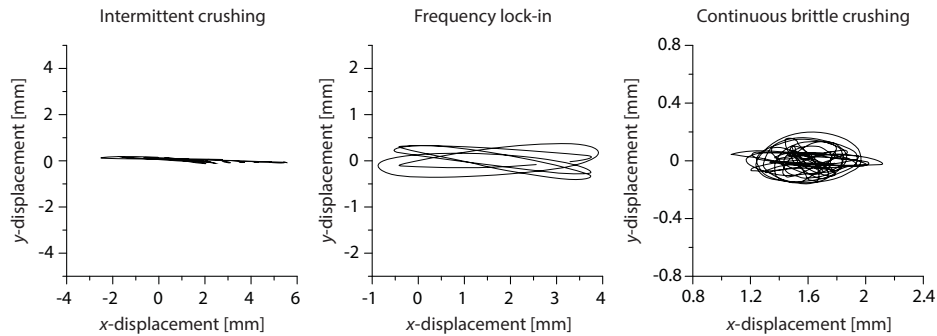


Figure 7.8: Structural displacement in the x-y plane during intermittent crushing, frequency lock-in, and continuous brittle crushing for a cylindrical structure.

based on the implementation for structures with multiple degrees of freedom, and structural shape as shown in the previous Sections of this Chapter. This allows to study the effects of ice action on single or multiple legs. An example of an implementation can be found in van den Berg (2013). Here important additional aspects which are specifically related to multi-legged structures are summarized.

Interaction between closely spaced piles, or legs of a multi-legged structure, needs to be considered for multi-legged structures. Three aspects which could be of importance are the formation of tensile cracks between the piles, rubble formation and blocking, and the dependence of the direction of ice loading on the leg spacing as illustrated in Figure 7.9.

Experimental studies show that the amount of rubble generation decreases with increasing inter-pile distance (Gürtner and Berger, 2006; Timco and Pratte, 1985). Pile interaction and rubble generation has been observed in these small-scale studies with pile spacing less than six pile diameters. Piles with a spacing of eight pile diameters showed no interaction. As the spacing between legs decreases, the forces in the direction of ice motion are smaller than the forces on a single leg in the same conditions. The force perpendicular to the direction of ice motion however increases resulting in a similar total force. During the interaction tensile cracks can form in the ice between the piles. Timco postulates that the cracks are caused by side motion of the interaction legs (Timco and Pratte, 1985).

A full-scale example of the formation of tensile cracks is the Confederations Bridge with a pile spacing of  $17.9D$  (Frederking et al., 2006). For such large leg spacing no interaction would be expected based on the experimental observations and therefore the tensile cracking in this case is unlikely to be caused by side motion of the piles. An alternative explanation could be the local slowing down of the ice sheet. There are not many observations and experimental results to consider but tensile cracking between the legs, rubble formation and blocking, and the change in direction of ice loading should be considered in the simulation as they are potential limiting the development of ice-induced vibrations.

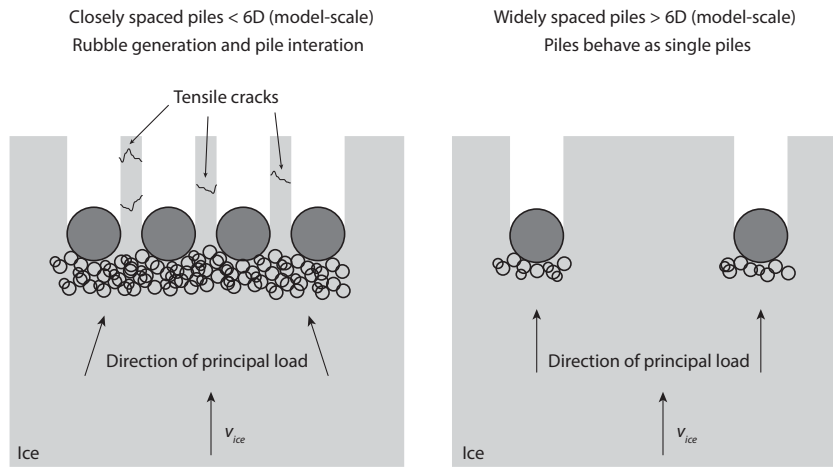


Figure 7.9: Left: Pile interaction for multi-legged structures indicating the development of tensile cracks, rubble formation, and the direction of principal loading. Right: No pile interaction.

Another aspect to consider is the effect of leg sheltering as illustrated in Figure 7.10. Depending on the amount of legs of a structure different sheltering scenarios can occur. In the wake of the legs first hit by the ice, free boundaries of the ice are formed which can give rise to splitting failure of the ice thereby unloading part of the structure. Splitting failure can be taken into account by the implementation presented by van den Berg (2013) which shows reasonable correspondence with model-scale experiments.

7

### 7.3. VARIATION IN ICE PROPERTIES

In the simulations shown and discussed in this thesis the ice properties are assumed constant over the duration of a single simulation. Taking the variability of ice properties into account could be of importance in longer simulations or for the generation of realistic load signals over the lifetime of structures. For effects of changes in micro properties of the ice such as temperature, grain size, and salinity, which directly affect the ductile and brittle behavior of the ice, on the interaction process more data is needed and changes to the model are necessary which should take into careful consideration the phenomenological nature of the model.

Variability in macro-properties such as ice thickness, global variations in strength, or indentation velocity can be rather easily considered. An example of an ice sheet slowing down against a structure, and an ice sheet with sudden change in ice thickness are shown here. Changes in strength can be implemented by varying the value of  $K_2$  around a mean value in the model, scaling the other element parameters accordingly. For such approach the correlation between local strength values should be considered in order to avoid getting too much randomness in the model, which is already included in the randomly drawn offset value after failure. Care should be taken that the ice behavior in the

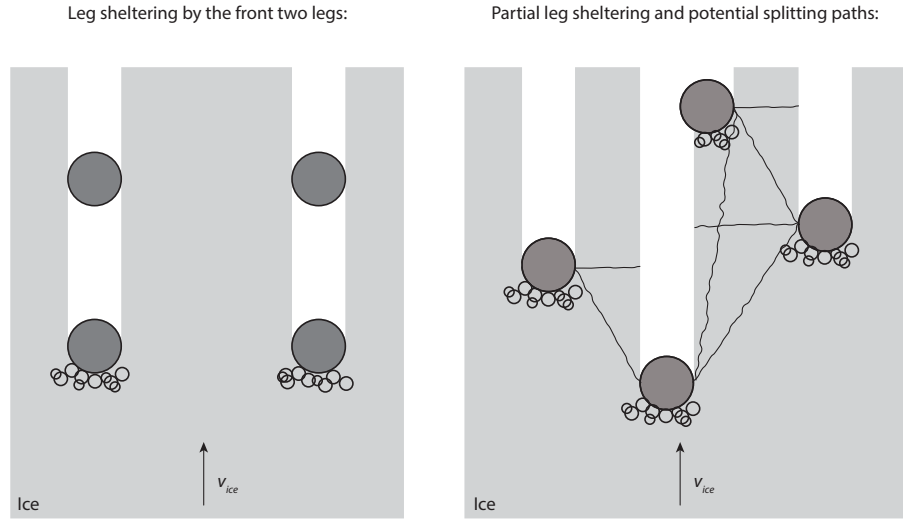


Figure 7.10: Leg sheltering examples for multi-legged structures. Left: two back legs in the wake of the front legs. Right: All legs at least partially loaded. Potential splitting paths are indicated.

model is still generally consistent with the experimental and full-scale observations on level ice action against vertically sided structures.

## 7

Simulation of a drifting ice sheet coming to a stop against a structure can be of interest for a quick study of the susceptibility of the structure to ice-induced vibrations over a wide range of velocities or the development of the large global loads which are associated with the event of an ice sheet slowing down. An example of such event is the Molikpaq May 12th 1986 event widely described in literature (Gagnon, 2012; Jefferies and Wright, 1988). For the simulation presented here an example structure is chosen with a natural frequency of 1.26 Hz, damping of 20 % of critical, and mass of  $160 \times 10^3$  tons reflecting the first mode of a large caisson like structure. The width of the structure is chosen as 80 m and ice thickness as 2.2 m. The maximum global load is set at 250 MN and the standard deviation limited to 0.1 to avoid the use of too many ice elements. Other ice properties and ratios between load levels are the same as used for the offshore wind turbine simulation at the beginning of this chapter (Table 7.2).

The mass of the ice is implemented as shown in Figure 7.11. The equation of motion for the ice mass given by:

$$\begin{aligned}
 M_{ice} \ddot{u}_{ice}(t) &= F_{driving}(t, u_{ice}, \dot{u}_{ice}) + F_{ice} \\
 F_{ice}(t, u_s, \dot{u}_s) &= \sum_{i=1}^N F_i(t, u_s, \dot{u}_s) \\
 F_i(t, u_s, \dot{u}_s) &= K_2 (u_{i,2}(t, u_s, \dot{u}_s) - u_{i,1}(t, u_s, \dot{u}_s))
 \end{aligned} \tag{7.3}$$

substituting  $\dot{u}_{ice}$  for  $v_{ice}$  in the equations of motion governing the ice elements (Equation 5.1). This way the effect of driving forces such as wind and currents, and inertia of

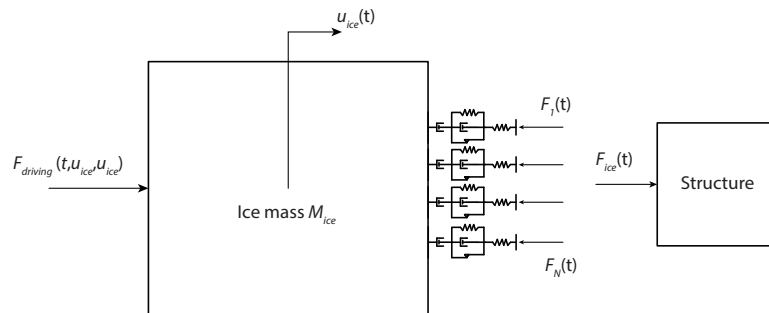


Figure 7.11: Implementation of a finite mass of an ice floe and driving forces in the model.

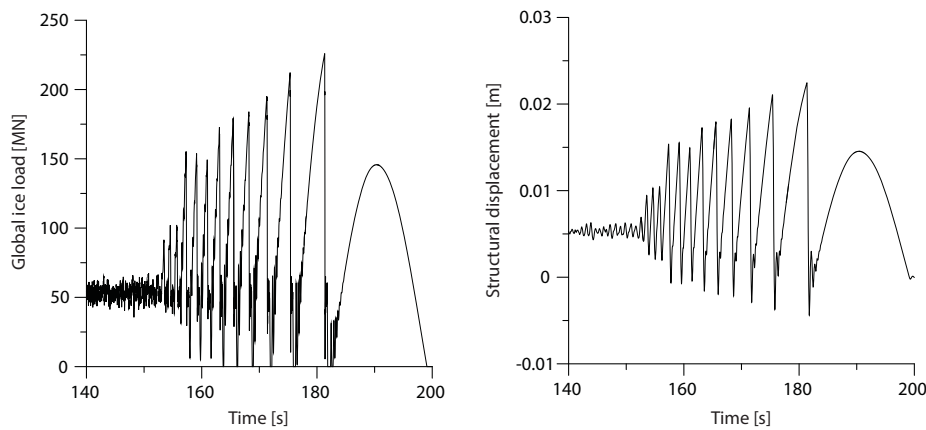


Figure 7.12: Simulation of a thick ice sheet coming to a stop against a large caisson structure. The initial velocity of the ice sheet is  $0.05 \text{ m s}^{-1}$

the ice can be easily incorporated. In the example presented next driving forces are not included.

For the simulation the initial velocity of the ice is taken as  $0.05 \text{ m s}^{-1}$  and the ice mass is  $2 \times 10^8$  tonnes roughly equal to the mass of a 7 by 15 square km ice floe of 2.2 m thickness. Results are shown in Figure 7.12. As the ice sheet slows down the interaction changes from continuous brittle crushing to intermittent crushing. Frequency lock-in is not observed, as a consequence of the large amount of structural damping. The peak load reaches a maximum right before the ice comes to rest against the structure. The maximum global load during the simulation gets close to the maximum possible global load of 250 MN. It is not likely that this value is reached as the ice sheet slows down and to develop the full maximum total load a long time of loading at a velocity equal to the transition velocity is required.

Local changes in thickness of the ice can have an effect on the duration and development

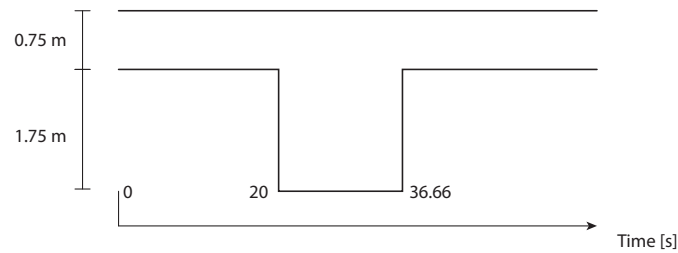


Figure 7.13: Simulation of an ice sheet with varying thickness acting against a structure.

of ice-induced vibrations, and in particular frequency lock-in. Especially after events which result in a high temporary load on the structure, such as an ice sheet at almost rest forming a large contact suddenly starting to move, a smooth previously formed circumferential cracked surface of the ice acting against the structure (Bjerkas et al., 2013), or the passing of a thick ice inclusion. An example is given for which the ice thickness changes according to the profile shown in Figure 7.13 representing a piece of rafted ice or an oversimplified consolidated layer of a ridge passing the structure. Structural properties are taken as 2.64 Hz, 2 % damping, and a mass of 11700 kg. The diameter is taken as 7.5 using the same ice as defined for the offshore wind turbine example in Table 7.2. The indentation velocity is chosen as  $0.03 \text{ m s}^{-1}$ .

The results are shown in Figure 7.14. What can be seen is that continuous brittle crushing is predicted to occur for the initial ice thickness of 0.75 m and the structure being at rest at  $t = 0$ . As soon as the thick ice inclusion hits the structure the global load increases significantly and interaction between the ice and structure leads to the development of frequency lock-in. When the thick inclusion has passed the global load drops, however the interaction persists and frequency lock-in is now observed in the ice conditions which previously led to continuous brittle crushing. This example illustrates the importance of initial conditions for the development of frequency lock-in which is a subject for future research.

## 7

### 7.4. DESIGN OF MODEL-SCALE EXPERIMENTS

Model-scale testing provides a unique way to investigate the behavior of structures in ice in a controlled environment. A general approach is to scale the structure and ice from the full-scale scenario to model-scale by the application of scaling laws. If observed, such scaling laws ascertain that the material behavior and observations in model-scale correspond to the material behavior and observations in full-scale.

With respect to ice-induced vibrations there exist several approaches and methods of scaling. For model-scale experiments a combination of scaling keeping the Froude number and Cauchy number constant is often applied (Palmer and Dempsey, 2009; Timco, 1984). A slightly different approach releasing some of the constraints on the scaling laws is proposed by Määttä et al. (2012). Yap (2011) proposes the application of Cauchy-

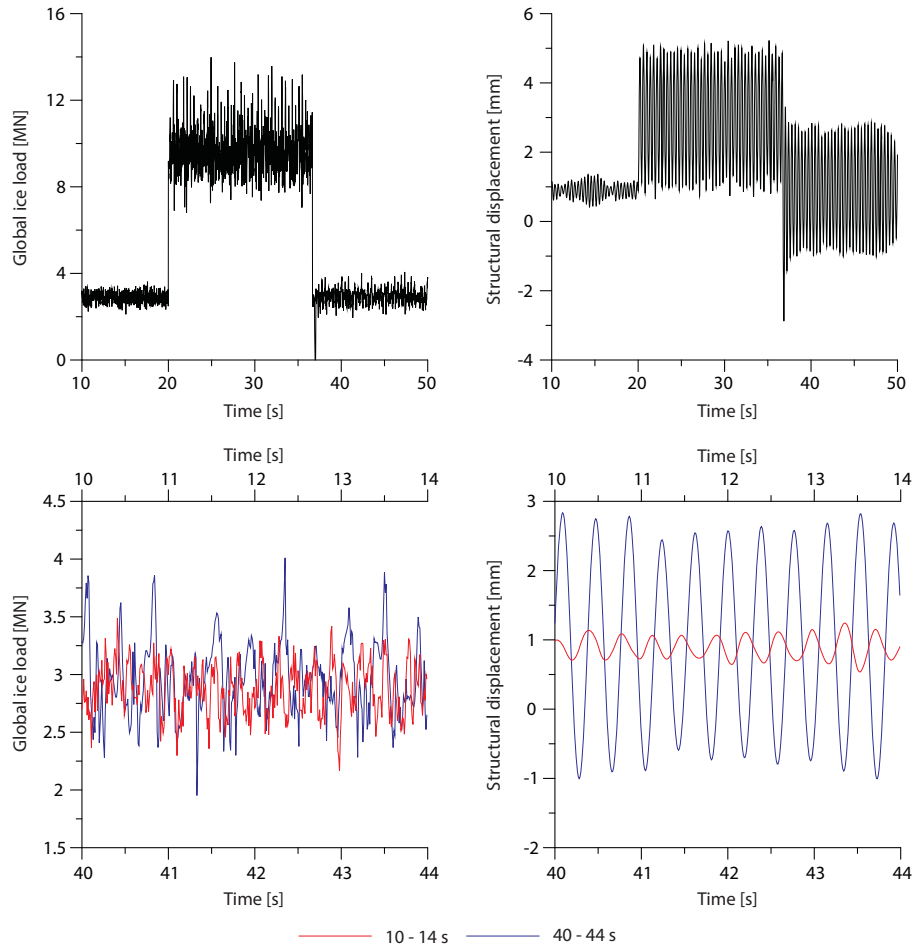


Figure 7.14: Simulation of an ice sheet with varying thickness acting against a structure. Top left: Global ice load. Top right: Structural displacement. Bottom left: Excerpts of global ice load for the intervals 10-14 seconds and 40-44 seconds. Bottom right: Excerpts of the structural displacement for the intervals 10-14 seconds and 40-44 seconds.

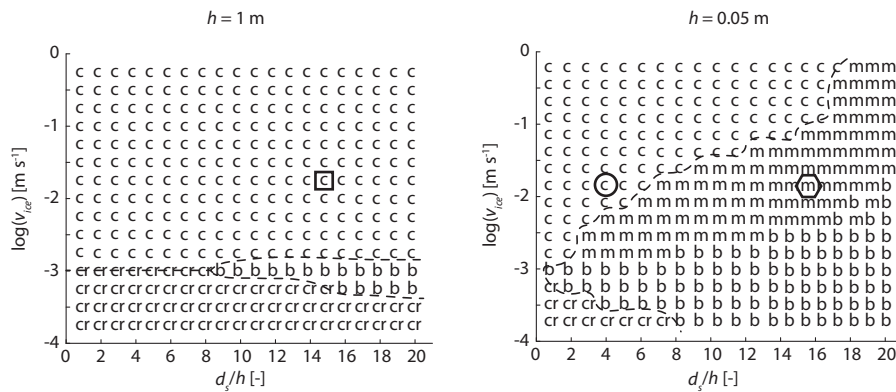


Figure 7.15: Failure map for 1 m thick and 0.05 m thin 'real' ice indicating the change of the buckling zone. Legend: cr – creep, c – crushing failure, b – buckling failure, m – mixed crushing and buckling failure. The square symbol indicates the full-scale event simulated in this Section. The hexagonal symbol indicates that mixed failure will occur when only the geometrical parameters are scaled. The circle symbol indicates the model-scale event simulated in this Section according to the here proposed scaling approach.

scaling and replica modeling based on a dimensionless parameter derived from recent experiments.

The application of scaling according to the Froude number and Cauchy number is consistent with the theory presented in this thesis when the failure modes of buckling, crushing, and creep are considered all together. A consequence of this approach is, however, the need of scaling down the ice strength and other material properties, as discussed already by Palmer and Dempsey (2009). The main challenge is to consistently scale all ice properties governing the time-dependent and loading rate dependent deformation behavior of the ice. This is almost impossible to control and, as a consequence, the interpretation of model-scale results for ice-induced vibrations should be done with great care.

An alternative choice which can be made is not to scale the ice, or so to say use 'real' ice. In this case only the geometry of the problem needs to be scaled down such as to fit in an ice basin. However, here the problem occurs that scaling down purely the geometry often results in buckling to be observed in the model-scale as illustrated by the failure maps in Figure 7.15 for an ice thickness of 1 m, the full-scale scenario, and an ice thickness of 0.05 m, the model-scale scenario. An interaction event at an aspect ratio of 15 and velocity of  $0.04 \text{ m s}^{-1}$  in full-scale, indicated by the rectangle symbol, could easily result in sustained frequency lock-in, however in model-scale mixed crushing and buckling occurs for this combination of parameters, indicated by the hexagon symbol, which gives a different response and loading as shown in Chapter 6. The ice properties used for generation of the failure maps in Figure 7.15 are shown in Table 7.3.

A choice which can be made is to drop the requirement of keeping a constant aspect ratio and to design the model-test for a reduced aspect ratio, thereby making sure that the observed failure mode remains crushing. This approach is illustrated here by numerical

Table 7.3: Input parameters for the ice used for the scaling simulations.

Parameter:	Input value:	Dimension:
$d_{ref}$	5	[m]
$h_{ref}$	0.4	[m]
$v_{ref,high}$	0.1	[m s <sup>-1</sup> ]
$f_{ref,peak}$	20	[Hz]
$v_{trans}$	0.001	[m s <sup>-1</sup> ]
$F_{ref,max}$	$10 \times 10^6$	[N]
$F_{ref,std}$	$1.6 \times 10^5$	[N]
$F_{ref,mean}$	$2 \times 10^6$	[N]
$F_{ref,mean,2}$	$5 \times 10^6$	[N]
$t_{ref,peak}$	60	[s]
$c$	0.3	[-]
$L$	40*h	[m]
$E$	$1 \times 10^9$	[N m <sup>-2</sup> ]
$\nu$	0.33	[-]
$\kappa$	10055	[kg (ms) <sup>-2</sup> ]
$\phi$	$\frac{\pi}{3}$	[rad]
$\chi$	512.5	[kg m <sup>-2</sup> s <sup>-1</sup> ]
$\rho$	950	[kg m <sup>-3</sup> ]
$\sigma_f$	$3 \times 10^5$	[N m <sup>-2</sup> ]
$\mu$	0.03	[-]



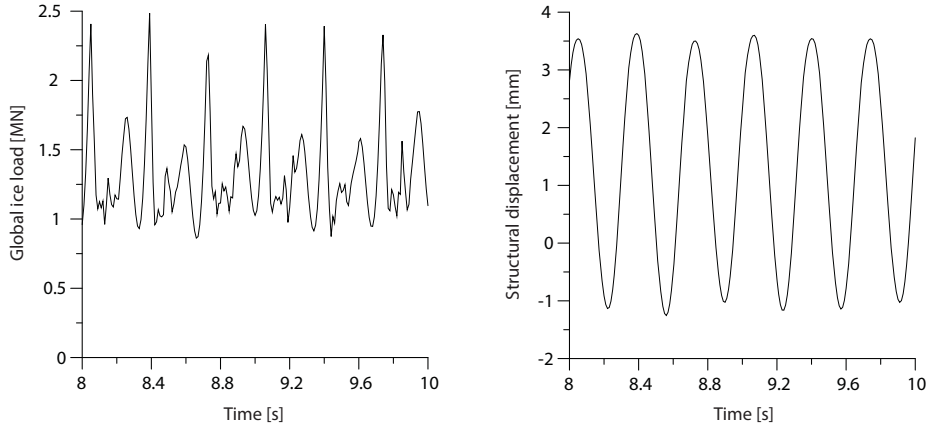


Figure 7.16: Simulation results showing frequency lock-in in full-scale conditions.

simulation. A full-scale structure with a natural frequency of 3 Hz, damping ratio of 1.5 % of critical, stiffness of  $15 \times 10^9 \text{ N m}^{-1}$ , and width of 15 m is placed in the 1 m full-scale ice conditions defined by the input parameters in Table 7.3 at a velocity of  $0.04 \text{ m s}^{-1}$ . The global load and displacement signals in Figure 7.16 show that frequency lock-in occurs for this structure in these ice conditions.

Model-scale conditions are now simulated by scaling the ice thickness down by an arbitrary factor  $\lambda_h = 20$  and the structural width by an arbitrary factor  $\lambda_w = 100$  such that the model-scale aspect ratio becomes 4 and the crushing failure mode is recovered as indicated by the circle symbol in Figure 7.15. To recover the same interaction in model-scale as observed in the full-scale simulation the dynamic properties of the structure need to be scaled according to:

$$\begin{aligned}
 M_{s,ms} &= \frac{M_{s,fs}}{\lambda_h \lambda_w} \\
 K_{s,ms} &= \frac{K_{s,fs}}{\lambda_h \lambda_w} \\
 C_{s,ms} &= \frac{C_{s,fs}}{\lambda_h \lambda_w}
 \end{aligned} \tag{7.4}$$

, where subscripts *ms* indicate model-scale properties and subscripts *fs* indicate full-scale properties. Results are shown in Figure 7.17. The ice load is scaled down significantly, but the structural displacement signal is the same as that for the full-scale scenario in terms of amplitude, mean value, and frequency. Frequency lock-in occurs in both cases. Figure 7.18 shows the results obtained for scaling according to the presented approach of a case of intermittent crushing at an ice velocity of  $0.01 \text{ m s}^{-1}$  for the same structure as used in the previous example. In this case the displacements of the structure for the full-scale case are the same as those for the model-scale case although with a phase-shift.

The two examples presented illustrate that the defined procedure can be an alternative

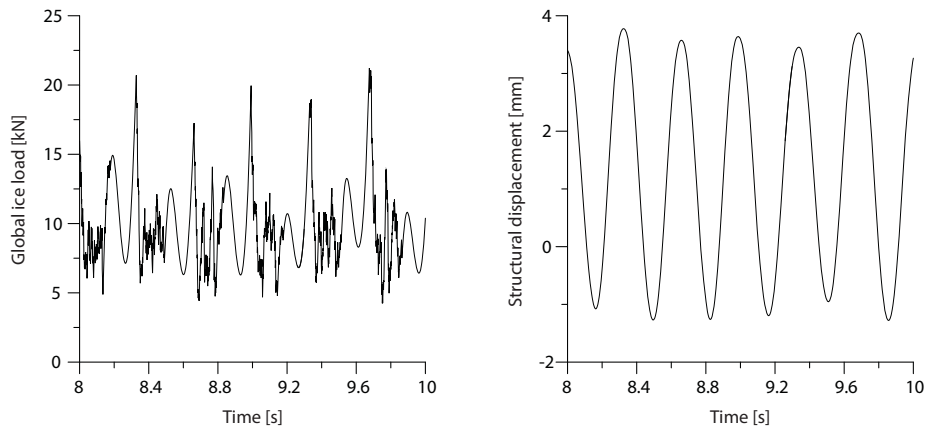


Figure 7.17: Simulation results showing frequency lock-in in scaled conditions.

approach to scaling which alleviates the need of scaling the ice properties. However it relies on several assumptions which require validation. The first assumption is that the global load levels depend linearly on ice thickness and structure width. The second assumption is that changes in ice thickness do not affect the ductile and brittle deformation and failure processes in the ice. Also, as the size of the structure is scaled down significantly the amount of individual contact zones decreases and the standard deviation of the ice load starts to play a more significant role as can be seen when comparing the global ice load signal in Figure 7.16 and Figure 7.17. When the standard deviation as a factor of the mean global load increases significantly the obtained results for structural oscillation in the model-scale scenario may change from those observed in full-scale.

7

## 7.5. CONCLUSION

On the basis of examples the practical application of the developed theory and model has been discussed and potential directions of further research have been identified.

Frequency lock-in can develop in higher structural modes for which the modal amplitude at the ice level is high and damping is sufficiently low. An example of a multi-degree-of-freedom model for an offshore wind turbine has been used to illustrate the development of lock-in in modes two and three. Higher modes which can easily be excited by the ice can disturb the lock-in process of lower modes by altering the relative velocity during the lock-in cycle.

It has been shown that it is important to consider external effects from wind, water, or other sources of excitation simultaneously with the ice-structure interaction in an integrated simulation. These actions can have both a limiting effect on the development of ice-induced vibrations, or an enabling effect.

Different structural shapes and angles of ice attack can be considered with the model as long as the main component of structural motion is assumed in the ice drift direction

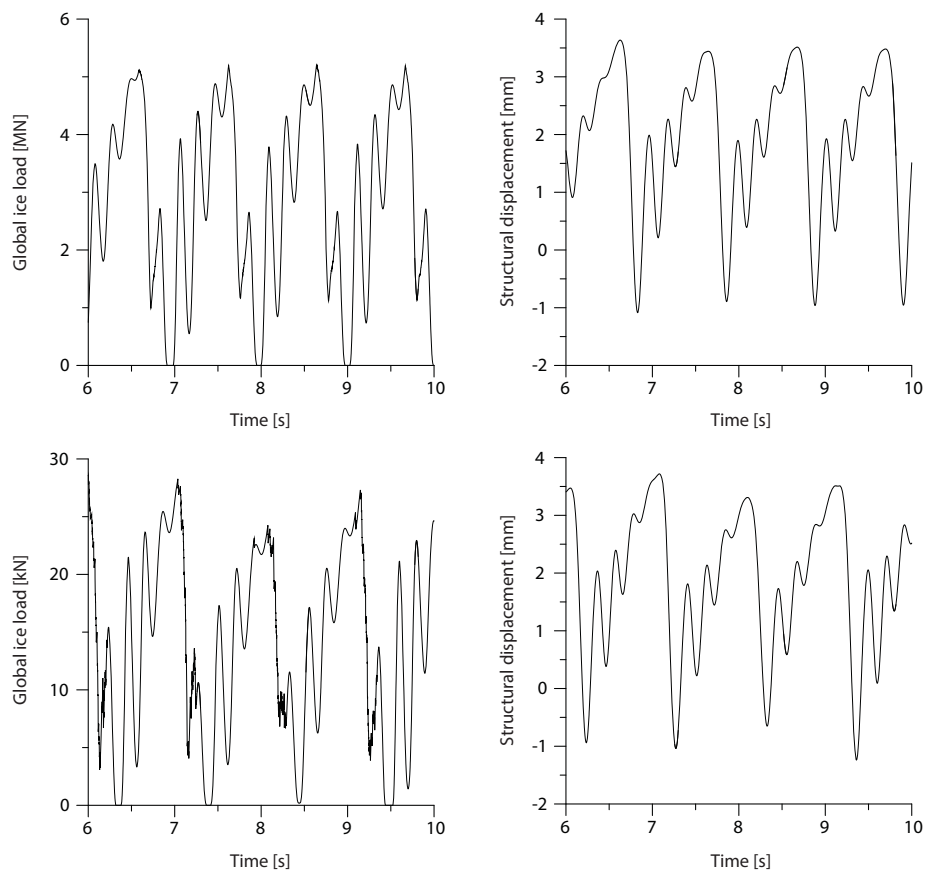


Figure 7.18: Simulation results showing intermittent crushing in full-scale (top) and scaled (bottom) conditions.

and reference measurements are used to define the input parameters of the model which contain the effect of shape and angle of attack. For a two dimensional analysis further steps need to be taken in order to assess the effect of friction, formation of radial cracks, and in general the two dimensionality of the problem. An approach containing some resistance in the cross-flow direction has been introduced which should be seen as a first step towards the development of a two dimensional model. Further development is proposed to follow after the general method of definition of input parameters and theory have been validated. For multi-legged structures additional aspects to take into consideration for modeling of the dynamic ice-structure interaction process have been identified as being leg-sheltering, splitting, and formation of rubble.

Variation of ice properties during a single simulation can be included taking into careful consideration the phenomenological nature of the model. For variations in micro-properties such as temperature, salinity, and density which have a direct effect on the ductile and brittle behavior of the ice additional experimental research is needed. Variation in macro properties such as velocity, thickness, or strength can be included in the model. An example of an ice sheet with a thick inclusion has been presented to show the importance of initial conditions for development of frequency lock-in.

Model-scale test design according to the commonly applied Froude-number and Cauchy-number scaling is consistent with the approach in this thesis. It is however challenging to scale the ductile and brittle deformation and failure processes in ice consistently and hence the interpretation of scale-model test results should be done with care. An alternative approach is to only scale the geometry of the problem, avoiding the occurrence of buckling for thinner ice at high aspect ratios by changing the aspect ratio. This results in a change in standard deviation of the global load which needs to be considered, but the dynamic behavior can be recovered as long as the standard deviation does not become dominant during the interaction. The defined approach can be a useful alternative, but requires validation following general validation of the approach and model presented in this thesis.



# 8

## CONCLUSION

The main goal of this work is to define a theory which explains the development of ice-induced vibrations and is consistent with the majority of experimental and full-scale observations available in literature. A secondary aim is to, based on this theory, develop a phenomenological model for the prediction of the interaction between level ice and vertically sided structures. To this end first a literature study into ice action on rigid structures and ice-induced vibrations has been performed and new forced-vibration experiments have been designed and executed. Based on these studies a governing mechanism has been defined and phenomenological model developed. The model has been consecutively applied to study the limiting effect of ice buckling on the development of ice-induced vibrations and illustrate the practical application of the theory.

The literature study of ice action against rigid vertically sided structures in Chapter 2 has resulted in the definition of several important observations. Level ice acting on a rigid vertically sided structure may fail in creep, crushing, bending, buckling, or a combination of those. Bending and buckling occur mainly for thin ice or wide structures, resulting in the formation of radial and circumferential cracks in the ice. Creep is the time dependent deformation and flow of material under permanent stress at low indentation velocities. Crushing is the failure mode which is primarily linked to the development of ice-induced vibrations. Crushing is characterized by the pulverization of ice in the contact zone and the spalling off of wedge shaped flakes at velocities above the transition from creep to crushing. The transition from creep to crushing is dependent on micro-properties of the ice, but no exact definition in terms of those yet exists. Around the transition the ice deforms in a ductile manner while at high velocities the ice deforms almost purely elastically. A key aspect is that the mean and maximum global load are largest for indentation with the transition velocity. Ice crushing is further characterized by discrete failure, local contact, and high pressure zones. The frequency of failure of single zones showed to be rather constant in small-scale experiments with only one or a few zones of contact, but to be distributed around a peak value in case of indentation against larger structures.

In Chapter 3 it has been shown that ice-induced vibrations can develop when flexible vertically sided structures are subject to loading by level ice. Three regimes can be generally distinguished being intermittent crushing, frequency lock-in, and continuous brittle crushing. Intermittent crushing and frequency lock-in are not observed for all structures and their development depends on the ratio between ice and structural properties. The intermittent crushing regime is defined by saw-tooth structural displacement and saw-tooth global ice load time traces. Experiments have shown that during interaction the local contact area and pressure increase as the relative velocity between ice and structure becomes small. Continuous brittle crushing occurs for all flexible structures at high enough ice sheet velocities for which the ice behavior is similar to crushing against rigid structures. Frequency lock-in vibrations can develop for flexible structures typically with a low natural frequency and low damping. The vibrations are characterized by being close to harmonic at a frequency slightly below a natural frequency of the structure. The maximum velocity of the structure at the location of ice action and in the direction of ice motion has been observed to roughly lie between 1 and 1.5 times the ice velocity. For structures with higher stiffness and natural frequency the boundaries of the lock-in regime can shift to lower velocities. During frequency lock-in the ice load is often greater in magnitude during the period the structure and ice move in the same direction as compared to the period during which they move in opposite direction.

Forced vibration experiments have been designed and executed with the aim to study the local deformation and failure process of level ice under harmonic deformation of the ice edge (Chapter 4). Such deformation closely resembles the deformation during frequency lock-in. During the experiments the development of the global ice load, local pressure, and local contact area have been measured by means of a tactile sensor. Results of the experiments have shown that the ice behavior changes according to the relative velocity between ice and structure. As soon as the relative velocity becomes small enough a change from brittle to transitional and ultimately to ductile behavior is observed. Both transitional and ductile behavior result in an increase of the global ice load which can be explained by an increase in contact area combined with an increase in mean contact pressure. The magnitude of the increase in contact area and mean contact pressure depends on the time period during which the relative velocity between ice and structure is small enough to cause ductile behavior of the ice. The longer the duration, the larger the contact area and mean pressure increase, resulting in a higher global load upon fracture of the ice. Indications of the trends in added mass and added damping of ice in interaction with a harmonically oscillating structure have been obtained. For low velocities the added damping is negative increasing towards zero for high velocities. The added mass is positive at low velocities and decreases with increasing velocity. A comparison between the trend in added damping with fluid-structure interaction shows that the trends are opposite, indicating that the mechanism causing vortex-induced vibrations to arise is physically different from the mechanism causing frequency lock-in in ice-induced vibrations.

On the basis of the literature study and performed indentation experiments a new theory has been proposed in Chapter 5. The theory is based on the observation that ice action on a vertically sided structure is controlled by the velocity dependent deformation and failure behavior of ice. At low loading rates a large contact area between ice and

structure can develop as a result of ductile deformations of the ice. This large contact area results in high global loads on the structure. At high loading rates the ice deforms more or less elastically and contact is only attained in specific zones of high pressure across the ice-structure interface. When a flexible structure is interacting with the ice the relative velocity changes continuously and when becoming small enough causes an increased contact area to develop resulting in an increased global load on the structure upon failure of the ice. Ice-induced vibrations develop when this increase in global load develops fast enough to provide sufficient energy to the structure.

A phenomenological model has been presented which captures the main aspects of the theory. The model includes, in a simplified manner, local contact between ice and structure, elastic deformation of ice, crushing failure, global creep, and ductile deformation resulting in an increase of contact between ice and structure at low loading rates. A method to define the model input parameters based on reference measurements has been developed. Based on simulation results and comparison with key observations from literature it has been concluded that the defined theory allows for a consistent model to be developed which captures level ice action on vertically sided structures in general.

Further validation of the theory and development of the model requires dedicated experiments to be performed. This is needed in order to make the step towards accurate quantitative comparison between simulation results and experiments or full-scale observations. It has been proposed that first tests with rigid structures focusing purely on the ice behavior during indentation for different velocities are executed.

As a next step the effect of ice buckling on the development of ice-induced vibrations has been studied theoretically in Chapter 6. To this end the developed phenomenological model has been expanded including a wedge beam on elastic foundation to account for the bending and buckling of the ice. Applicability of this model over a wide range of structural and ice conditions is illustrated based on the reproduction of model-scale failure maps of ice. The model can qualitatively capture the transitions from creep to crushing and buckling as a function of aspect ratio and velocity. Buckling failure has been shown to generally be a limiting case for ice-induced vibrations. A controlling factor is the buckling period, the time needed for buckling to lead to failure of the ice in bending, which has to be smaller than a period of intermittent crushing or frequency lock-in. An interesting combination of parameters has been discovered which predicts the buckling failure of ice on a rigid structure, but results in long period of sustained intermittent crushing on a flexible structure of the same size. This is understood as a consequence of the drops in ice load during intermittent crushing which allow the beam to bend back to the equilibrium in-plane position before the critical bending stress in the beam resulting in bending failure could be reached. Although it is challenging to predict conditions under which such scenario might occur, the obtained result clearly shows that buckling does not necessarily prevent the occurrence of ice-induced vibrations.

Finally the practical application of the developed theory and model has been illustrated on the basis of example calculations and discussion in Chapter 7. An example of a simplified multi-degree of freedom model of an offshore wind turbine illustrates how frequency lock-in can develop in higher structural modes. It has been shown that it is



important to consider external effects from wind, water, or other sources of excitation simultaneously with the ice-structure interaction in an integrated simulation. These actions can have both a limiting effect on the development of ice-induced vibrations, or an enabling effect. The implementation of structural shape and multi-legged structures has been discussed. Implementation of variation in ice properties has been discussed and an example of a thick ice inclusion has been presented to illustrate the importance of initial conditions for the development of frequency lock-in. Model-scale test design according to the common applied Froude-number and Cauchy-number scaling is consistent with the approach in this thesis. It is however challenging to scale the ductile and brittle deformation and failure processes in ice consistently and hence the interpretation of scale-model test results should be done with care. An alternative approach to only scale the geometry of the problem and changing the aspect ratio has been introduced. The defined approach can be a useful scaling alternative, but requires validation.

## REFERENCES

- Bjerkas, M., Meese, A., and Alsos, H. S. (2013). Ice-induced vibrations - observations of a full scale lock-in event. In *Proceedings of the 23rd International Offshore and Polar Engineering Conference*, pages 1272–1279, Anchorage, Alaska.
- Bjork, B. (1981). Ice-induced vibration of fixed offshore structures. part 2: Experience with Baltic lighthouses. Technical report, Ship Research Institute of Norway, Information Department.
- Blanchet, D., Churcher, A., Fitzpatrick, J., and Badra-Blanchet, P. (1988). An analysis of observed failure mechanisms for laboratory, first-year and multi-year ice. In *Proceedings of the IAHR Ice Symposium*, volume 3, pages 89–136, Sapporo, Japan.
- Blenkarn, K. A. (1970). Measurements and analysis of ice forces on Cook Inlet structures. In *Proceedings of the Second Annual Offshore Technology Conference*, volume II, pages 365–378, Houston, Texas.
- Brown, T. G. and Määttänen, M. (2009). Comparison of Kemi-I and Confederation Bridge cone ice load measurement results. *Cold Reg. Sci. Technol.*, 55:3–13.
- Dempsey, J. P. (2000). Research trends in ice mechanics. *Int. J. Solids Struct.*, 37:131–153.
- Dorival, O., Metrikine, A. V., and Simone, A. (2008). A lattice model to simulate ice-structure interaction. In *Proceedings of the ASME International Conference on Offshore Mechanics and Arctic Engineering*, volume 3, pages 989–996, Estoril, Portugal.
- Engelbrektson, A. (1983). Observations of a resonance vibrating lighthouse structure in moving ice. In *Proceedings of the Seventh International Conference on Port and Ocean Engineering under Arctic Conditions*, volume 2, pages 855–864, Helsinki, Finland.
- Eranti, E. (1992). Dynamic ice structure interaction, theory and applications. VTT Publications 90, VTT Technical Research Centre of Finland.
- Evers, K.-U. and Jochmann, P. (1993). An advanced technique to improve the mechanical properties of model ice developed at the hsva ice tank. In *Proceedings of the 12th International Conference on Port and Ocean Engineering under Arctic Conditions*, volume 2, pages 877–888, Hamburg, Germany.
- Finn, D. W., Jones, S. J., and Jordaan, I. J. (1993). Vertical and inclined edge-indentation of freshwater ice sheets. *Cold Reg. Sci. Technol.*, 22:1–18.
- Frederking, R. M. W., Kubat, I., and Prinsenberg, S. (2006). Response of two piers on Confederation Bridge to ice loading event of April 4, 2003. In *Proceedings of the 18th IAHR International Symposium on Ice*, volume 1, pages 231–238, Sapporo, Japan.

- Gabbai, R. D. and Benaroya, H. (2005). An overview of modeling and experiments of vortex-induced vibration of circular cylinders. *J. Sound Vib.*, 282:575–616.
- Gagnon, R. (2011a). An inside look at ice-crushing induced vibration and lock-in. In *Proceedings of the 21st International Conference on Port and Ocean Engineering under Arctic Conditions*, pages 339–348, Montreal, Canada.
- Gagnon, R. (2014). First lab tests of the blade runners concept for reducing ice induced vibration of structures. In *Proceedings of the 22nd IAHR International Symposium on Ice*, pages 282–289, Singapore.
- Gagnon, R. E. (1999). Consistent observations of ice crushing in laboratory tests and field experiments covering three orders of magnitude in scale. In *Proceedings of the 15th International Conference on Port and Ocean Engineering under Arctic Conditions*, volume 2, page 12, Helsinki, Finland.
- Gagnon, R. E. (2011b). A numerical model of ice crushing using a foam analogue. *Cold Reg. Sci. Technol.*, 65:335–350.
- Gagnon, R. E. (2012). An explanation for the Molikpaq May 12, 1986 event. *Cold Reg. Sci. Technol.*, 82:75–93.
- Gautier, D. L., Bird, K. J., Charpentier, R. R., Grantz, A., Houseknecht, D. W., Klett, T. R., Moore, T. E., Pitman, J. K., Schenk, C. J., Schuenemeyer, J. H., Sørensen, K., Tennyson, M. E., Valin, Z. C., and Wandrey, C. J. (2009). Assessment of undiscovered oil and gas in the arctic. *Science*, 324(5931):1175–1179.
- Gopalkrishnan, R. (1993). *Vortex-induced forces on oscillating bluff cylinders*. PhD thesis, Massachusetts Institute of Technology, Cambridge, USA.
- Gürtner, A. and Berger, J. (2006). Results from model testing of ice protection piles in shallow water. In *Proceedings of the 25th International Conference on Offshore Mechanics and Arctic Engineering*, volume 2, pages 693–698, Hamburg, Germany.
- Gürtner, A., Bjerkas, M., Forsberg, J., and Hilding, D. (2010). Numerical modelling of a full scale ice event. In *Proceedings of the 20th IAHR International Symposium on Ice*, page 16, At Lathi, Finland.
- Hansen, M., Sørensen, J., Voutsinas, S., Sørensen, N., and Madsen, H. (2006). State of the art in wind turbine aerodynamics and aeroelasticity. *Progress in Aerospace Sciences*, 42(4):285 – 330.
- Hendrikse, H. and Metrikine, A. (2015). Interpretation and prediction of ice induced vibrations based on contact area variation. *Int. J. Solids Struct.*, 75-76:336–348.
- Hendrikse, H. and Metrikine, A. (2016a). Edge indentation of ice with a displacement-controlled oscillating cylindrical structure. *Cold Reg. Sci. Technol.*, 121:100–107.
- Hendrikse, H. and Metrikine, A. (2016b). Ice-induced vibrations and ice buckling. *Cold Reg. Sci. Technol.*, 131:129–141.

- Hendrikse, H., Metrikine, A., and Evers, K.-U. (2012). A method to measure the added mass and added damping in dynamic ice-structure interaction: deciphering ice induced vibrations, part 3. In *Proceedings of the 21st IAHR International Symposium on Ice*, Dalian, China.
- Hendrikse, H., Renting, F. W., and Metrikine, A. V. (2014). Analysis of the fatigue life of offshore wind turbine generators under combined ice- and aerodynamic loading. In *Proceedings of the ASME 33rd International Conference on Ocean, Offshore and Arctic Engineering*, volume 10, page 10, San Francisco, California.
- Huang, G. and Liu, P. (2009). A dynamic model for ice-induced vibration of structures. *J. Offshore Mech. Arct. Eng.*, 131(1):6.
- Huang, Y., Shi, Q., and Song, A. (2007). Model test study of the interaction between ice and a compliant vertical narrow structure. *Cold Reg. Sci. Technol.*, 49:151–160.
- ISO19906 (2010). Petroleum and natural gas industries - arctic offshore structures.
- Izumiyama, K., Irani, M. B., and Timco, G. W. (1994). Influence of compliance of structure on ice load. In *Proceedings of the 12th IAHR International Symposium on Ice*, volume 1, pages 229–238, Trondheim, Norway.
- Izumiyama, K. and Uto, S. (1997). Ice loading on a compliant indenter. In *Proceedings of the 16th International Conference on Offshore Mechanics and Arctic Engineering*, volume 4, pages 431–436, Yokohama, Japan.
- Jefferies, M. G., Rogers, B., Hardy, M., and Wright, B. (2011). Ice load measurement on Molikpaq: methodology and accuracy. In *Proceedings of the 21st International Conference on Port and Ocean Engineering under Arctic Conditions*, volume 2, page 13, Montreal, Canada.
- Jefferies, M. G. and Wright, W. H. (1988). Dynamic response of 'Molikpaq' to ice-structure interaction. In *Proceedings of the Seventh International Conference on Offshore Mechanics and Arctic Engineering*, volume 4, pages 201–220, Houston, Texas.
- Jeong, S. and Baddour, N. (2008). Influence of flow on ice-induced vibrations of structures. In *Proceedings of the Canadian Society for Mechanical Engineering Forum*, page 5, Ottawa, Ontario.
- Jeong, S. and Baddour, N. (2010). Comparison of characteristic failure frequency models for ice induced vibrations. *JP Journal of Solids and Structures*, 4(3):115–137.
- Joensuu, A. and Riska, K. (1988). "jään ja rakenteen välinen kosketus" (contact between ice and structure). Report M-88, Helsinki University of Technology, Laboratory of Naval Architecture and Marine Engineering. (in Finnish).
- Jordaan, I. J. (2001). Mechanics of ice-structure interaction. *Eng. Fract. Mech.*, 68:1923–1960.

- Kamesaki, K., Yamauchi, Y., and Kärnä, T. (1996). Ice force as a function of structural compliance. In *Proceedings of the 13th IAHR International Symposium on Ice*, volume 1, pages 395–402, Beijing, China.
- Kärnä, T. (1992). A procedure for dynamic soil-structure-ice interaction. In *Proceedings of the Second International Offshore and Polar Engineering Conference*, pages 764–771, San Francisco, California.
- Kärnä, T., Andersen, H., Gürtner, A., Metrikine, A., Sodhi, D. S., Loo, M., Kuiper, G., Gibson, R., Fenz, D., Muggeridge, K., Wallenburg, C., Wu, J.-F., and Jefferies, M. G. (2013). Ice-induced vibrations of offshore structures - looking beyond ISO 19906. In *Proceedings of the 22nd International Conference on Port and Ocean Engineering under Arctic Conditions*, page 12, Helsinki, Finland.
- Kärnä, T. and Jochmann, P. (2003). Field observations on ice failure modes. In *Proceedings of the 17th International Conference on Port and Ocean Engineering under Arctic Conditions*, pages 839–848, Trondheim, Norway.
- Kärnä, T., Kamesaki, K., and Tsukuda, H. (1999). A numerical model for dynamic ice-structure interaction. *Comput. Struct.*, 72:645–658.
- Kärnä, T., Kolari, K., Jochmann, P., Evers, K.-U., Xiangjun, B., Määttänen, M., and Martonen, P. (2003). Ice action on compliant structures. Research Notes 2223, VTT Technical Research Centre of Finland.
- Kärnä, T. and Muhonen, A. (1990). Preliminary results from ice indentation tests using flexible and rigid indentors. In *Proceedings of the Tenth IAHR International Symposium on Ice*, volume 3, pages 261–275, Espoo, Finland.
- Kärnä, T. and Turunen, R. (1989). Dynamic response of narrow structures to ice crushing. *Cold Reg. Sci. Technol.*, 17:173–187.
- Kerr, A. D. (1978). On the determination of horizontal forces a floating ice plate exerts on a structure. *J. Glaciol.*, 20(82):123–134.
- KorzHAVIN, K. (1971). Action of ice on engineering structures. Technical Report Translation TL260, U.S. Army Cold Regions Research and Engineering Laboratory.
- Lu, W., Lubbad, R., and Løset, S. (2014). In-plane fracture of an ice floe: A theoretical study on the splitting failure mode. *Cold Reg. Sci. Technol.*, 110:77–101.
- Määttänen, M. (1978). On conditions for the rise of self-excited ice-induced autonomous oscillations in slender marine pile structures. Research Report No. 25, Winter Navigation Research Board.
- Määttänen, M. (1983). Modelling the interaction between ice and structures. In *Proceedings of the Seventh International Conference on Port and Ocean Engineering under Arctic Conditions*, volume 2, pages 745–759, Helsinki, Finland.

- Määttänen, M. (1988). Ice-induced vibrations of structures - self-excitation. In *Proceedings of the Ninth IAHR International Symposium on Ice*, volume 2, pages 658–665, Sapporo, Japan.
- Määttänen, M. (1999). Numerical model for ice-induced vibration load lock-in and synchronization. In *Proceedings of the 14th IAHR International Symposium on Ice*, volume 2, pages 923–930, Potsdam, New York.
- Määttänen, M. and Järvinen, E. (2003). Baltic aids-to-navigation ice-induced vibration measurements 2003. Report, Helsinki University of Technology.
- Määttänen, M., Løset, S., Metrikine, A., Evers, K.-U., Hendrikse, H., Lønøy, C., Metrikin, I., Nord, T., and Sukhorukov, S. (2012). Novel ice induced vibration testing in a large-scale facility: deciphering ice induced vibrations, part 1. In *Proceedings of the 21st IAHR international Symposium on Ice*, pages 946–958, Dalian, China.
- Määttänen, M., Marjavaara, P., and Saarinen, S. (2011). Ice crushing pressure distribution against a compliant stiffened panel. In *Proceedings of the 21st International Conference on Port and Ocean Engineering under Arctic Conditions*, Montreal, Canada.
- Matlock, H., Dawkins, W. P., and Panak, J. J. (1969). A model for the prediction of ice-structure interaction. In *Proceedings of the First Annual Offshore Technology Conference*, pages 687–694, Houston, Texas.
- Metrikin, I. (2011). Applicability of the Tekscan I-scan tactile sensor system for ice loads measurements in model testing. Hydralab-iv technical report, Norwegian University of Science and Technology, Trondheim, Norway.
- Michel, B. and Blanchet, D. (1983). Indentation of an s<sub>2</sub> floating ice sheet in the brittle range. *Ann. Glaciol.*, 4(1):180–187.
- Michel, B. and Toussaint, N. (1977). Mechanisms and theory of indentation of ice plates. *J. Glaciol.*, 19(81):285–300.
- Muhonen, A. (1996). *Evaluation of three ice-structure interaction models*. PhD thesis, Helsinki University of Technology.
- Muhonen, A., Kärnä, T., Eranti, E., Riska, K., Järvinen, E., and Lehmus, E. (1992). Laboratory indentation tests with thick freshwater ice. Research Notes 1370, VTT Technical Research Centre of Finland.
- Nakazawa, N. and Sodhi, D. S. (1990). Ice forces on flat, vertical indentors pushed through floating ice sheets. Special Report 90-14, US Army Cold Regions Research and Engineering Laboratory.
- Neill, C. R. (1976). Dynamic ice forces on piers and piles. An assessment of design guidelines in the light of recent research. *Can. J. Civ. Eng.*, 3:305–341.
- Nevel, D. E. (1980). *Bending and Buckling of a Wedge on an Elastic Foundation*, pages 278–288. Springer Berlin Heidelberg, Berlin, Heidelberg.

- Nordlund, O.-P., Kärnä, T., and Järvinen, E. (1988). Measurements of ice-induced vibrations of channel markers. In *Proceedings of the Ninth IAHR International Symposium on Ice*, volume 1, pages 537–548, Sapporo, Japan.
- Palmer, A. and Bjerkas, M. (2013). Synchronisation and the transition from intermittent to locked-in ice-induced vibration. In *Proceedings of the 22nd International Conference on Port and Ocean Engineering under Arctic Conditions*, page 12, Helsinki, Finland.
- Palmer, A. and Dempsey, J. (2009). Model tests in ice. In *Proceedings of the 20th International Conference on Port and Ocean Engineering under Arctic Conditions*, Lulea, Sweden.
- Palmer, A., Yue, Q., and Guo, F. (2010). Ice-induced vibrations and scaling. *Cold Reg. Sci. Technol.*, 60:189–192.
- Palmer, A. C., Goodman, D. J., Ashby, M. F., Evans, A. G., Hutchinson, J. W., and Ponter, A. R. S. (1983). Fracture and its role in determining ice forces on offshore structures. *Ann. Glaciol.*, 4:216–221.
- Peyton, H. R. (1968). Sea ice forces. In *Ice Pressures Against Structures, compiled by L. Gold and G. Williams, NRC Techn. Memo No. 92*, Ottawa, Canada.
- Ponter, A. R. S., Palmer, A. C., Goodman, D. J., Ashby, M. F., Evans, A. G., and Hutchinson, J. W. (1983). The force exerted by a moving ice sheet on an offshore structure part i. the creep mode. *Cold Reg. Sci. Technol.*, 8:109–118.
- Saeki, H., Hirayama, K., Kawasaki, T., Akagawa, S., Kato, K., Kamesaki, K., Saka, K., and Kurokawa, A. (1996). JOIA project of study on ice load. In *Proceedings of the 13th IAHR International Symposium on Ice*, volume 1, pages 17–27, Beijing, China.
- Sarpkaya, T. (1978). Fluid forces on oscillating cylinders. *J. Waterw. Port Coast. Ocean Eng.*, 104:275–291.
- Schulson, E. and Duval, P. (2009). *Creep and Fracture of ice*. Cambridge university press.
- Schwarz, J. (1971). The pressure of floating ice-fields on piles. In *Proceedings of the IAHR International Symposium on Ice and Its Action on Hydraulic Structures*, page 12, Reykjavik, Iceland.
- Schwarz, J. and Jochmann, P. (2001). Ice force measurements within the LOLEIF-project. In *Proceedings of the 16th International Conference on Port and Ocean Engineering under Arctic Conditions*, volume 2, pages 669–682, Ottawa, Canada.
- Sédillot, F. (1998). The Hibernia gravity base structure. In *Proceedings of the Eighth International Offshore and Polar Engineering Conference*, volume 1, pages 654–659, Montreal, Canada.
- Shih, L. (1991). Analysis of ice-induced vibrations on a flexible structure. *Appl. Math. Modelling*, 15:632–638.

- Shkhinek, K., Zhilenkov, A., Thomas, G., and Gebson, R. (2011). The vibration of fixed offshore structures under ice action. In *Proceedings of the SPE Arctic and Extreme Environments Conference & Exhibitions*, page 9, Moscow, Russia.
- Singh, S. K., Timco, G. W., Frederking, R. M. W., and Jordaan, I. J. (1990). Tests of ice crushing on a flexible structure. In *Proceedings of the Ninth Offshore Mechanics and Arctic Engineering Symposium*, volume 4, pages 89–94, Houston, Texas.
- Sodhi, D. S. (1979). Buckling analysis of wedge-shaped floating ice sheets. In *Proceedings of the Fifth International Conference on Port and Ocean Engineering under Arctic Conditions*, volume 1, pages 797–810, Trondheim, Norway.
- Sodhi, D. S. (1988). Ice-induced vibrations of structures. In *Proceedings of the Ninth IAHR International Symposium on Ice*, volume 2, pages 625–657, Sapporo, Japan.
- Sodhi, D. S. (1991). Effective pressures measured during indentation tests in freshwater ice. In *Proceedings of the Sixth International Cold Regions Engineering Specialty Conference*, pages 619–627, Hanover, New Hampshire.
- Sodhi, D. S. (1995). An ice-structure interaction model. *Mechanics of Geomaterial Interfaces*, 42:57–75.
- Sodhi, D. S. (1998). Nonsimultaneous crushing during edge indentation of freshwater ice sheets. *Cold Reg. Sci. Technol.*, 27:179–195.
- Sodhi, D. S. (2001). Crushing failure during ice-structure interaction. *Eng. Fract. Mech.*, 68:1889–1921.
- Sodhi, D. S. and Morris, C. E. (1984). Ice forces on rigid, vertical, cylindrical structures. Report 84-33, US Army Cold Regions Research and Engineering Laboratory.
- Sodhi, D. S., Takeuchi, T., Nakazawa, N., Akagawa, S., and Saeki, H. (1998). Medium-scale indentation tests on sea ice at various speeds. *Cold Reg. Sci. Technol.*, 28:161–182.
- Takeuchi, T., Sakai, M., Akagawa, S., Nakazawa, N., and Saeki, H. (2001). On the factors influencing the scaling of ice forces. In *Proceedings of the IUTAM Symposium on Scaling Laws in Ice Mechanics and Ice Dynamics*, pages 149–160, Fairbanks, Alaska.
- Timco, G. W. (1980). The mechanical properties of saline-doped and carbamide (UREA)-doped model ice. *Cold Reg. Sci. Technol.*, 3:45–56.
- Timco, G. W. (1984). Ice forces on structures: physical modelling techniques. In *Second IAHR State-of-the-art report on ice forces on structures, special volume of proceedings IAHR symp. on Ice*, page 34.
- Timco, G. W. (1987). Indentation and penetration of edge-loaded freshwater ice sheets in the brittle range. *J. Offshore Mech. Arct. Eng.*, 109(3):287–294.
- Timco, G. W. (1991). Laboratory observations of macroscopic failure modes in freshwater ice. In *Proceedings of the Sixth International Cold Regions Engineering Specialty Conference*, pages 605–614, West Lebanon, New York.



- Timco, G. W. (2007). Thickness dependence of the failure modes of ice from field observations on wide structures. In *Proceedings of the 19th International Conference on Port and Ocean Engineering under Arctic Conditions*, volume 1, pages 286–295, Dalian, China.
- Timco, G. W., Irani, M. B., Tseng, J., Liu, L. K., and Zheng, C. B. (1992). Model tests of dynamic ice loading on the Chinese JZ-20-2 jacket platform. *Can. J. Civ. Eng.*, 19:819–832.
- Timco, G. W. and Pratte, B. D. (1985). The force of moving ice cover on a pair of vertical piles. In *Proceedings Canadian Coastal Conference*, pages 349–362, St. John's, Newfoundland, Canada.
- Toyama, Y., Sensu, T., Minami, M., and Yashima, N. (1983). Model tests on ice-induced self-excited vibration of cylindrical structures. In *Proceedings of the Seventh International Conference on Port and Ocean Engineering under Arctic Conditions*, volume 2, pages 834–844, Helsinki, Finland.
- Tsuchiya, M., Kanie, S., Ikejiri, K., Yoshida, A., and Saeki, H. (1985). An experimental study on ice-structure interaction. In *Proceedings of the Seventeenth Annual Offshore Technology Conference*, pages 321–327, Houston, Texas.
- van den Berg, M. (2013). Ice induced vibration in jack-up structures. Master's thesis, Delft University of Technology.
- Venturella, M. A., Patil, M. J., and S., M. L. (2011). Modal analysis of the ice-structure interaction problem. *J. Offshore Mech. Arct. Eng.*, 133:18.
- Vershinin, S. A. and Iliady, A. A. (1990). A new approach to dynamic ice-flexible structure interaction. In *Proceedings of the Tenth IAHR International Symposium on Ice*, volume 3, pages 73–80, Espoo, Finland.
- Withalm, M. and Hoffmann, N. P. (2010). Simulation of a full-scale ice-structure-interaction by an extended Matlock-model. *Cold Reg. Sci. Technol.*, 60:130–136.
- Yap, K. T. (2011). *Level Ice-Vertical Structure Interaction: Steady-state self-excited vibration of structures*. Thesis for the degree of doctor of philosophy, National University of Singapore.
- Yue, Q., Bi, X., Zhang, X., and Kärnä, T. (2002). Dynamic ice forces caused by crushing failure. In *Proceedings of the 16th IAHR International Symposium on Ice*, volume 3, pages 231–237, Dunedin, New Zealand.
- Yue, Q., Qu, Y., Bi, X., and Kärnä, T. (2007). Ice force spectrum on narrow conical structures. *Cold Reg. Sci. Technol.*, 49:161–169.
- Yue, Q., Zhang, X., Bi, X., and Shi, Z. (2001). Measurements and analysis of ice induced steady state vibration. In *Proceedings of the 16th International Conference on Port and Ocean Engineering under Arctic Conditions*, pages 413–421, Ottawa, Canada.

- Yue, Q. J. and Li, L. (2003). Ice problems in Bohai Sea oil exploitation. In *Proceedings of the 17th International Conference on Port and Ocean Engineering under Arctic Conditions*, page 13, Trondheim, Norway.
- Ziemer, G. and Evers, K.-U. (2014). Ice model tests with a compliant cylindrical structure to investigate ice-induced vibrations. In *Proceedings of the ASME 33rd International Conference on Ocean, Offshore and Arctic Engineering*, volume 10, page 8, San Francisco, California.



# A

## POST-PROCESSING OF TACTILE SENSOR MEASUREMENTS

The obtained tactile sensor measurements presented in this work and corresponding article (Hendrikse and Metrikine, 2016a) have been post-processed in order to remove noise and obtain a better view of the dynamic processes at the ice-structure interface. The procedure of post-processing is illustrated in Figure A.1.

The first step in the process is to tare the measurements by removing the artificial load effects originating from statistical variation in the pressure sensor material and bending of the sensor around the cylindrical structure. This results in a “Nett” force as opposed to a “Gross” force which includes these variations. The tare procedure was carried out using the Tekscan® I-Scan software designed for this purpose.

The second step in the process is to identify the contact area which transfers the load from ice to the structure. During interaction the sensor picks up a load transferred by both intact ice as well as ice rubble on top and below the intact ice which is generated upon events of local fracture. The pressure by ice rubble has two observable effects on the global ice load. The first is an increase in the global load due to a static component generated by the presence of rubble resting against the structure. Due to its static nature and relatively constant magnitude throughout the experiment this pressure does not have a significant effect on the dynamic interaction process. The second effect is the transient pressure generated after the ice fractures, an event which occurs when material is pushed up and down from the interface. This pressure affects the global load at moments of fracture in the brittle regime, however it has no influence on the load in the ductile regime and its duration is short. Both these effects are considered to be of marginal importance to the dynamic ice-structure interaction problem and therefore filter the pressure generated by rubble from the results by defining a contact zone with

---

This Chapter has been published as part of an article in Cold Regions Science and Technology, 2016 (Hendrikse and Metrikine, 2016a).

a height of 35 mm. This zone covers more than half the thickness of the ice and encompasses the wedge shaped front of the ice edge. The effect of this approach on the obtained global load signal is shown in Figure A.1. For each experiment it is verified that the reduction in global load by application of this procedure on average does not exceed more than 2% in the ductile regime and 5% in the brittle regime. The difference in percentages was chosen because of the larger effect of rubble generated by fracture on the global load in the brittle regime when compared to the ductile regime. The frequency content of the signal as well as the overall characteristics are not influenced by this approach as shown in Figure A.1.

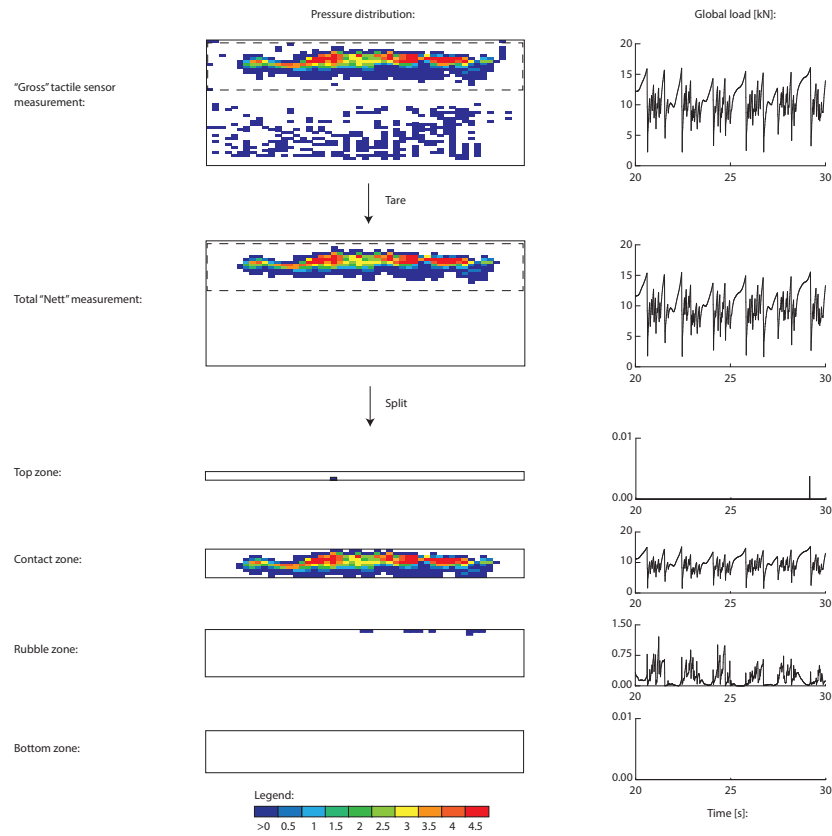


Figure A.1: Post-processing of tactile sensor measurements. First a tare of the measurements is executed resulting in a reduction of noise in the measurements which occurs as a result of bending of the tactile sensor and natural statistical variations in the material. Second the pressure by ice rubble is removed in order to identify the contact area which transfers the majority of the load from the ice to the structure. The dashed box indicates an area covered by the thickness of the ice sheet and half the circumference of the cylinder. The contact zone contains the data considered for further evaluation.



# B

## DETERMINATION OF ADDED MASS AND ADDED DAMPING

This Appendix deals with the theory for determination of added mass and added damping from data obtained from forced vibration experiments. In the first Section the theoretical approach is introduced. In Section 2 the problems which were encountered during forced vibration experiments in ice are described, as well as the attempted solutions.

### B.1. THEORY FOR DETERMINATION OF ADDED MASS AND ADDED DAMPING

The basic components of a forced vibration setup in ice are shown in Figure B.1. An ice sheet moves with a constant velocity  $v_{ice}$  [m s<sup>-1</sup>] towards a rigid indenter of whose motion  $u_f(t)$  [m] is controlled to be harmonic with a fixed amplitude and frequency. During the experiment the global ice load on the structure  $F_{ice}(t)$  [N] and displacement are simultaneously measured at the ice level. The latter merely serves as a check of the prescribed motion of the structure. The obtained load signal can be analyzed to show the components in phase with the velocity and acceleration of the structure, which represent the added damping and added mass of the ice during ice-structure interaction respectively. The obtained results can be used to study the stability of the prescribed harmonic motion.

Without loss of generality, the co-ordinate of the structure during the forced vibration experiment can be described by:

$$u_f(t) = A_f \sin(\omega_f t) \tag{B.1}$$

---

Parts of this Chapter have been published in the proceedings of the IAHR international Symposium on Ice 2010 (Hendrikse et al., 2012).



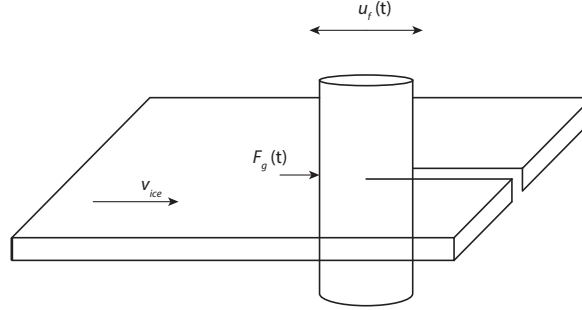


Figure B.1: Illustration of a forced vibration experiment in ice.

where  $A_f$  [m] and  $\omega_f$  [ $s^{-1}$ ] are the controlled amplitude and angular frequency of the structure, and  $t$  is time [s].

The global load on the structure from the ice as a result of this motion,  $F_{ice}(t)$ , is measured during the experiment. The spectral component of this global load at the frequency of oscillation of the cylinder is characterized by the following two expressions:

$$F^{sin}(\omega_f) = \frac{2}{T_f} \int_{t_0}^{t_0+T_f} F_{ice}(t) \sin(\omega_f t) dt \quad (B.2)$$

$$F^{cos}(\omega_f) = \frac{2}{T_f} \int_{t_0}^{t_0+T_f} F_{ice}(t) \cos(\omega_f t) dt \quad (B.3)$$

where  $F^{sin}$  is the part of the global load in phase with the acceleration of the structure [N], and  $F^{cos}$  is the part in phase with the velocity of the structure [N].  $T_f$  is the period of controlled oscillation of the structure [s], and  $N$  is the number of periods in the measured global load signal which are included in the integration [-]. Note that though the measured force may be not exactly periodic, Equation (B.2) and (B.3) characterize the chosen spectral component of the global load rather accurately.

If the motion of the structure is purely harmonic, the added mass can be determined from the component of the ice load in phase with the acceleration:

$$M_{add} = \frac{F^{sin}(\omega_f)}{A_f \omega_f^2} \quad (B.4)$$

where  $M_{add}$  is the added mass [kg].

Similarly, the added damping can be determined from the component of the global load in phase with the velocity:

$$C_{add} = -\frac{F^{cos}(\omega_f)}{A_f \omega_f} \quad (B.5)$$

where  $C_{add}$  is the added damping [ $kg s^{-1}$ ].

## B.2. PROBLEMS ENCOUNTERED DURING THE FORCED VIBRATION EXPERIMENTS

The obtained data from the forced vibration experiments consists of time traces (row data) of the ice load and displacement. The global ice load is found by integration of the local pressures, obtained from the tactile sensor data, over their respective area of action. For each pressure area the component in the direction of forced motion is taken into account to correct for the fact that the pressures are measured normal to the surface of the cylinder. A dynamic friction coefficient of 0.1 is used to account for the friction between ice and the outer steel surface of the cylinder. During and after the tests several problems were encountered influencing the results of the intended analysis. The problems encountered and the attempted solutions are discussed in the following paragraphs.

The tactile sensor measurements and laser displacement measurements were facilitated by two different computers and were started at different time moments resulting in a loss of synchronization in time between the load and displacement signals. Also the durations of the signals are unequal. This problem has been solved by visually inspecting both the displacement signal and the force signal and synchronizing the point of first failure, the point where the indentation is stopped and the points of major ice failure. Because the phase shift between the force and displacement signal is of key importance to the determination of added mass and added damping, this procedure resulted in a small loss of quantitative accuracy of the results.

The large ice load caused the actuator to slip upon first contact resulting in a shift of the equilibrium position of its motions. This affects the mean displacement of the structure, but does not affect the results significantly as the amplitude and frequency of forced vibration remained approximately equal to the desired ones. In order to obtain a sinusoidal signal with a zero mean value for the displacement, the signal is shifted up or down, depending on the direction of the occurring slip, over the range where the interaction is present.

The large ice load caused that the actuator was incapable of exactly controlling the acceleration of the structure. This affects the analysis significantly as for a non-sinusoidal motion of the cylinder the method described in Section B.1 is not valid. Therefore it has to be concluded that here a loss of quantitative accuracy of the results is obtained. However, since the periodicity and amplitude of the motion are approximately maintained an identification of trends in the added mass and added damping is still considered to be possible.

The displacement signals obtained from the experiments are not completely sinusoidal. To take this into account the general approach to the identification of the added mass and added damping as described in the previous Section is modified. As an additional first step the part of the measured displacement signal in phase with the desired sinusoidal displacement signal is calculated:

$$u^{sin}(\omega_f) = \frac{2}{T_f} \int_{t_0}^{t_0+T_f} u_m(t) \sin(\omega_f t) dt \quad (\text{B.6})$$

Table B.1: Reduced test matrix showing amplitude of vibration at ice action point, velocity of indentation and frequency of vibration of the tests for which the added mass and added damping components could be determined approximately. Multiple test signals are available for the frequencies marked with an asterisk.

$A_f$ [mm]	11	22	44	66
$v_{ice}$ [mm s <sup>-1</sup> ]	$\omega_f$ [s <sup>-1</sup> ]	$\omega_f$ [s <sup>-1</sup> ]	$\omega_f$ [s <sup>-1</sup> ]	$\omega_f$ [s <sup>-1</sup> ]
20	1.8	0.9	0.45	
30	2.7			
40	3.6*	1.8	0.9	
50	4.5*	2.25		0.75
60	5.4		1.35	
70	6.3*	3.15		
100		4.5		

where  $u_m(t)$  is the measured displacement obtained from the laser signals [m]. For a perfect sinusoidal pattern with the exact forced frequency and amplitude Equation B.6 would yield:

$$u^{sin}(\omega_f) = A_f \quad (B.7)$$

For a non-perfect signal a reduced or increased amplitude is found without jeopardizing the phase shift, therefore the parameter can be used to give a measure for the resemblance of the actual signal with the perfect sine. Test series where the difference between  $u^{sin}$  and  $A_f$  is considered to be too large (>5%) are removed from the results. For the remaining signals the procedure as described in Section B.1 is followed.

In some of the cases the measuring range of the laser sensors showed to be insufficient to record the large occurring displacements. This happened when the slip of the actuator became very large resulting in a large offset of the mean displacement. For some of the cases the identification of added mass and added damping could still be performed as only one of the two lasers showed to be out of range. The remaining cases could not be used for further analysis and were therefore discarded. The reduced test matrix containing only the results which could be used for the analysis is shown in Table B.1.

# C

## IMPLEMENTATION OF STRUCTURAL MODELS

In this Appendix the governing equations for the structural models used in Chapter 7 are defined. The first Section contains the equations for the simplified offshore wind turbine model. The second Section contains the equations for the cylindrical structure model.

### C.1. IMPLEMENTATION OF A SIMPLIFIED OFFSHORE WIND TURBINE

A one-dimensional beam model of an offshore wind turbine is considered to illustrate the development of frequency lock-in in higher structural modes and the effect of additional, besides the ice load, external loads on the structure on the ice-structure interaction process. The in-plane motion is analyzed taking into account, in a simplified manner, various properties of the support structure, transition piece, and tower. A schematic overview of the model is given in Figure C.1, whose main element is an Euler-Bernoulli beam for which the lateral motion is governed by the following equation of motion:

$$EI \frac{\partial^4 u_i(z, t)}{\partial z^4} + (\rho_i A + \mu_i) \frac{\partial^2 u_i(z, t)}{\partial t^2} + \frac{\partial}{\partial z} \left( T_i(z) \frac{\partial u_i(z, t)}{\partial z} \right) + K_i u_i(z, t) = F_i(\dot{u}_i, u_i, t) \quad (\text{C.1})$$

where  $u_i(z, t)$  is the lateral displacement of part  $i$  of the wind turbine [m],  $EI$  is the bending stiffness [ $\text{N m}^2$ ],  $\rho_i$  is the mass density of the wind turbine material [ $\text{kg m}^{-3}$ ],  $A$  is the cross-sectional area [ $\text{m}^2$ ],  $K_i$  is a linear soil stiffness acting on part 1 only [ $\text{N m}^{-2}$ ],  $\mu_i$  is the added mass of the submerged parts of the structure [ $\text{kg m}^{-1}$ ],  $F_i$  is the total non-linear external load acting on the structure [ $\text{N m}^{-1}$ ], and  $T_i(z)$  is the axial compressive force acting over the length of the beam, given by:

$$T_i(z) = g \left( M_{top} - A \rho_i \left( -z_i + \sum_{j=1}^i L_j \right) + A \sum_{j=i}^5 \rho_j L_j \right) \quad (\text{C.2})$$

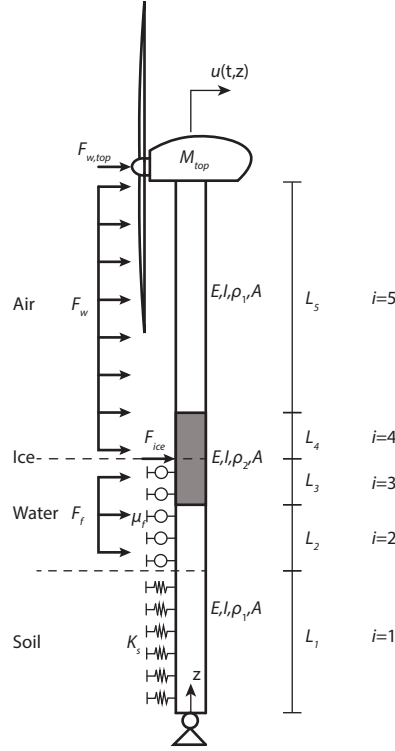


Figure C.1: One-dimensional beam model of an offshore wind turbine in level ice conditions. The rotor-nacelle assembly is modeled as a point mass and the interaction between blades and wind is taken into account using the blade element theory in combination with momentum theory.

with  $M_{top}$  the mass of the rotor nacelle assembly [kg],  $g$  the gravitational constant, and  $z$  the coordinate along the length of the structure [m].

Part one ( $i = 1$ ) of the model represents the pile section embedded in the soil. The boundary condition at the bottom is chosen as pinned:

$$u_1(0, t) = \frac{\partial^2 u_1(z, t)}{\partial z^2} \Big|_{z=z_1} = 0 \quad (C.3)$$

The true interaction at the pile tip is complex and therefore the choice of a pinned connection might seem arbitrary. A completely free boundary indeed would be more accurate, however it was found that a restraint on the displacement is needed in order to describe the displacement shape of the structure correctly which resulted in the choice of a pinned connection.

Part two ( $i = 2$ ) of the model represents the submerged part of the foundation pile which runs from the seabed to the transition piece. Over this length the added mass of sur-

rounding water is taken into account directly in the equation of motion by means of  $\mu_f$ . Interaction with the fluid is further described by application of Morison's equation for the drag on a submerged cylinder:

$$F_f(z, t) = \frac{1}{2} \rho_f C_{D,f} D (v_f - \dot{u}_i(z, t)) |v_f - \dot{u}_i(z, t)| \quad (C.4)$$

where  $v_f$  is the assumed constant current velocity [ $\text{m s}^{-1}$ ],  $\rho_f$  is the mass density of the surrounding water [ $\text{kg m}^{-3}$ ],  $D$  is the diameter of the structure [ $\text{m}$ ], and  $C_{D,f}$  is the drag coefficient for a cylinder submerged in water [-].

The transition piece is represented by parts three and four ( $i = 3, 4$ ) of the beam, where the border between these parts defines the ice action point. Part three is submerged and subject to the same conditions as part two. Part four is located above water and subject to aerodynamic loading taken into account as a drag force described by Morison's equation:

$$F_a(z, t) = \frac{1}{2} \rho_a C_{D,a} D (v_a(z, t) - \dot{u}_i(z, t)) |v_a(z, t) - \dot{u}_i(z, t)| \quad (C.5)$$

where  $\rho_a$  is the mass density of air [ $\text{kg m}^{-3}$ ],  $C_{D,a}$  is the drag coefficient for a cylinder in air [-], and  $v_a$  is the time and space dependent wind speed taken into account as:

$$v_a(z, t) = v_{rna}(t) \left( \frac{z}{z_{rna}} \right)^{\frac{1}{7}} \quad (C.6)$$

where  $z_{rna}$  is the location of the rotor nacelle assembly, and  $v_{rna}$  is the wind speed at that location taken as a set of random velocities generated with a Weibull distribution according to:

$$f(v, \alpha_a, \beta_a) = \frac{\beta_a}{\alpha_a} \left( \frac{v}{\alpha_a} \right)^{\beta_a - 1} \exp - \left( \frac{v}{\alpha_a} \right)^{\beta_a} \quad (C.7)$$

with  $\beta_a$  equal to 2 and:

$$\alpha_a = \frac{v_{avg}}{0.886} \quad (C.8)$$

where  $v_{avg}$  is the mean wind speed at the height of the rotor nacelle assembly [ $\text{m s}^{-1}$ ].

Part five ( $i = 5$ ) represents the tower which is subject to aerodynamic loading as described for part four. The rotor nacelle assembly is taken into account as a point mass with the non-linear interaction between wind and blades represented by a point load. The boundary conditions at the top are given by:

$$\begin{aligned} \frac{\partial^2 u_5(z, t)}{\partial z^2} \Big|_{z=L} &= 0 \\ EI \frac{\partial^3 u_5(z, t)}{\partial z^3} \Big|_{z=L} &= F_{top}(v_{rna}, t) + M_{top} \frac{\partial^2 u_5(z, t)}{\partial t^2} \Big|_{z=L} \end{aligned} \quad (C.9)$$

The wind load is taken into account by application of the blade element theory in combination with the momentum theory as described in Hansen et al. (2006).

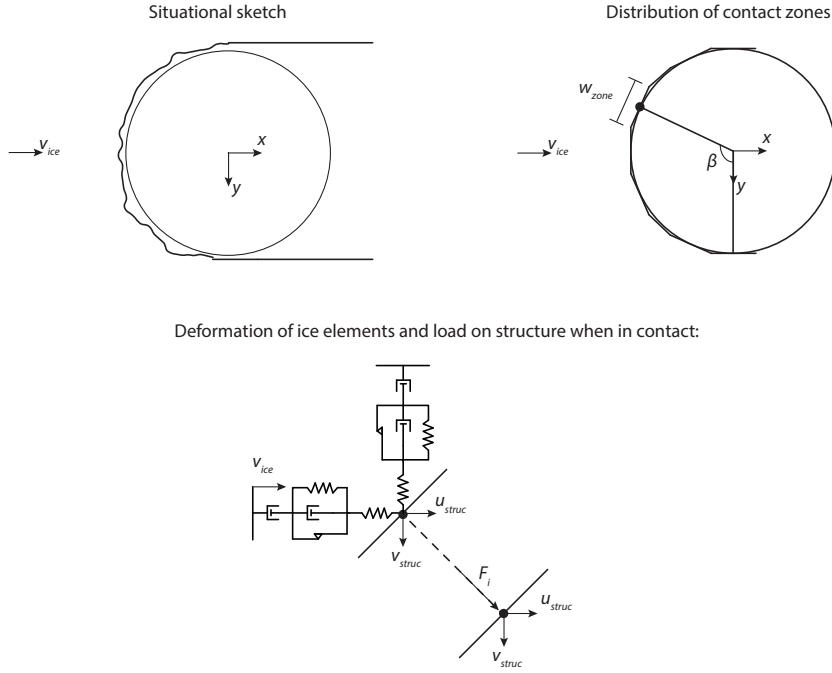


Figure C.2: Overview of first step towards a two-dimensional model for ice action on vertically sided structures.

Interface conditions between the parts of the structure are defined by the continuation of displacements, angular rotations, bending moments, and shear forces. Ice action is taken into account as a point load in the interface condition for the shear force between parts three and four which is given by:

$$\left( EI \frac{\partial^3 u_4(z, t)}{\partial z^3} + T_4(z_4) \frac{\partial u_4(z, t)}{\partial z} - EI \frac{\partial^3 u_3(z, t)}{\partial z^3} - T_3(z_3) \frac{\partial u_3(z, t)}{\partial z} \right) \Big|_{z=z_{ice}} = F_{ice}(\dot{u}_3, u_3, t) \quad (\text{C.10})$$

## C.2. IMPLEMENTATION OF A CYLINDRICAL STRUCTURE

For a cylindrical structure interacting with an ice floe as shown in Figure C.2 which is free to move in  $x$  and  $y$  direction the approach is as follows. The circumference of the cylinder is split up into  $N$  interaction zones with a width  $w_{zone}$  equal to the width of an interaction zone obtained from reference measurements as defined in Chapter 5. The global reference angle  $\beta_i$  for element  $i$  given by:

$$\beta_i = 2 \arctan\left(\frac{0.5w_{zone}}{0.5d_s}\right) \quad (\text{C.11})$$

For each zone two ice elements are introduced, one acting in the direction of the ice drift

which is chosen to coincide with the global  $x$  direction, and one in the cross-wise direction, or the global  $y$  direction. Both elements only give compression resistance and the element in  $x$  direction is pushed forward with the ice velocity. The equations of motion for both elements are given by:

$$\begin{aligned}
 u_{i,1}(t) &= \begin{cases} u_{i,2}(t) & \text{no contact} \\ u_s(t) & \text{contact} \end{cases} \\
 \dot{u}_{i,2}(t) &= \begin{cases} v_{ice} & \text{no contact} \\ \frac{K_2}{C_2}(u_s(t) - u_{i,2}(t)) + v_{ice} & \text{contact stick} \\ \left(\frac{K_2}{C_1} + \frac{K_2}{C_2}\right)(u_s(t) - u_{i,2}(t)) + \frac{K_1}{C_1}(u_{i,3}(t) - u_{i,2}(t)) & \text{contact slip} \\ \quad + v_{ice} + \frac{F_{slip}}{C_1} & \end{cases} \\
 \dot{u}_{i,3}(t) &= \begin{cases} v_{ice} & \text{no contact} \\ \frac{K_2}{C_2}(u_s(t) - u_{i,2}(t)) + v_{ice} & \text{contact} \end{cases} \\
 v_{i,1}(t) &= \begin{cases} v_{i,2}(t) & \text{no contact} \\ v_s(t) & \text{contact} \end{cases} \\
 \dot{v}_{i,2}(t) &= \begin{cases} 0 & \text{no contact} \\ \frac{K_2}{C_2}(v_s(t) - v_{i,2}(t)) & \text{contact stick} \\ \left(\frac{K_2}{C_1} + \frac{K_2}{C_2}\right)(v_s(t) - v_{i,2}(t)) + \frac{K_1}{C_1}(v_{i,3}(t) - v_{i,2}(t)) & \text{contact slip} \\ \quad + \frac{F_{slip}}{C_1} & \end{cases} \\
 \dot{v}_{i,3}(t) &= \begin{cases} 0 & \text{no contact} \\ \frac{K_2}{C_2}(v_s(t) - v_{i,2}(t)) & \text{contact} \end{cases}
 \end{aligned} \tag{C.12}$$

Contact occurs when either the  $x$  offset or  $y$  offset is crossed at which point both elements are assumed simultaneously in contact with the structure in that contact zone. The elements are not coupled and only give a resistance in compression. The load in  $x$  and  $y$  direction on the structure is then given by:

$$\begin{aligned}
 F_{x,i} &= \sin(\beta_i)^2 K_2 (u_{i,1} - u_s) + \cos \beta_i \sin(\beta_i) K_2 (v_{i,1} - v_s) \\
 F_{y,i} &= -\sin(\beta_i) \cos(\beta_i) K_2 (u_{i,1} - u_s) + \cos(\beta_i)^2 K_2 (v_{i,1} - v_s)
 \end{aligned} \tag{C.13}$$

Failure is set to occur when the total deformation equals the critical deformation:

$$\sqrt{(u_{i,1} - u_s)^2 + (v_{i,1} - v_s)^2} - \delta_{crit} > 0 \tag{C.14}$$

, where only the compressive deformation is considered. If one of the elements is in tension that deformation component is set to zero.





# ACKNOWLEDGEMENTS

My journey as a PhD student has come to an end and looking back it has been an amazing experience which resulted in many memories I will treasure forever. I consider myself lucky to have been given the opportunity to work with, and learn from, so many devoted researchers and experienced engineers. Being part of three 'groups' I never lacked an enthusiastic colleague to discuss my work with or whom I could ask for help. I wish to thank all of you from the SAMCoT project and the groups of Dynamics of Solids and Structures and Offshore Engineering at TU Delft for your input, support, and for all the fun we had over the past years.

My main supervisor Andrei deserves a special word of thanks. Thank you for making the effort in persuading me that my dream is not to become a bridge engineer, but to do research on ice-induced vibrations. You gave me the freedom to pursue my own ideas and you were always there when it really mattered. You made me a more confident person by making me volunteer to give presentations at every possible occasion. Our conference visits and trips to Norway have resulted in many great stories which illustrate the friendship we have developed over the years, and which I treasure.

This PhD project would not have been as rewarding and such a great experience without the existence of SAMCoT and its devoted project leader and my second supervisor Sveinung. I wish to thank you for arranging the possibilities for me to experience the Arctic by taking me to Svea and on board the Oden. It is these trips which have left the biggest impression on me the past years. Thank you also for taking the time to teach me about ice engineering and share your experience and stories with me.

I wish to thank Knut for leading our work package in SAMCoT and Mauri for always being available to share his experience with respect to ice-induced vibrations. All the people at HSVA I thank for their help during the experimental campaign and the great spirit during the long days in the basin. Thank you Guido for your involvement in my work and the discussions on scaling over the years.

Several people have contributed to making me feel at home during my stays in Norway. First of all Torodd, despite the fact that we were forcefully put together in WP3 it has been a great pleasure working with you. Thanks for showing me a bit of Norway, and for saving me from all the near accidents while attempting to ski and mountain-bike. Sergey and Anna for the warm welcome every time I came to Trondheim, the great fun while waiting for the first ice-station on the Oden, and for coming to visit me in The Hague during the hard times when I could not visit you. And finally, Maria Azucena, for all the warm welcomes, discussions in Dutch, and for your support and enthusiasm throughout the years.

My friends who were there when things did not go as planned, who stuck around, and who became so important to me during the last two years. Mathis, no longer among us,

we should have been able to celebrate this moment together. Jesse, Hildo, Philip, and Vincent, thank you for the friendship and always reminding me that I can do this. My culinary brothers from the Persch, Mathijs, Robin and Robbert, for being there when I needed it most. Martijn, my oldest friend, thank you for being my paranymph. I hope I can return the favor one day soon. And finally Bas who was always close by, despite the distance.

My parents I would like to thank for creating the possibilities for me which allowed me to become who I am today, and for their everlasting support and believe in me. I wish to thank my sister for her help with the experiments related to the design of the cover of this book and the actual design itself, and I wish to thank my brother for standing beside me during my defence. It is really great to be able to share this with you.

Finally, Vroukje, I cannot begin to thank you enough. You were there to celebrate every small victory along the way, something I would have never done myself. Thank you for your help in finishing this thesis and allowing me to work on it day and night for several weeks. You deserve all the credits for pulling us through the challenging times the past years. I am looking forward to the future in which our evenings together will no longer be filled with dynamics, that I promise.

# PUBLICATIONS BY THE AUTHOR

## JOURNAL PUBLICATIONS

1. **H. Hendrikse**, A. Metrikine (2015). Interpretation and prediction of ice induced vibrations based on contact area variation. *Int. J. Solids Struct.*, 75-76:336-348.
2. **H. Hendrikse**, A. Metrikine (2016). Edge indentation of ice with a displacement-controlled oscillating cylindrical structure. *Cold Reg. Sci. Technol.*, 121:100-107.
3. **H. Hendrikse**, A. Metrikine (2016). Ice-induced vibrations and ice buckling. *Cold Reg. Sci. Technol.*, 131:129-141.

## CONFERENCE PUBLICATIONS

1. **H. Hendrikse**, A. Metrikine, K.-U. Evers (2012). A method to measure the added mass and added damping in dynamic ice-structure interaction: Deciphering ice induced vibrations, Part 3. In *Proceedings of the 21st IAHR International Symposium on Ice*, Dalian, China.
2. **H. Hendrikse**, G.L. Kuiper, A.V. Metrikine (2011). Ice induced vibrations of flexible offshore structures: the effect of load randomness, high ice velocities and higher structural modes. In *Proceedings of the 21st International Conference on Port and Ocean Engineering under Arctic Conditions*, Montreal, Canada.
3. **H. Hendrikse**, F.W. Renting, A.V. Metrikine (2014). Analysis of the fatigue life of offshore wind turbine generators under combined ice- and aerodynamic loading. In *Proceedings of the ASME 33rd International Conference on Ocean, Offshore and Arctic Engineering*, San Francisco, California.
4. **H. Hendrikse**, A.V. Metrikine (2013). The influence of friction at the ice-structure interface on ice induced vibrations. In *Proceedings of the 22nd International Conference on Port and Ocean Engineering under Arctic Conditions*, Espoo, Finland.
5. M. Määttänen, S. Løset, A. Metrikine, K.-U. Evers, **H. Hendrikse**, Lønøy, C., Metrikin, I., Nord, T., Sukhorukov, S. (2012). Novel ice induced vibration testing in a large-scale facility: Deciphering ice induced vibrations, Part 1. In *Proceedings of the 21st IAHR International Symposium on Ice*, Dalian, China.
6. A. Sinitsyn, T. Sinitsyna, **H. Hendrikse** (2016). Ice station for ramming test on OATRC 2013. In *Proceedings of the 23rd IAHR International Symposium on Ice*, Ann Arbor, Michigan.
7. A. Tsouvalas, **H. Hendrikse**, A. Metrikine (2014). The completeness of the set of modes for various waveguides and its significance for the near-field interaction with vibrating structures. In *Proceedings of the 9th International Conference on Structural Dynamics*, Porto, Portugal.
8. S. Verichev, A. Metrikine, R. Plat **H. Hendrikse** (2011). Dynamics of the vertical hydraulic transport system for deep sea mining. In *Proceedings of the ASME 30th International Conference on Ocean, Offshore and Arctic Engineering*, Rotterdam, The Netherlands.



# SAMENVATTING

Het afgelopen decennium is de interesse voor offshore ontwikkelingen in gebieden waar de zee voor een deel van het jaar bedekt is met ijs sterk toegenomen. De olie- en gas sector kijkt naar het Noordpool gebied waar een groot deel van de nog onontdekte olie en gas voorraad op de wereld gevonden kan worden. Voor de wind energie sector zijn locaties zoals de Baltische zee en de grote meren in Noord-Amerika interessant.

Duurzame ontwikkelingen op zee kunnen bijdragen aan een toekomst met een goede balans tussen conventionele en groene energie, vooropgesteld dat de gebouwde constructies veilig zijn. Om deze constructies te kunnen ontwerpen is het belangrijk inzicht te hebben in de krachten die drijvend ijs kan uitoefenen op de constructie en de interactie tussen het ijs en de constructie. Voor constructies die gefundeerd zijn op de zeebodem en waarvan de buitenzijde haaks op het wateroppervlak staat is het van belang om door ijs geïnduceerde trillingen in beschouwing te nemen. Deze trillingen ontstaan als gevolg van de dynamische interactie tussen het ijs en de constructie en resulteren in grote krachten op de constructie en mogelijke vermoeiing van het materiaal. Door ijs geïnduceerde trillingen zijn het onderwerp van deze thesis.

In de jaren zestig van de vorige eeuw zijn er twee theorieën gepresenteerd die de oorsprong van de trillingen mogelijk verklaren. Ondanks dat er over de jaren vele observaties zijn gedaan die niet overeenkomen met voorspellingen op basis van deze theorieën worden ze nog steeds het meest gebruikt om het ontstaan van door ijs geïnduceerde trillingen te voorspellen. Er bestaat tot op heden geen model gebaseerd op deze theorieën dat toepasbaar is voor een breed scala aan scenario's. Dit is een reden om de bestaande data opnieuw te onderzoeken met als doel een theorie te definiëren die alle, of de meerderheid van de, observaties kan verklaren en op basis waarvan een breed toepasbaar model ontwikkeld kan worden.

Het doel van dit onderzoek is om een theorie te definiëren die verklaart hoe door ijs geïnduceerde trillingen ontstaan wanneer een plaat ijs tegen een offshore constructie aan drijft waarvan de zijde haaks op het wateroppervlak staat. Om dit doel te bereiken zijn eerst een groot deel van de bestaande experimentele observaties geanalyseerd. Op basis van deze analyse zijn belangrijke observaties gekozen die op zijn minst door de theorie verklaart moeten worden. Nieuwe experimenten zijn uitgevoerd waarbij de constructie een gecontroleerde trilling onderging met als doel om een beter beeld te kunnen krijgen van de processen die optreden in het gebied waar het contact tussen het ijs en de constructie plaats vindt.

Op basis van de literatuur studie en de uitgevoerde experimenten is een nieuwe theorie ontwikkeld. De theorie is gebaseerd op de observatie dat het van de relatieve snelheid tussen ijs en constructie afhankelijke vervormings- en faalgedrag van het ijs de interactie tussen ijs en constructie bepaald. Wanneer ijs langzaam belast wordt kan het contact

tussen het ijs en de constructie zich ontwikkelen over een groot oppervlak als gevolg van grote vervormingen in het ijs. Dit grote contact oppervlak zorgt ervoor dat er een hoge kracht op de constructie ontstaat. Wanneer het ijs echter snel belast wordt ontstaat er alleen contact in specifieke zones, wat ervoor zorgt dat er een lagere kracht op de constructie wordt uitgeoefend. Wanneer een beweegbare constructie wordt belast door het ijs ontstaat er een wisselende relatieve snelheid waarmee het ijs belast wordt. Als gevolg hiervan zijn er periodes waarin de kracht van het ijs hoog is, die zich afwisselen met periodes waarin de kracht lager is. De door ijs geïnduceerde trillingen kunnen zich ontwikkelen wanneer tijdens de periodes van hoge kracht voldoende energie aan de constructie wordt overgedragen.

Op basis van deze nieuw ontwikkelde theorie is een model voor de simulatie en voorspelling van door ijs geïnduceerde trillingen ontwikkeld. Het is aangetoond dat het model consistent is met de meeste van de bestaande experimentele observaties. Een theoretische studie naar het effect van het uitknikken van het ijs laat zien dat knik over het algemeen de ontwikkeling van door ijs geïnduceerde trillingen belemmert, echter er zijn situaties waarin het tegenovergestelde mogelijk is. De praktische toepassing van het model is aan de hand van gesimuleerde voorbeelden behandeld met daarbij de focus op meer gedetailleerde modellen van constructies en het ontwerp van experimenten.

# CURRICULUM VITAE

21 Juli 1986	Born in Woerden, the Netherlands
September 2004 - September 2007	Bachelor of Science Delft University of Technology Faculty of Civil Engineering and Geosciences
September 2007 - September 2010	Master of Science ( <i>cum laude</i> ) <i>Structural Engineering</i> Delft University of Technology Faculty of Civil Engineering and Geosciences Section of Structural Mechanics
September 2010 - September 2011	Researcher <i>Riser dynamics and deep-water mining</i> Delft University of Technology Faculty of Civil Engineering and Geosciences Section of Structural Mechanics Dynamics of Solids and Structures
September 2011 - September 2016	Ph.D. Research <i>Ice-induced vibrations</i> Delft University of Technology Faculty of Civil Engineering and Geosciences Section of Structural Mechanics Dynamics of Solids and Structures